



Vaal University of Technology

PHOTOCATALYTIC DEGRADATION OF DYES AND PESTICIDES IN THE PRESENCE OF IONS.

Kwena Yvonne Pete (207064814)

Dissertation for the degree of **Magister Technologiae** submitted in the Department of Chemical Engineering, Faculty of Engineering and Technology, Vaal University of Technology.

Supervisor: Prof. Ochieng Aoyi

Co-supervisor: Prof. Maurice S. Onyango

March 2015

DECLARATION

I, Kwena Yvonne Pete, declare that this dissertation is my own work. It is submitted for the degree of Magister Technologiae in the Department of Chemical Engineering, Vaal University of Technology, Vanderbijlpark. It has not been submitted before for any degree or examination to any other University.

Kwena Yvonne Pete

Candidate: Name

Signature

Prof. Ochieng Aoyi

Supervisor: Name

Signature

Prof. Maurice. S. Onyango

Co-Supervisor: Name

Signature

DEDICATION

This dissertation is dedicated to my parents, Mr. Selepe Wilson and Mrs. Mmatlou Justina Pete, also to my brothers and sisters.

ACKNOWLEDGEMENTS

The research work for this MTech-thesis was executed at the Laboratory of Green Chemistry, Lappeenranta University of Technology in Mikkeli (Finland). I am very appreciation of my supervisors Professor Ochieng Aoyi and Prof Maurice Onyango for the opportunity to carry out this study and for the encouragement to finish the research for this degree. I wish to express my deep gratitude to Prof. Mika Sillanpää and Dr. Repo for giving me the opportunity and encouragement to execute my experimental work at the Laboratory of Green Chemistry in Finland. In addition, thank you for the invaluable guidance in experimental work, data analysis, and preparation of manuscripts. The financial supports from European Union and the City of Mikkeli, Finland and the Water Research Commission in South Africa are acknowledged with much appreciatively.

I wish also to extend my warmest appreciations to the research group of the Laboratory of Green Chemistry for all the assistance and encouragement. Most of all I am very grateful to Irina Levchuk and Olga Oleksiienko for their invaluable guidance during my experimental work and Tero for being my extra hands in the laboratory. I wish also to thank the Vaal University of Technology for providing the founding with which the project would not have been possible. My thanksgiving is also extended to the VUT international office team, Mr. Wiseman Jack, Mr. Simon Mohlala, Mr. Lebohang Sebiloane and Venessa Bradbury for their contributions in making my trip to Finland a success.

My deepest thanks to my family, mostly my parents, Mr. Wilson and Mrs. Mmatlou Pete, for their endless support during my entire life. Particularly, they encouraged me to further studies right from the beginning and I would also like to thank my elder sisters, Shirley, Maphuti, Kgabo, Phuti and elder brothers, Tlou and Rangwane for always inspiring and encouraging me. Not forgetting my niece, Lebogang Pete, for all the ups and downs she went through to have my proposal submitted to higher degree office when I was in Europe. This work is dedicated to them. To end with, I thank God for enabling me to make this work possible.

LIST OF PUBLICATIONS

- I. Pete Kwena Yvonne & Aoyi Ochieng. 2014. Analysis of Kinetic Models in Heterogeneous Catalysis of Methyl Orange Using TiO₂/Silica Composite Photocatalyst. Paper presented at International Conference on Chemical and Metallurgical Engineering. Johannesburg, South Africa, 15th-16th April
- II. Pete Kwena Yvonne & Aoyi Ochieng. 2014. Photodegradation of dye in the presence of metal ions using composite catalyst. International Conference on Composite Materials and Renewable Energy Applications (ICCMREA-2014). Sousse, Tunisia, 22nd-24th January
- III. Pete Kwena Yvonne, Sillanpää Mika, Onyango Maurice & Aoyi Ochieng. 2014. Analysis of Kinetics and Isotherms Equilibrium Modeling for the Photocatalytic Reduction of Cr(VI) in the Presence of Dye on Composite Photocatalyst. Paper presented at Global Conference on Applied Sciences and Environment Research (GCAEER), Okinawa, September (Also accepted to the Journal of Chemistry and Chemical Engineering)
- IV. Aoyi Ochieng, Pete Kwena Yvonne & Apollo Seth. 2012. Application of zeolite and chitosan beads for the photocatalytic degradation of methylene blue dye. Paper presented at 7th Egerton UNIVERSITY international conference: Research and Expo, Njoro, 26th-28th September.

ABSTRACT

Water pollution caused by organic and inorganic contaminants represents an important ecological and health hazard. Simultaneous treatment of organic and inorganic contaminants had gradually gained great scientific interest. Advanced oxidation processes such as photocatalysis, using TiO_2 as a photocatalyst, have been shown to be very robust in the removal of biorecalcitrant pollutants. These methods offer the advantage of removing the pollutants, in contrast to conventional techniques. At present, the main technical challenge that hinder its commercialization remained on the post-recovery of the photocatalyst particles after water treatment. Supporting of the photocatalyst on the adsorbent surface is important as it assists during the filtration step, reducing losses of the materials and yielding better results in degrading pollutants. To overcome this challenge, in this study composite photocatalysts of TiO_2 /zeolite and TiO_2 /silica were prepared and investigated to explore the possible application in the simultaneous removal of organic and inorganic compounds from contaminated water. The main objective of this study was to investigate the heterogeneous photocatalytic degradation of organic compounds in the presence of metal ions using composite photocatalysts. The Brunauer–Emmett–Teller (BET), Scanning Electron Microscopy and Energy Dispersive X-ray (SEM-EDX), Raman spectroscopy (RS) and zeta potential (ZP) analyses were used to characterize the prepared composite photocatalysts.

The successive composite photocatalysts were used in a semi-batch reactor under an irradiation intensity of 5.5 mW/m^2 (protected by a quartz sleeve) at $25 \pm 3^\circ\text{C}$ for the photocatalytic degradation of synthetic textile (methyl orange) and agricultural (atrazine) wastewater in the presence of ions. The effect of operating parameters such as TiO_2 composition on supporting material, particle size, composite photocatalyst loading, initial pollutant concentration and pH were optimized. The effects of inorganic salts and humic acid on dye and pesticides degradation were also studied, respectively. The performance of the photocatalyst reactor was evaluated on the basis of color removal, metal ion reduction, total organic carbon (TOC) reduction, intermediates product analysis and modeling of kinetics and isotherms. Different kinetic and isotherm models were introduced and applied in this work. Important aspects such as error functions with the optimal magnitude were used for the selection of the best suitable model.

The optimum conditions found during photocatalytic tests include 10 wt% TiO₂ in the zeolite composite, 6.25 g/L composite concentration, 25 mg/L dye concentration and pH 3. The extent of color removal and metal reduction after 3 h of irradiation was 99.7% and 80% at acidic conditions for the single and binary systems, respectively. The optimum conditions for the degradation of atrazine at an initial concentration of 10 mg/L were 15% TiO₂ in the silica composite, 6.25 g/L of TiO₂/silica composite concentration, with a particle size of 38-75 μm at pH 5.1. The Langmuir isotherm model fitting experimental data suggested the surface homogeneity of the prepared composite photocatalyst for dye and pesticide. The kinetics of methyl orange dye by supported TiO₂ followed pseudo-second-order mechanism while atrazine followed pseudo-first-order mechanism. Competitive photocatalytic degradation experiments showed that both composite photocatalyst had a preferential binding capacity for Cr(VI) and As(III) during the Cr(VI)-dye and As(III)-pesticide binary systems. The presence of inorganic salts and humic acid had a suppressing effect on methyl orange and atrazine degradation, respectively. From the present results it can be concluded that there is a synergistic effect between the photocatalytic degradation of organic compound and reduction of metal ions. Such a synergistic effect is likely to be attributed to two kinds of effects from zeolite and silica supporting material: adsorption effect and electron trap effect.

Table of Contents

DECLARATION	ii
DEDICATION	iii
ACKNOWLEDGEMENTS	iv
LIST OF PUBLICATIONS	v
ABSTRACT.....	vi
NOMENCLATURE	xvi
LIST OF SYMBOLS	xvi
CHAPTER 1	1
1. INTRODUCTION	1
1.1 General background	1
1.2 Problem statement.....	2
1.3 Main objective	3
1.4 Specific objectives	3
1.5 Justification of the research.....	3
1.6 Arrangement of the dissertation.....	4
CHAPTER 2	5
2. LITERATURE REVIEW	5
2.1 Wastewater containing dyes.....	5
2.2 Wastewater containing herbicides	6
2.3 Wastewater containing heavy metals and humic substances	7
2.4 Wastewater treatment methods	8
2.5 Fundamentals and mechanism of TiO ₂ photocatalysis	10

2.5.1	Heterogeneous TiO ₂ photocatalysis	10
2.5.2	Homogeneous photo-Fenton reaction	13
2.6	Photoactivity and photocatalytic properties of TiO ₂	14
2.7	Developments in photocatalyst immobilization and supports.....	15
2.7.1	Photocatalytic membrane.....	16
2.7.2	Modification of photocatalyst by doping	16
2.7.3	Photocatalyst support material	18
2.8	Isotherms and kinetics modelling	21
2.8.1	Langmuir isotherm.....	21
2.8.2	Freundlich isotherm	22
2.8.3	Sips isotherm (Langmuir-Freundlich).....	23
2.8.4	Isotherm shape	23
2.9	Kinetics modelling	24
2.9.1	Pseudo-first-order model.....	24
2.9.2	Pseudo-second-order model.....	24
2.10	Goodness of fit.....	25
CHAPTER 3		27
3.	MATERIALS AND METHODS.....	27
3.1	Materials	27
3.2	Synthesis of TiO ₂ /zeolite and TiO ₂ /silica composite photocatalysts	28
3.3	Characterization of composite photocatalysts.....	28
3.3.2	SEM instrumentation	28
3.3.4	Zeta potential	29

3.4	Photocatalysis experiments	29
3.5	Kinetics and Equilibrium modelling	30
3.6	Sample preparation	31
3.6.1	Sample preparation for chromogenic agent	32
3.6.2	Sample preparation for FTIR and GC-MS analyses	32
3.7	Analysis of solutions	33
CHAPTER 4		35
4.	RESULTS AND DISCUSSION	35
4.1	Material Characterization.....	35
4.1.1	BET Surface Area	35
4.1.2	SEM- EDX analysis	36
4.1.3	Raman Spectroscopy.....	40
4.1.4	Isoelectric Point Measurements (IEP).....	42
4.2	Photocatalytic degradation of dye by TiO ₂ /zeolite and TiO ₂ /Silica photocatalyst.....	43
4.2.1	Effect of particle size of the supporting material	46
4.2.2	Effect of TiO ₂ composition on supporting material	48
4.2.3	Effect of composite photocatalyst concentration	51
4.2.4	Effect of dye initial concentration.....	53
4.2.5	Effect of solution pH.....	54
4.2.6	Effect of inorganic salt.....	57
4.2.7	Equilibrium modelling of methyl orange degradation	60
4.2.8	Kinetics modelling of methyl orange degradation	65
4.2.9	Photocatalytic reduction with single substrate: Cr(VI)	69

4.2.10	A comparison of method analysis of Cr(VI) reduction in the mixed system.....	70
4.2.11	Photocatalytic degradation of the dye and reduction of Cr (VI), binary system.....	72
4.3	Mineralization	78
4.3.1	TOC analysis.....	79
4.3.2	Identification and evolution of inorganic ions	81
4.3.3	Degradation of intermediate products.....	82
4.4	Photocatalytic degradation of pesticides.....	84
4.4.1	Effect of composite photocatalyst size.....	84
4.4.2	Effect of composite photocatalyst loading	84
4.4.3	Effect of atrazine concentration	86
4.4.4	Equilibrium modelling of atrazine degradation	87
4.4.5	Kinetics modeling of atrazine degradation	91
4.4.6	Effect of solution pH.....	92
4.4.7	Photocatalytic reduction with single substrate: As(III).....	93
4.4.8	Photocatalytic degradation of atrazine and reduction of As(III).....	95
4.4.9	Effects of As(III) and humic acid on the photodegradation of atrazine.....	97
4.4.10	Identification of intermediate products	99
CHAPTER 5	101
5.	CONCLUSIONS AND RECOMMENDATIONS	101
5.1	Conclusions.....	101
5.2	Recommendations.....	103
REFERENCES	104
APPENDIX: Characterization of composite photocatalysts.....		115

List of figures

Figure 2.1. Schematic diagram showing the generation of oxidative species in a photocatalytic study.....	12
Figure 2.2. Steps in heterogeneous catalytic reaction	13
Figure 2.3. Stages of excitation with a sensitizer in the presence of an adsorbed organic.	17
Figure 2.4. Surface silanol OH groups at the at the silica surface.	20
Figure 3.1. Experimental setup	30
Figure 4.1. SEM images and EDX spectra of zeolite	37
Figure 4.2. SEM images and EDX spectra of 10% TiO ₂ supported on different zeolite particles.....	38
Figure 4.3. SEM images and EDX spectra of silica.....	39
Figure 4.4. SEM images and EDX spectra of TiO ₂ /silica.....	40
Figure 4.5. Raman spectra of 10% TiO ₂ /zeolite and 15% TiO ₂ /silica	41
Figure 4.6. Zeta potential of TiO ₂ /silica as a function of pH.....	43
Figure 4.7. Adsorption of methyl orange over TiO ₂ /zeolite and TiO ₂ /silica	45
Figure 4.8. Boxplots built up with data values obtained at different treatment processes	46
Figure 4.9. Effect of zeolite particle size	47
Figure 4.10. Effect of silica particle size	48
Figure 4.11. Photocatalytic degradation of methyl orange over different loading of TiO ₂ supported on zeolite.....	49
Figure 4.12. Photocatalytic degradation of methyl orange over different loading of TiO ₂ supported on silica	50
Figure 4.13. Effect of TiO ₂ /zeolite composite photocatalyst concentration on dye degradation.....	52
Figure 4.14. Effect of TiO ₂ /silica composite photocatalyst concentration on dye degradation.....	53
Figure 4.15. Effect of initial concentration on TiO ₂ /zeolite and TiO ₂ /silica.....	54
Figure 4.16. Effect of solution pH on dye degradation over TiO ₂ /zeolite	55

Figure 4.17. Effect of solution pH on dye degradation over TiO ₂ /silica	57
Figure 4.18. Effect of ions on methyl orange dye over TiO ₂ /zeolite	58
Figure 4.19. Effect of ions on methyl orange dye over TiO ₂ /silica	60
Figure 4.20. Linear transform of Langmuir and Freundlich isotherm over TiO ₂ /zeolite and TiO ₂ /silica...	61
Figure. 4.21. Photodegradation isotherms of methyl orange on TiO ₂ /zeolite.....	63
Figure 4.22. Photodegradation isotherms of methyl orange on TiO ₂ /silica	64
Figure 4.23. Linear and nonlinear regression of pseudo first order and pseudo second order model by TiO ₂ /zeolite composite photocatalyst.	66
Figure 4.24. Linear nonlinear regression of pseudo first order (a) and pseudo second order by TiO ₂ /silica composite photocatalyst.....	68
Figure 4.25. Photocatalytic reduction of Cr(VI) over (a) TiO ₂ /zeolite and (b) TiO ₂ /silica.....	70
Figure 4.26. Photocatalytic reduction of Cr(VI) in the presence of methyl orange.....	71
Figure 4.27. UV–vis absorption spectra of Cr(VI), (b) methyl orange and Cr(VI) + methyl orange	71
Figure 4.28. Effect of TiO ₂ /zeolite concentration on dye degradation in the presence of Cr(VI)	73
Figure 4.29. Effect of TiO ₂ /silica concentration on dye degradation in the presence of Cr(VI).....	74
Figure 4.30. Effect of TiO ₂ /zeolite concentration on Cr(VI) reduction in the presence of dye	75
Figure 4.31. Effect of TiO ₂ /silica concentration on Cr(VI) reduction in the presence of dye.	76
Figure 4.32. Effect of Cr(VI) initial concentration on dye degradation (black bars) over TiO ₂ /zeolite	77
Figure 4.33. Effect of Cr(VI) initial concentration on dye degradation (black bars) over TiO ₂ /silica	78
Figure 4.34. TOC reduction at different dye concentration	79
Figure 4.35. TOC reduction at different pH values	80
Figure 4.36. Time-course of inorganic ions concentration during heterogeneous photocatalysis treatment of an aqueous solution of methyl orange on TiO ₂ /zeolite	81
Figure 4.37. FTIR spectra of raw methyl orange; and extracted methyl orange	83

Figure 4.38. Effect of particle size for atrazine degradation on TiO ₂ /silica.....	85
Figure 4.39. Effect of TiO ₂ /silica concentration on pesticide degradation	86
Figure 4.40. Effect of atrazine concentration on TiO ₂ /silica.....	87
Figure 4.41. Linear transform of Langmuir isotherm over TiO ₂ /silica.....	88
Figure 4.42. Linear transform of Freundlich isotherm over TiO ₂ /silica	89
Figure 4.43. Isotherms modelling for degradation of atrazine on TiO ₂ /silica composite photocatalyst.....	90
Figure 4.44. Pseudo first and second order modelling for pesticide degradation on TiO ₂ /silica.....	92
Figure 4.45. Effect of solution pH on atrazine degradation on TiO ₂ /silica.....	93
Figure 4.46. Effect of solution pH on atrazine degradation on TiO ₂ /silica composite photocatalyst	94
Figure 4.47. Effect of As(III) initial concentration on atrazine degradation on TiO ₂ /silica	96
Figure 4.48. Final As(III) reduction in the presence of atrazine alone and atrazine/Humic acid mixture..	96
Figure 4.49. Effect of HA initial concentration on degradation of atrazine in the absence and presence of As(III)	98
Figure 4.50. FTIR spectra of raw atrazine and extracted atrazine	99
Figure 4.51. Time-course of inorganic ions concentration during heterogeneous photocatalysis treatment of atrazine.....	100
Figure A1. SEM-EDX analysis of Zeolite alone	116
Figure A2. SEM-EDX analysis of TiO ₂ supported on 0.2-0.5 mm zeolite.....	117
Figure A3. SEM-EDX analysis of TiO ₂ supported on 0.5-1 mm zeolite.....	118
Figure A4. SEM-EDX analysis of TiO ₂ supported on 1-1.2 mm zeolite.....	119
Figure A5. SEM-EDX analysis of Silica alone.....	120
Figure A6. SEM-EDX analysis of 38-75 μm TiO ₂ /silica composite photocatalyst.....	121
Figure A7. SEM-EDX analysis of 75-150 μm TiO ₂ /silica composite photocatalyst.....	122
Figure A8. SEM-EDX analysis of Analysis of 150-250 μm TiO ₂ /silica composite photocatalyst.....	123

List of Tables

Table 2.1. Advantages and disadvantages of the current methods of dye removal from industrial effluents	9
Table 2.2. The list of error functions	26
Table 4.1. Surface area of TiO ₂ supported onto zeolite	36
Table 4.2. Paired T-test on the difference of TiO ₂ Composition supported on zeolite	49
Table 4.3. Paired T-test on the difference of TiO ₂ Composition supported on zeolite	51
Table 4.4. Linear Fitting results of Langmuir and Freundlich isotherms for the degradation of methyl orange on composite photocatalysts.	62
Table 4.5. Values of R _L obtained for linear regression of Langmuir isotherm	62
Table 4.6. Nonlinear Fitting results of Langmuir and Freundlich isotherms for the degradation of methyl orange onto composite photocatalysts.	64
Table 4.7. Kinetic parameters for methyl orange photodegradation over TiO ₂ /zeolite composite photocatalyst	67
Table 4.8. Kinetic parameters for methyl orange photodegradation over TiO ₂ /silica composite photocatalyst	69
Table 4.9. GC/MS analytical results	82
Table 4.10. Linear Fitting results of Langmuir and Freundlich isotherms for the degradation of atrazine on TiO ₂ /silica composite photocatalyst.....	88
Table 4.11. Values of R _L obtained for linear regression of Langmuir isotherm	89
Table 4.12. Isotherm parameters for Atrazine pesticides over TiO ₂ /silica composite photocatalyst.....	91
Table 4.13. Kinetic parameters for the degradation of atrazine onto composite photocatalyst.	92
Table A1 Physical characteristics of zeolite and composite (TiO ₂ /zeolite)	115

NOMENCLATURE

LIST OF SYMBOLS

C_e	Equilibrium concentration	mmol/L or mg/L
C_i	Initial concentration	mmol/L or mg/L
e^-	Electron	-
E_{cb}	Conduction band	-
E_g	Band gap	-
E_{vb}	Valence band	-
h^+	Hole	-
$h\nu$	Photon energy	-
k_1	Pseudo-first-order rate constant	1/min
k_2	Pseudo-second-order rate constant	g/mmol min
K_{ads}	Equilibrium constant of adsorption	mmol/L
K_F	Freundlich affinity constant	L/mmol
K_L	Langmuir affinity constant	L/mmol
n_F	Freundlich heterogeneity factor	-
t	Time	h
T	Temperature	K or °C
q_e	Equilibrium adsorption capacity	mmol/g
q_m	Maximum adsorption capacity	mmol/g
q_t	Adsorption capacity at time t	mmol/g
R^2	Coefficient of determination/correlation coefficient	-
R_L	Constant separation factor	-
χ^2	Nonlinear chi-square test	-
α	Absorption coefficient	-
λ	Wavelength	nm

ABBREVIATIONS

AOPs	Advanced oxidation processes
ARE	The average relative error
BET	Brunauer–Emmett–Teller
EABS	Sum of absolute errors
EDAX	Energy Dispersive Analysis of X-ray
ERRSQ	The sum of the square of the errors
FTIR	Fourier transform infrared spectroscopy
GCMS	Gas chromatography mass spectroscopy
HPLC	High performance liquid chromatography
HS	Humic substances
ICP-OES	Inductively coupled plasma optical emission spectrometry
MPSD	Marquardt’s percent standard deviation
NOM	Natural organic matter
R&D	Research and development
RMSE	Residual root mean square error
RS	Raman spectroscopy
SEM	Scanning electron microscope
SSE	Sum of the squares of the errors
TOC	Total organic carbon
UV	Ultraviolet
UV-vis	Ultraviolet-visible spectroscopy
WHO	World Health Organization
WWTP	Wastewater treatment plants
ZP	Zeta potential

CHAPTER 1

1. INTRODUCTION

The world faces enormous challenges ahead as drinkable water runs short due to natural disasters, population increase, and water pollution. The rapid industrialization and large number of contaminants entering the water supply from human activities, contribute to exacerbate this challenge. In addition, several health problems are associated with the lack of access to clean drinking water. Different water sources are contaminated with multiple recalcitrant contaminants such as pesticides, organic matter and heavy metal ions. Recently, water reuse has emerged as a serious issue in preserving global water. Therefore, there is a need for providing potable water using inexpensive water treatment method.

1.1 General background

The fast growth of industry, agriculture and the worldwide concern for environmental conservation is becoming increasingly problematic in view of water pollution by inorganic and organic compounds. Chemical pollution from inorganic and organic compounds such as heavy metals, dyes and pesticides is one of the main threats to water quality (Bhatnagar and Sillanpää, 2009). These chemicals enter the natural water bodies in several different ways, either discharged directly, such as industrial effluents or from WWTP. They may also enter the aquatic medium indirectly through application of plant health products such as biocides and fertilizers in agriculture. In general, water-soluble substances can be transported and spread more easily in the water cycle. These compounds are nonbiodegradable, highly toxic and frequently accumulate in the food chain. If ingested beyond the acceptable concentration level, their toxicities could lead to serious damage not only to human health but also to plants and animals (Repo, 2011).

The most problematic recalcitrant organics co-contaminated with metal ions are dyes and pesticides from the dye and agricultural industrial effluents. Amongst all water pollutants, metal ions such as arsenic, chromium, copper, lead and mercury (Bhatnagar and Sillanpää, 2009) often co-exist with these organic compounds in wastewater. Treatment of wastewater containing organic and metal pollutants is a complex worldwide environmental problem, as the two components must be treated independently. In addition these chemicals revealed a

significant difference in molecular weight, chemical composition and toxicity (Aksu, 2005). With growing demand of good quality water, one of a few attractive alternatives to resolve these environmental issues is the possible reuse of wastewater. Countless practical strategies and solutions have been implemented to produce more viable water resources. Currently presented water treatment methods such as adsorption or coagulation simply concentrate the pollutants present by transferring them to other phases, thus not reducing them into an active compound. These have led to the rapid R&D in the field of “Advanced Oxidation Processes (AOPs)” as the innovative and low cost wastewater treatment methods (Chong *et al.*, 2010).

1.2 Problem statement

The presence of biorecalcitrant wastes such as dyes, pesticides and metal ions in water is a huge environmental concern worldwide. These chemicals have shown a significant difference in molecular weight, chemical composition and toxicity in water and wastewater. Due to their high toxicity and the associated environmental hazards, occurrence of dyes, pesticides and metal ions in water and wastewater can cause serious damage to human beings even at very low concentrations. In addition, due to their complex aromatic chemical structure and synthetic origin, dyes and pesticides are hardly biodegradable using conventional methods. Metals are also not biodegradable and can accumulate in living tissues, thus becoming concentrated throughout the food chain. Although at low doses they are essential micronutrients for plants and animals, in high doses can negatively affect the health of most living organisms.

Treatment of wastewater containing both inorganic and organic pollutants is a challenge as the two compounds must be treated independently. Moreover, the occurrence of ions in wastewater can affect the treatment efficiency of organic pollutants since they can compete with the dye and pesticides molecules for the binding sites. Conventional water and wastewater treatment methods such as chemical and membrane methods involve high operating costs and could produce toxic secondary wastes into the ecosystem. Therefore, UV heterogeneous photocatalytic degradation using TiO₂ particles is an effective and low cost technique to degrade aromatic pollutants co-existing with ions from the industrial and municipal wastewater. However, the application of TiO₂ in the form of slurry is still experiencing technical challenges such as recombination difficulties and its functionality towards the practicality as an industrial process include its post-separation after water treatment. The fine powder particles of the TiO₂ tend to form agglomeration during the process.

Such particles agglomeration is highly detrimental in views of particles size preservation, surface-area reduction and its reusability lifespan. To address this problem in this work, a composite photocatalyst is prepared by supporting TiO₂ powder onto supporting materials namely, zeolite and silica in such a way as to provide the accessibility of the photocatalyst. Due to its unique uniform pores, adsorption capability and straight channels, zeolite seem to be the potential material whilst silica is light transparent in nature and provides large surface area. Therefore, this work will address the problems of bio-recalcitrance of the pollutants, effect of ions on photodegradation and catalyst separation.

1.3 Main objective

The main aim of this work was to investigate the heterogeneous photocatalytic degradation of dyes and pesticides in the presence of ions.

1.4 Specific objectives

- a) To prepare TiO₂ composite photocatalyst and apply it to determine the effect of different operating parameters on photodegradation;
- b) To determine the effect of water matrix (salts) on the photodegradation of dye;
- c) To evaluate the effect of humic substance on the photodegradation of herbicide;
- d) To analyze the reaction kinetics and isotherms modelling and
- e) To identify the intermediate organic and inorganic products after photocatalysis process.

1.5 Justification of the research

Investigations on the wastewater treatment area have been conducted in two main groups: treatment of single and multi-component solutions. Although results achieved by single component solutions are suitable for predicting the behavior of such solutions, wastewater streams containing a single compound are very rare and the results cannot be applicable to actual wastewater. While studies on multi-component solutions are beneficial to employ for real wastewater streams in larger scale. It was also considered that the real wastewater might contain substances that could compete with the target contaminant for the oxidizing agent, such as dyes and pesticides in the presence of ions. This usually results in a decrease in process efficiency. Therefore, it was desirable to optimize the effects of different parameters of the dye

and pesticides solutions to achieve a better photocatalytic efficiency using the prepared composite photocatalysts in the wastewater treatment applications. Traditional methods have been used to determine these effects for removing the toxic compounds, however these techniques are ineffective. Therefore, the development of an effective treatment process employing low cost composite photocatalyst that can convert contaminants into non-toxic is required. This research would also contribute to a more sustainable future by reusing wastewater while promoting low operation cost.

1.6 Arrangement of the dissertation

A general introduction to the subject of water and wastewater treatment is provided in Chapter 1. Comprehensive literature review is presented in Chapter 2 on wastewater contaminated with different organic and inorganic pollutants, wastewater treatment methods, fundamentals of photocatalysis, properties of TiO_2 , and types of photocatalysts support, isotherm and kinetics modelling. Chapter 3 presents the methodology employed to achieve the objectives of the thesis. It discusses the experiments that were conducted. It consists of procedures, methods, equipment, and other relevant information that was used for conducting the experiments. Chapter 4 focuses on the photodegradation of methyl orange dye and atrazine pesticide in the single or binary system. Here, results obtained from studies on the adsorption, photolysis and photodegradation of the dye and pesticides in the presence of ions are presented. The isotherms and kinetic modelling of the dye and pesticides degradation are performed. An in-depth analysis and comparison of the results are also presented in this chapter. The conclusions drawn from this work including recommendations for future work arising from this project are presented in Chapter 5. Appendix provide the table and figures that were not included in the context of the report, but are used for supporting some content.

CHAPTER 2

2. LITERATURE REVIEW

Good water quality is one of the basic needs to our existence, however; many water sources in urban and rural communities are contaminated with wide range of compounds at different concentrations such as dyes, pesticides, organic matter and heavy metal ions, some of which need to be treated independently. Furthermore, in view of large-scale plant for water treatment as well as industries, the water quality of the effluents can fluctuate considerably with time. The way of selecting the treatment method depends on the characteristics of the wastewater stream regulations and cost.

There are several chemical and physical methods available to remove contaminants in water and wastewater, such as adsorption by activated carbon, Fenton's reagent and ozonation. Due to the large number of aromatic rings found in dyes and pesticides, these method are ineffective. Therefore, advanced oxidation processes are being considered as an emerging technology to handle large volumes of textile and agricultural wastewater. Among these processes, heterogeneous photocatalysis is believed to be a simple and effective technique for water and wastewater (Chong *et al.*, 2010). Modeling of isotherm and kinetics, however, has become important for a fast and successful process design. The most commonly used adsorption isotherms are still the Langmuir and Freundlich models. Moreover, hazardous organic and inorganic compounds usually co-exist in streams of practical wastewaters, and the simultaneous photocatalytic treatment of organic and inorganic pollutants will show profits in both economics and technology.

2.1 Wastewater containing dyes

A great number of industries such as textile, paint, printing, pharmaceuticals, paper and pulp are very organic and water based chemicals intensive, which results in the production of large volumes of wastewater. Main contaminants specifically originating in polluted textile wastewater are highly recalcitrant characterized by high chemical oxygen demand, suspended solids and dyes giving intense colour (Venceslau *et al.*, 1994). The classifications of dyes include reactive dyes, cationic-basic dyes anionic-direct, non-ionic-and disperse dyes (Banat *et al.*, 1996). The azo or anthraquinone types are the common chromophores in anionic and

non-ionic dyes. Due to their aromatic structures, dyes are more resistant to removal and therefore remain coloured for a long period of time in the wastewater. Among these dyes, reactive dyes are widely used in textile industries due to their favorable characteristics of water-fast and simple application procedures with low energy consumption (Hao *et al.*, 2000). Methyl orange is one of important dyes which is widely used in textile industry. Several studies discovered the carcinogenic nature and toxicity of this dye. It absorbs blue-green light in acidic solution which lead to red solution. Whilst at high pH values it absorbs blue-green and red light which makes its solution appear yellow. If this dye comes in contact with certain drugs in the human body, it can lead to asthmatic reactions in people (Calza *et al.*, 2006).

2.2 Wastewater containing herbicides

Beside dyes, the presence of pesticides and their derivatives poses threat to surface and groundwater due to their high solubility which makes their distribution very easy in the environment. The main sources of pesticide contamination are wastewater from agricultural industries, formulation of pesticides and manufacturing plants (Beitz *et al.*, 1994). They contribute significantly in the economic production of a wide range of fruits, vegetables, cereals, fiber and oil crops in many countries. Irrespective of their benefits, humans and animals are potentially exposed to pesticides in most places, especially in food. Exposure to pesticides have raised considerable health concern to humans and other living things as the compounds are persistent and carcinogenic in nature even at low concentrations (Eriksson *et al.*, 2007).

Pesticides are divided into various classes, of which the most critical are organochlorine and organophosphorous compounds. Due to their hydrophobicity and low chemical degradation rates, organochlorine pesticides have accumulated in biological tissues. On the other hand, organophosphorous pesticides are known to degrade fast depending on their method of application, formulation and the growing stage of the plant (Aksu, 2005). Atrazine has been used since 1958 as herbicide to control broad leaf weeds in the production of corn, sugarcane, winter wheat, nuts and conifers. It is commonly used at rates of 1.12 to 2.24 kg/ha, which results in soil concentrations of 3 to 6 mg/kg (Alvey and Crowley, 1996). The half-life of atrazine varies from 45 days to 3-5 years (Armstrong *et al.*, 1967) depending on the environmental conditions. The solubility of atrazine in water is 33 mg/L at 25°C and it is resistant to hydrolysis at neutral pH. Due to its extensive use and moderate persistence in the environment, atrazine is frequently identified in ground and surface waters, in precipitation and

in gas phase (Tang *et al.*, 2012). Reported concentrations in ground and surface water are typically 100 ng/L or less, however; Ren and Jiang (2002) have detected levels above 30 µg/L.

2.3 Wastewater containing heavy metals and humic substances

The emission of heavy metals is another major global concern due to their high toxicity and variety as they are considered carcinogen (Kabra *et al.*, 2004). Among all water contaminants, metal ions such as chromium and arsenic are the most widespread in the environment. In addition, these metal ions often co-occur with organic pollutants in different wastewater streams including municipal and industrial wastes. Chromium is a heavy metal, naturally found in rocks, animals, plants, and soil and its exploitation has increased due to the extensive use of chromate and dichromate in textile, photoengraving processes, leather tanning and the electroplating industry (Park *et al.*, 2005). It is available in two common oxidation states naturally, namely; trivalent and hexavalent forms. Hexavalent chromium (Cr(VI)) is mobile and potentially toxic whilst Cr(III) at neutral or alkaline pH is readily precipitated on a variety of inorganic and organic substrates (Schrank *et al.*, 2002). The maximum acceptable level in chromium polluted wastewater is 0.05 mg/L. With this limit it is necessary for industries to treat their waste to reduce the chromium to a satisfactory level. The preferred treatment is to reduce Cr(VI) to less harmful Cr(III), which can be sorbed in neutral or alkaline solutions as Cr(OH)₃ (Schrank *et al.*, 2002).

Arsenic exists naturally and it is extensively distributed in the earth's crust. It normally enters groundwater through natural weathering from arsenic-bearing minerals and sediments in groundwater aquifers. Additionally, many human activities such as coal combustion, mining, use of pesticides and fertilizers has generated great deposits of tailings with arsenic concentrations. Its long-term exposure can result in health hazards such as urinary bladder and skin cancer (Meng *et al.*, 2000). As a result, the World Health Organization (WHO, 2006) has decreased the standard level for arsenic in drinking water from 50 to 10 µg/L and most industrialized countries also consider 10 µg/L as a standard concentration limit. The maximum recommended levels for arsenic waste product, however; can be as much as 10-50 times less depending on the country's regulations (WHO, 2006). Inorganic arsenic exists in groundwater mainly in nonionic trivalent (As(III)) and ionic pentavalent (As(V)) forms in different proportions subject to environmental conditions. The species of arsenic in water is generally determined by redox conditions, pH, adsorption reactions and biological activity. As(III) is

more toxic than As(V) and problematic to remove from wastewater by most methods. In view of this, As(III) is typically removed by first oxidizing it to less toxic As(V) (Sharma and Shon, 2009).

Humic substances and heavy metals often exist simultaneously in the environment and they may affect arsenic removal either through interfering with the process treatment or competing with arsenic for active sites (Li *et al.*, 2012). It has been reported in the study conducted by Moura *et al.* (2007) that 3–28% of the dissolved organic matter in effluents from WWTP are humic substances. Humic substances classically denote a large portion of natural organic matter (NOM) dispensing in sediments, soils and waters. Fulvic acid (FA) and humic acid (HA) are two major components of humic substances, and they vary in molecular weight and functional group contents. Regardless of variances, their common functional groups such as phenol, carboxyl, hydroxyl, amine and quinine groups make it possible that HA and FA in water could lead to health hazard to the ecological and environment. HA/FA has strong complexation ability with heavy metals and thus increasing their transportation and distributions in waters (Morales *et al.*, 2012). Since As(V) can be removed more efficiently than As(III), and the presence of HA reduces arsenic removal efficiency, and therefore a treatment method for the simultaneous As(III) oxidation and HA removal is highly necessary in arsenic removal procedures.

2.4 Wastewater treatment methods

The most widely used methods of organic pollutants removal from dye and pesticides containing industrial effluents are physical, chemical and biological or combinations of these methods in wastewater treatment plants (Galindo *et al.*, 2001). Each of these treatment methods has short-comings (Table 2.1) and may then affect drinking water quality. Therefore there is a need to find alternative treatment method that is cost effective to completely degrade and mineralize recalcitrant organic pollutants to non-toxic compounds.

Adsorption has been widely applied to remove organic and heavy metal ions pollutants present in wastewaters which have been generated from industries such as textile, agricultural and mining industries. This treatment method may produce effluents that contain a suitable effluent limit of target dyes, pesticides and metals. However, due to state-of-the-art of adsorption technique, the development of new adsorbents has intensified lately. Currently, organic polymers chemically modified with functional groups such as amine, carboxylic and phosphate

have been utilized to assist remove organic and inorganic compound from contaminated wastewater (Crini, 2005). In spite of having a high amount of active sites for metal binding, their drawbacks include slow kinetics, irreversible adsorption of target compounds and loss of mechanical stability (Jal *et al.*, 2004).

Table 2.1. Advantages and disadvantages of the current methods of dye removal from industrial effluents (Robinson *et al.*, 2001).

	Advantages	Disadvantages
Physical/chemical methods		
Fenton's reagent	effective for decolorization of both soluble and insoluble dyes	It generates sludge
Ozonation	Applied in gaseous state: no alteration of volume	Short half-life (20 min)
Photochemical	No sludge	Formation of by-products
Electrochemical destruction	Breakdown compounds are non-hazardous	High cost of electricity
Electrokinetic coagulation	Economically feasible	High sludge production

Adsorption processes using activated carbon (AC) is broadly employed to treat pollutants from wastewater. Due to its adsorptive properties, the application of AC involves purification, detoxification, filtration and altering the concentration of various liquid and gaseous materials (Joana *et al.*, 2007). Activated carbon is very active for adsorbing cationic, mordant, and acid dyes to a slightly lesser extent, dispersed and reactive dyes (Raghavacharya, 1997). The removal rates can be modified by using higher doses, although regeneration or re-use may reduce the performance and efficiency of dye removal. The carbon also has to be re-energized or else discharge of the concentrates has to be considered. Reactivation can lead to 10±15% loss of the sorbent. The drawback of using adsorption processes is that the adsorbent needs to be regenerated, which contribute to the cost of the operation and sometimes is a very time-

consuming process. Nevertheless, these methods are non-destructive, since they just transfer the contaminant from water to solid matrix (Hoffman & Martin, 1995).

Fenton's reagent is an appropriate chemical means of treating polluted wastewaters which are not easily treated using biological treatment. The main detriment of this method is sludge generation through the flocculation of the reagent and the dye molecules. The sludge, which contains the concentrated impurities, still requires removal (Slokar and Le Marechal, 1997). More details on Fenton's reagent is discussed in section 2.3.2. Coagulation may be good for dispersive dyes, however it may not eradicate highly soluble dyes and it produces a large quantity of sludge. Oxidation by ozone is proficient of degrading phenols, pesticides, chlorinated hydrocarbons, and aromatic hydrocarbons (Xu and Lebrun, 1999). Ozonation alone is not effective for disperse dyes (Solozhenko *et al.*, 1995). The main benefit of ozone is that can be applied in its gaseous state and hence does not increase the quantity of sludge. The disadvantage of ozonation is its short half-life, normally being 20 minutes and is also not economically viable since continuous ozonation is essential due to its short half-life. This time duration can be further reduced if dyes are existing, with stability being influenced by the occurrence of salts and pH. In alkaline conditions, ozone decomposition is enhanced and therefore attentive monitoring of the discharge pH is essential (Slokar and Le Marechal, 1997).

2.5 Fundamentals and mechanism of TiO₂ photocatalysis

2.5.1 Heterogeneous TiO₂ photocatalysis

Several authors have reported the fundamentals of photophysics and photochemistry underlying the heterogeneous photocatalysis engaging the TiO₂ semiconductor (Gaya and Abdullah, 2008; Fujishima *et al.*, 2000). Titanium dioxide is an extensively investigated material as a photocatalyst for stimulating a series of reductive and oxidative reactions on its surface. From a mechanistic point of view, when photon energy ($h\nu$) supplied equal or greater than the bandgap energy, ΔE_g of the semiconductor, the excited electron in the valence band is shifted to the empty conduction band. This leads to the generation of a positive hole (h_{vb}^+) in the valence band and an electron (e_{cb}^-) in the conduction band. As a result, electron-hole pairs are produced in the photocatalytic reaction.



where e_{cb}^- and h_{cb}^+ are the electrons in the conduction and valence band, correspondingly. When the surface of the photocatalyst absorbs a specific amount of energy, an electron from the valence band moves to the conduction band, thereby leaving a positive “hole” in the valence band. The electrons in the valence band react easily with the surface bound H_2O to release $\bullet OH$ radicals, whereas, e_{cb}^- react with O_2 to yield superoxide radical anion of oxygen.



This reaction hinders the combination of the electron and the hole which are produced in the first step. The $\bullet OH$ and $O_2^{\bullet -}$ formed can react with the dye and pesticides molecules and thus accountable for the degradation of the organic pollutants. Bandgap excitation of TiO_2 causes charge separation followed by scavenging of electrons and holes by surface adsorbed species (Fig. 2.1). Basically, the oxidative and reductive reactions do not occur concurrently. Therefore, when an accretion of electron take place in the conduction band, the electron is then recombined with the positive hole in the absence of the photocatalyst. As the photocatalytic reaction continues in preference to the positive hole-electron recombining, efficient electron consumption is hence essential to promote the photocatalytic oxidation. The equation of the recombination of positive hole and electron is given (Eq. (2.6)):



Since the photocatalysis reaction follows on the photon activated surface of TiO_2 , the comprehending of the reaction stages that includes photodegradation of organics is desired in the formulation of kinetic expression. For heterogeneous photocatalysis and prolonged time, the organic pollutants are degraded to their corresponding intermediates and further mineralized to salts, carbon dioxide and water.



According to Pirkanniemi and Sillanpää (2002), the overall heterogeneous photocatalysis as represented by (Eq. (2.7)) involves five steps which are demonstrated in Fig. 2.2:

- a. Mass transfer of the organic contaminant(s) in the liquid phase to the TiO_2 surface.

- b. Adsorption of the organic contaminants onto the photon activated TiO_2 surface
- c. Photocatalysis reaction for the adsorbed phase on the TiO_2 surface.
- d. Desorption of the intermediates products from the TiO_2 surface.
- e. Mass transfer of the intermediates from the interface region to the bulk fluid. In terms of rate determination, the overall rate of reaction is equal to the slowest step.

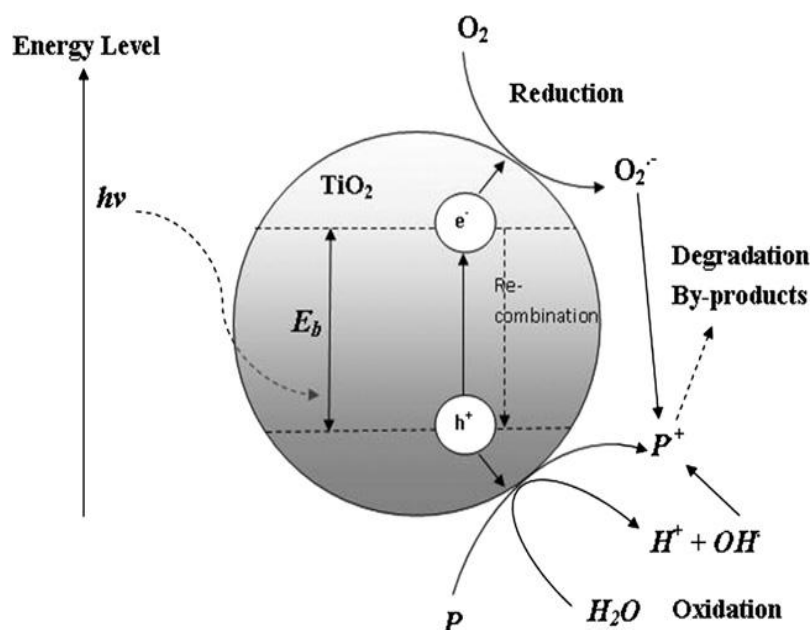


Figure 2.1. Schematic diagram showing the generation of oxidative species in a photocatalytic study (Chong *et al.*, 2010).

When the mass transfer stages (a and e) are compared with the reaction stages (b, c and d), the organic concentrations in the immediate of the active sites are vague from those in the bulk liquid phase. At this stage, the mass transfer steps are not rate limiting and do not influence the overall rate of photocatalytic reaction. The study completed by Vinodgopal and Kamat (1992) reported the reliance of the photodegradation rate of the organic surrogate on surface coverage of the photocatalysts employed. This outlines the significance of molecules adsorption or surface contact with the photocatalyst during the photocatalytic degradation process. If the mass transfer steps are rate restrictive, a modification in the aeration or liquid flow conditions past the TiO_2 photocatalyst may change the overall photocatalytic reaction rate.

2.5.2 Homogeneous photo-Fenton reaction

The Fenton reaction is a treatment method that does not involve any light irradiation as matched with the heterogeneous TiO₂ photocatalysis reaction, while the photo-Fenton react up to a light wavelength of 600 nm. Several studies on the photo-Fenton degradation on extended variety of organic contaminants such as chlorophenol (Pera-Titus *et al.*, 2004), pesticides (Fallmann *et al.*, 1999) and phenolic compounds have been performed (Gernjak *et al.*, 2007). The photo-Fenton reaction is more effective in the presence of light, thus causing prompt H₂O₂ decomposition by ferrous or ferric ions and resulting in the production of radicals. Such soluble iron hydroxyl does not only absorb UV radiation but also visible light. The Fenton and photo-Fenton reaction could occur concurrently with TiO₂ photocatalysis during UV-Vis irradiation period. The mechanism for the Fenton reaction is given in (Eq. (2.8)):



The Fe²⁺ can be returned back to Fe³⁺ through different mechanisms:

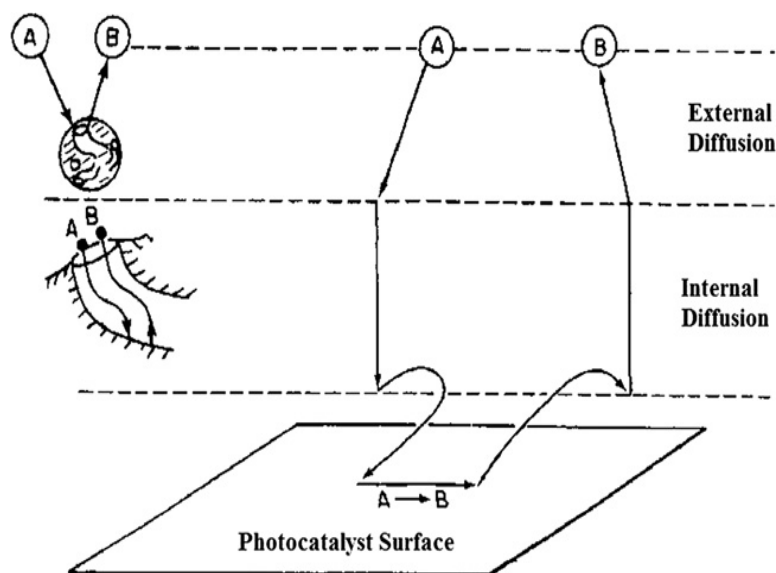
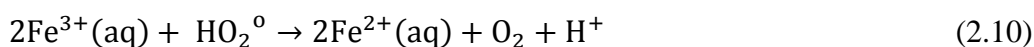
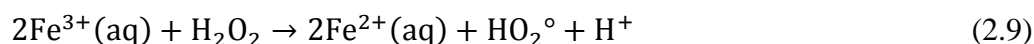


Figure 2.2. Steps in heterogeneous catalytic reaction (Fogler, 1999)

The rate of photo-Fenton was described to be positively improved during the presence of a light source when compared to the dark condition. This can be explained by the regeneration of Fe²⁺ (aq) from the photochemical effect of light and the coexisting generation of the OH⁻

radicals during the process. Such a reversion cycle of $\text{Fe}^{2+}(\text{aq}) / \text{Fe}^{3+}(\text{aq}) / \text{Fe}^{2+}(\text{aq})$ constantly produce OH^- , provided that the concentration of H_2O_2 in the system is considerable. Despite its higher photoactivity than the heterogeneous photocatalysis, photo-Fenton practicable operation is mainly reliant on numerous water quality constraints. De Laat *et al.* (2004) has reported that the generation of the highly photoactive iron complexes during photo-Fenton reaction is highly influenced by ions content and water pH. Pignatello (1992) reported that the pH 2.8 was the common optimum pH for photo-Fenton reaction. At such low pH, the precipitation does not occur and further encourages the presence of dominant iron species of $[\text{Fe}(\text{OH})]^{2+}$ in water. The existence of ions such as carbonate (CO_3^{2-}), phosphate (PO_4^{3-}), sulphate (SO_4^{2-}) and chlorine (Cl^-) have the potential to increase the water pH and efficiently slow down the photo-Fenton reaction rate. Both CO_3^{2-} and PO_4^{3-} have unfavorable effect on the reaction, as they precipitate the iron and as well as scavenges the OH^- radicals. Gernjak *et al.* (2007) has shown that a pH of 4.0-5.0 was found to be adequate to sustain the photo-Fenton reaction with 2-6 mM of iron for the commencement of the treatment.

2.6 Photoactivity and photocatalytic properties of TiO_2

Titanium dioxide is frequently an investigated photocatalyst due to its substantial range of practical features. It holds good physical and chemical stability and it is insoluble in water, hydrochloric and dilute sulfuric acid (Material Safety Data Sheet, 2012). Inertness to chemical environment and long-term photostability has made TiO_2 an important semiconductor material in different practical applications and in commercial products ranging from cosmetics to catalysts, paints to pharmaceuticals, and sunscreens to solar cells in which TiO_2 is used as a desiccant, or brightener (Kamat, 2012). In addition to this benefits, TiO_2 is also an inexpensive material. The most common polymorphs of TiO_2 are rutile and anatase. The band gaps of anatase and rutile are 3.2 eV and 3.0 eV, correspondingly. Till now, photocatalytic properties, mechanisms, and surface reactions of TiO_2 have been under extensive investigation (Hoffmann and Martin, 1995).

Photoactivity is applied during self-cleaning surfaces and in dye-sensitized solar cells, on the other hand photocatalytic activity is essential in processes and where the degradation of organic compound is required. Both TiO_2 forms, anatase and rutile have been reported to be photoactive and have photocatalytic properties, however; based on many studies, anatase is more effective than rutile. In studies by Kawahara *et al.* (2002), TiO_2 catalyst have presented that there is a

synergistic effect on the photocatalytic properties between anatase and rutile and that both forms are desirable to produce an effective photocatalyst. They were further reported that a photo-induced interfacial electron transfer from anatase to rutile accelerates TiO₂ photocatalytic activity. Furthermore, Liu and Liu (2008) reported that the photogenerated electrons in the rutile conduction band form superoxide radicals and the holes in the anatase valence band play a vital role in oxidation reactions. However, Agrios *et al.* (2003) reported an opposing study that the electron transfer takes place from rutile to anatase. Since rutile contains Ti³⁺ ions which are electron donors, it was proposed that the electron transfer occurs from rutile to anatase particles.

The obstacles associated with TiO₂ are recombination challenges and its application in a narrow solar range. As mentioned in section 2.4, the bandgap of rutile is $E_g = 3.0$ eV which agrees to a wavelength of 414 nm whereas of anatase is $E_g = 3.2$ eV, corresponding to 388 nm. Therefore, anatase to be activated, an extra energy is required and both polymorphs absorb UV light only; thus, it is only photoreactive within 4% of the solar energy limits. Since TiO₂ undergoes fast recombination of electrons and holes during the photoactivation, it declines its productivity in photoactivity and also as a photocatalytic material. Detailed investigation on understanding the photoactive materials' structure and electron/hole transport is critical to achieve high photocatalytic degradation efficiency. There have been countless efforts adopted to decrease the difficulty of recombination and also to extend the narrow solar absorption range to the visible region. The photocatalytic activity of TiO₂ may be adjusted by changing its physicochemical properties such as its crystal structure, particle size, and surface area (Yu *et al.*, 2007).

2.7 Developments in photocatalyst immobilization and supports

Ever since the finding of a photocatalytic effect on water splitting by Fujishima and Honda (1972) using TiO₂ semiconductor, many studies have prepared some methods for modifying TiO₂ catalyst, thus distinguishing its physical properties and determining its photocatalytic performances to the surface-oriented nature of photocatalysis reaction (Fujishima and Honda, 1972). The most common technique to modify the photocatalytic activity of TiO₂ can be achieved through doping with transitional metal ions and/or nonmetals and supporting the semiconductor onto activated carbon, silica, and zeolite (Chong *et al.*, 2010). The highest decomposition rate for propylamide (herbicide) was obtained with supports having medium adsorption strengths, such as silica (Torimoto *et al.*, 1996).

2.7.1 Photocatalytic membrane

Many investigations have employed microns size immobilizers to fix catalyst that improve surface contact with pollutants and inhibits the membrane fouling. A membrane itself could be used as immobilizer to fix the photocatalyst (Kwak and Kim, 2001). The practice of the membranes has been targeted due to the fact that the photocatalytic reaction can initiate on the membrane surface and the treated wastewater could be constantly discharged without losing photocatalyst particles. The membranes can be prepared using different materials and thus include from $\text{TiO}_2/\text{Al}_2\text{O}_3$ composite membranes (Choi *et al.*, 2007), TiO_2 supported on polymer and metallic membranes or doted polymer membranes having TiO_2 particles entrapped within the membrane structure during the membrane fabrication operation (Artale *et al.*, 2001). Photocatalytic membranes may experience many technical complications such as membrane structure corrosion, low photocatalytic activity and loss of deposited TiO_2 semiconductor layer over time. To overcome the difficulties associated with the TiO_2 membrane coating, an attempt of using membranes without any deposited TiO_2 layer can be configured into a slurry-membrane hybrid system.

2.7.2 Modification of photocatalyst by doping

Composite photocatalyst with dyed sensitizers, metals and non-metals doping onto semiconductor surface, predominantly TiO_2 is one of the attractive engineering alternatives that have been invented to enlarge the activity of TiO_2 photocatalyst (Chong *et al.*, 2010). The basis in making use of these material is to balance both the half-reaction rates of the photocatalytic reaction by adding electron acceptor and modifying the photocatalyst structure. Figure 2.3 represents the application of different mechanisms to improve the photoactivity of the catalysts. The occurrence of electron acceptors could scavenge the excited electrons and altogether avoid the recombination of electrons hole pairs. In the dye sensitized coupling, the excited dye molecules under illumination can provide more electrons to the conduction band for improving the formation of electron hole pairs (Fig. 2.3a). Since Fermi levels of noble metals such as Ag, Ni, Cu, Pt, Rh, and Pd are lower than that of TiO_2 photocatalyst, they could be deposited on the TiO_2 surface to improve the charge separation (Ni *et al.*, 2007). Photoexcited electrons can be shifted from the conduction band of TiO_2 to metal particles deposited on the surface TiO_2 , whereas photogenerated holes in the valence band persevere on TiO_2 . This reduces the possibility of electron-hole recombination, following in efficient

separation and enhanced photocatalytic activity. Many studies have found that the properties of these kinds of composites depend highly on the size of the metal particle, dispersion and composition. When the size of the metal particle is less than 2.0 nm, the composites show remarkable photocatalytic activity (Turner *et al.*, 2008). It has been reported by Sakthivel *et al.* (2004) that a high concentration of metal particles diminishes photon absorption by TiO₂ and allows the metal particles to become electron-hole recombination centers, resulting in poorer efficiency.

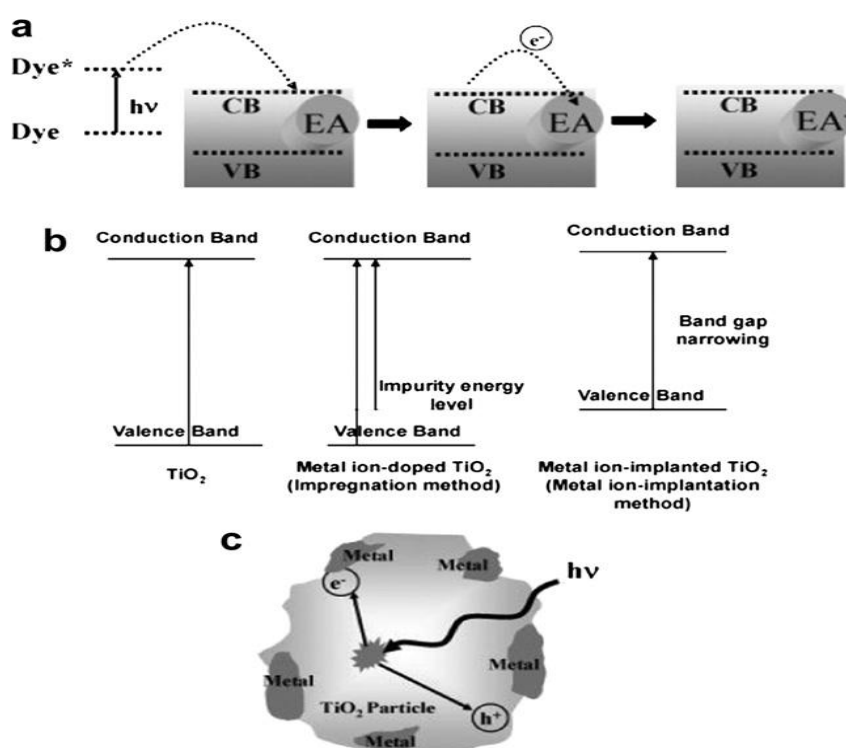


Figure 2.3. (a) Stages of excitation with a sensitizer in the presence of an adsorbed organic electron acceptor; (b) Arrangement of TiO₂ band structures, chemically ion-doped TiO₂ and physically ion-implanted TiO₂; (c) Electron capture by a metal in contact with a catalyst surface (Malato *et al.*, 2009).

Though noble metals were reported to be effective in increasing the surface charge separation, their operating cost-effectiveness for an industrial practice is usually substituted by more cost-effective transition or non-metals doping. However, the mechanism of such transition and nonmetals doping is not the same as the noble metals doping. For transition and nonmetals doping, the TiO₂ is incorporated into the TiO₂ crystal lattice (Asahi *et al.*, 2001). Such incorporation presents impurity in the bandgap of TiO₂ and thus, decreases the photonic energy

requirements (Fig. 2.3c). The use of non-metal dopants (N, C, F, S) is reported to improve the feasibility of TiO₂ catalysts for large scale application (Fujishima *et al.*, 2008). Further research attempts is required to provide a detailed information of the photoactivity kinetics, so as to expand the photooxidation efficiency for wastewater treatment.

2.7.3 Photocatalyst support material

As already mentioned in section 1.2, the use of TiO₂ in the form of a fine powder after wastewater treatment is troublesome and expensive. Therefore, researchers have found a different solution to these problems by using immobilized photocatalyst, to avoid the filtration problem. However, the competence of immobilized reactors may be hindered by lower mass transfer area and the availability of photocatalyst surface to the reactants and photons. In order to overcome this difficult, efficient material supports with adsorption capability that would bring the contaminants into close contact with the catalyst surface where the hydroxyl radicals predominantly exist would be used (Turchi and Ollis, 1990). Supporting materials such as glass beads, fiber, glass, silica, and zeolite have been used to modify the TiO₂ structure.

2.7.3.1 Activated carbon as supporting material

Activated carbon is a commonly used photocatalyst support material for the water and wastewater treatment for removing organic and inorganic contaminants. The application of activated carbon in treatment process is mainly reliant on the pore structure of porous carbons. These properties have attracted broad research as a potential support in the photocatalysis processes. As a photocatalyst support material, the activated carbon can accelerate the photodegradation efficiency by allowing an increasing amount of substrate to come in contact with the TiO₂ by means of adsorption (Shan *et al.*, 2010). The investigation done by Hermann *et al.* (1999) on the synergy effects specified that an improved adsorption of the pollutants onto the activated carbon followed closely by a transfer through an interphase to the TiO₂ phase, thus resulting in a complete photocatalytic degradation process. Further investigation done by Uchida *et al.* (1993) reported that though the oxidation rates of a specific compound were lower with the TiO₂ supported on activated carbon, complete mineralization rates were greater than the unsupported TiO₂. Although activated carbon has some benefits as a photocatalyst support in promoting the photocatalytic process, its application requires a reactor that efficiently exposes the photocatalyst surface to the photons of light. Furthermore it is also a costly

supporting material and the surface chemistry of a carbon may obstruct effective coating of TiO₂ on it (Khan, 2003).

2.7.3.2 *Fibers as supporting material*

Glass, carbon fibers and woven fiber cloths have been considered as material supports in groundwater denitrification and in photocatalytic degradation of wastewater contaminants. Most of these fibers show a longitudinal morphology or protruded rod-shape. When fibrous supports are used, loss of pressure and pore diffusion resistance are lower than with pellet shaped catalysts (Matatov-Meytal and Sheintuch, 1998). Another good advantage of fiber catalysts is its transparency of UV light in photocatalytic applications. Matatov-Meytal and Sheintuch (1998) studied Pd impregnated glass fiber catalysts in denitrification of groundwater and found that the material was stable in the pH range 4.5-8.5.

2.7.3.3 *Zeolite as supporting material*

Zeolites are naturally occurring aluminosilicate minerals, which can also be made at commercial level, which can be more optimized, purified and monolithically structured. Possibly clinoptilolite is the most abundant amongst the natural zeolite classes as well as readily available and inexpensive (Ming and Dixon, 1987). Taking into account their highly crystalline structure, zeolites contain silicon, aluminum and oxygen forming an internal framework with cavities and channels, where cations and/or small molecules may exist. Due to their unique porosity properties, zeolites afford a wide variety of applications from photocatalysis to the ion exchange and separation processes known as molecular sieves.

Ammonium ion is often formed during the biodegradation of pyridine and quinoline due to its transformation of N from pyridine and quinoline. Bai *et al.* (2010) applied a specific bio-zeolite composed of mixed bacteria for degrading pyridine-and quinoline. The modified zeolite was used for biodegradation and adsorption in two types of wastewater, sterile synthetic and coking wastewater. It was found that both pyridine and quinoline degraded all together by the mixed bacteria. In addition, zeolites can be good candidate as photocatalyst supports due to their unique uniform pores and straight channels. Since they provide large surface area, most of degradable molecules find it easier to diffuse to the channels and cages of the order of 4–14Å resulting in the enhanced degradation. Additional study by Ichiura *et al.* (2003) has confirmed that, due to the high adsorption capacity, the role of zeolite particles in the TiO₂-zeolite

composite is to escalate the number of the nitrogen oxide and that of the dye molecules near the active sites of the TiO_2 . The photocatalytic activity of TiO_2 -based zeolite composites is improved due to the zeolite acting as supporting material for the homogeneous dispersion of TiO_2 particles on its surface. Additionally, the zeolite plays a positive impact in the processes of charge and electrons transfer during the photocatalytic reaction, which subsequently decreases the recombination of the charge carriers (Dubey *et al.*, 2006).

2.7.3.4 Silica as supporting material

Silica materials such as silica gels and mixed oxides of silica titania have been used as photocatalyst supports to overcome the separation of the photocatalyst after the photocatalytic reaction in aqueous systems (Shan *et al.*, 2010). Since synthetic silica has a higher surface area than naturally occurring forms of silica, the synthetic silica provide the best adsorption and catalyst support structure for heterogeneous photocatalysis. Figure 2.4 shows the different types of surface silanol OH. The surface charge of a mineral surface is the result of the protonation-deprotonation of surface functional groups (mostly OH).

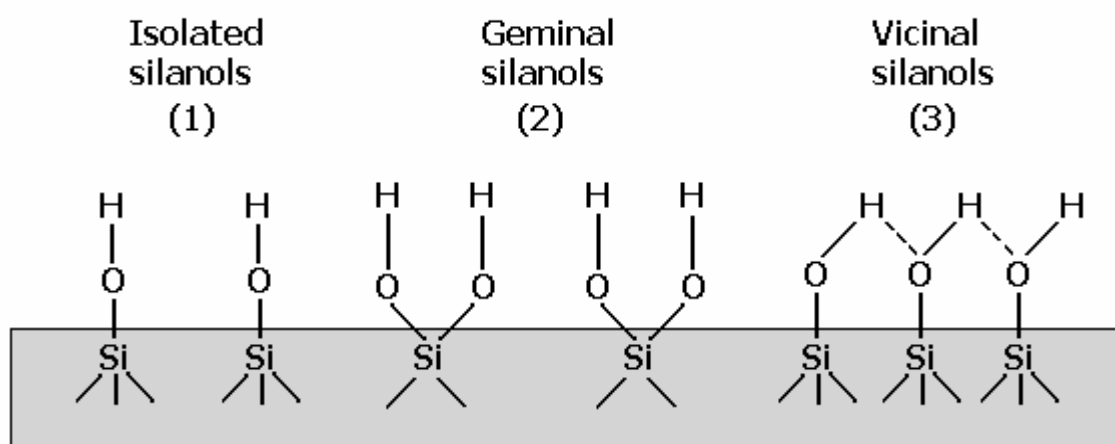


Figure 2.4. Surface silanol OH groups at the silica surface (Zhuravlev, 2000).

The SiOH surface groups are the principal species. The surface concentration of SiOH_2^+ is highest at pH 0, while the concentration of SiO^- increases with an increasing pH and maximum concentration of SiO^- is at pH 8 (Londeree, 2002). Moreover, Silica, on the other hand, have many advantages over activated carbon as a photocatalyst support. The transparency of silica progressively allows the penetration of photons to the photocatalyst surface. This is extremely beneficial and allows for a fixed-bed reactor design that can be highly efficient with respect to

input energy. In addition, silica has high mechanical strength, thermal stability, and can be synthetically formed into any shape, such as cylindrical pellets (Yamazaki *et al.*, 2001).

Silica-modified TiO₂ was reported to exhibit a better photocatalytic performance than TiO₂ itself. The TiO₂/SiO₂ photocatalysts permit the supporting of the catalyst on both external surfaces and internal surfaces within the porous silica matrix where contaminants are adsorbed. In the study carried out by Anderson and Bard (1997), a strong synergy between titania and silica as a composite oxide was found and it was further reported that the presence of the supporting material was considered to encourage the efficiency by increasing the concentration of the substrate near the TiO₂ sites relative to the solution concentration. However, for substrates that are not readily adsorbed to the surface of silica, the degradation rates were lower compared to a slurry of pure TiO₂.

2.8 Isotherms and kinetics modelling

Isotherm studies defines the amount of component adsorbed on the adsorbent surface versus the adsorbate amount in the fluid phase at equilibrium. One of the main stages in data experimental analysis is the fitting of adsorption isotherm equations. Langmuir and Freundlich models are still the most commonly used adsorption isotherms even though they were first introduced over 100 years ago (Freundlich, 1906). Though Langmuir isotherms have initially been derived for the gas phase adsorption, they were later modified for the liquid-solid systems application.

2.8.1 Langmuir isotherm

It has been reported that the expression for the rate of photocatalytic degradation of organic substrates such as dyes and pesticides with irradiated TiO₂ follows the Langmuir–Hinshelwood law for the four possible conditions (Konstantinou and Albanis, 2004);

- a) The reaction takes place between two adsorbed materials.
- b) The reaction initiates between a radical in solution and an adsorbed substrate molecule.
- c) The reaction initiates between a radical linked to the surface and a substrate molecule in solution.
- d) The reaction take place with the both of species being in solution.

The Langmuir isotherm follows the Henry's law at low concentrations and thus there is a linear relationship between the adsorption capacity and adsorbate concentration in the solution, but, at high concentrations the Langmuir isotherm approaches a constant capacity value in liquid-solid system, the nonlinear form of the Langmuir isotherm model is described by the following equation (Langmuir, 1918);

$$q_e = \frac{q_m K_L C_e}{1 + K_L C_e} \quad (2.11)$$

where, q_m (mg/L) and K_L (L/mg) are the Langmuir constants related to adsorption capacity and rate of adsorption, respectively, q_e is dye concentration at equilibrium onto adsorbent (mg/L), C_e is dye/pesticide concentration at equilibrium in solution (mg/L). A plot of $1/q_e$ vs. $1/C_e$ allows the empirical constants K_L and q_m to be evaluated from the intercept and slope of the linear regression. The linear expression of the Langmuir isotherm model is given by the following equation;

$$\frac{C_e}{q_e} = \frac{1}{q_m K_L} + \frac{C_e}{q_m} \quad (2.12)$$

The essential characteristic of the Langmuir isotherm can be described by a separation factor which is called the equilibrium constant, R_L : The equilibrium factor thus is defined as:

$$R_L = \frac{1}{1 + K_L} \times \frac{1}{C_o} \quad (2.13)$$

where K_L is the affinity constant (mg^{-1}), C_o is the initial concentration of the adsorbate (mg/L). The R_L value is to be favorable at ($0 < R_L < 1$); unfavorable ($R > 1$), linear ($R = 1$ and irreversible ($R_L = 0$)).

2.8.2 Freundlich isotherm

As the Langmuir isotherm, the Freundlich isotherm consist of two parameters and is the simplest isotherm that takes into account the equilibrium heterogeneity of the surface. The Freundlich isotherm simply refers to adsorption process in which the number of adsorption sites is large relative to the number of pollutant molecules. It was one of the earliest empirical isotherms applied for describing adsorption equilibrium, but was later interpreted as sorption on heterogeneous surfaces or surfaces supporting sites of different affinities. According to this

model, the adsorbed mass per mass of adsorbent can be expressed by a power law function of the solute concentration, C_e (Freundlich, 1906):

$$q_e = K_f C_e^{1/n_f} \quad (2.14)$$

where K_f is the Freundlich constant related to adsorption capacity, q_e (mg/g), n_f is measure of the surface heterogeneity, ranging between 0 and 1. For linearization of the data, the Freundlich equation is written in logarithmic form:

$$\log q_e = \log K_f + \left(\frac{1}{n_f}\right) \log C_e \quad (2.15)$$

2.8.3 Sips isotherm (Langmuir-Freundlich)

The Sips isotherm is a combination of the Langmuir and Freundlich isotherms and can be derived using either equilibrium or thermodynamic approach (Langmuir, 1918).

$$q_e = \frac{q_m (K_s C_e)^{n_s}}{1 + (K_s C_e)^{n_s}} \quad (2.16)$$

where K_s is the affinity constant and n_s defines the surface heterogeneity. When n equals unity, the Sips isotherm goes back to the Langmuir isotherm and predicts homogeneous adsorption. On the other hand, deviation of n_s value from the unity specifies heterogeneous surface. At low concentrations the Sips isotherm returns to Freundlich type equation and at high concentrations, seems to approach constant value (Langmuir, 1918).

2.8.4 Isotherm shape

There are four different isotherm shapes that are commonly observed (Giles *et al.*, 1974). The C-shape isotherm is when a line is passing through the origin. It describes a system where the ratio between the concentration of the compound in solution and adsorbed on the solid is equal at entire concentration range. Such type of isotherm can only be achieved for low concentrations in practice. The L-type isotherm suggests a progressive saturation of the solid with or without of a plateau. Most of the isotherm equations are of this nature. The H-type isotherm is an exceptional case of the L-type isotherm with an extreme high initial slope demonstrating strong adsorbate–adsorbent connections (Covelo *et al.*, 2007). Lastly, the S-type isotherm, even though quite rarely observed, at low adsorbate concentrations, it indicates a low

adsorption affinity and improved adsorption after the point of inflection at which some adsorption has already taken place.

2.9 Kinetics modelling

Kinetics and mechanistic studies on heterogeneous catalysis of the water and wastewater contaminants are valuable for scale-up operation. The appropriate application of kinetic models for the interpretation of experimental data allows the design and optimization of photoreactor system with sufficient capacity and minimal non-illuminated reactor volume as well as quality control in photocatalyst selection (Chong *et al.*, 2010). Similarly, as in the case of isotherms studies (Langmuir and Freundlich), in most cases kinetics has been fitted by the two simplest models: pseudo-first- and pseudo-second-order equations (Azizian and Bashiri, 2008).

2.9.1 Pseudo-first-order model

The model was called the pseudo first order model due to the fact that it was allied with the kinetics of one-site adsorption governed by the rate of the surface reaction. The nonlinear equation is given as:

$$q_t = q_e(1 - \exp(-k_1 t)) \quad (2.17)$$

For linearization of the data, the pseudo first order model is written as:

$$\ln(q_e - q_t) = \ln q_e - k_1 t \quad (2.18)$$

where q_t and q_e are the adsorption capacity (mmol/g) at time t and at equilibrium respectively, while k_1 represents the pseudo first order rate constant (min^{-1}). Earlier the pseudo first order model was derived for special cases such as ion-exchange by natural zeolites (Boyd *et al.*, 1947) and biosorption by aerobic granular sludge.

2.9.2 Pseudo-second-order model

The pseudo-first-order model was generalized to two-site-occupancy adsorption to form a pseudo second order equation:

$$q_t = \frac{q_e^2 k_2 t}{1 + q_e k_2 t} \quad (2.19)$$

where k_2 is the pseudo second order rate constant (g/mmol min) and the linear form pseudo second order is given as follows:

$$\frac{t}{q_t} = \frac{1}{k_2 q_e^2} + \frac{t}{q_e} \quad (2.20)$$

Azizian (2004) derived the pseudo-second-order model using classical theory of adsorption/desorption by presumptuous of a low initial concentration of adsorbate. Based on this derivation, k_2 was a complex function of the initial concentration of adsorbate, its equilibrium surface capacity as well as the rates of the adsorption and desorption. Later on Azizian's assumptions were argued by Liu and Liu (2008), who recognized that his derivation was relevant in the initial stage of the adsorption (small value of t) and certainly did not require the assumption of a low initial concentration. It has been identified that this model is able to estimate experimental q_e values reasonably well and is not very sensitive to the influence of the random errors (Plazinski *et al.*, 2009).

2.10 Goodness of fit

Goodness of fit is a fundamentally key parameter that approximate how well the predicted curve correlates with the experimental data. Usually least squares method is used to measure the degree of the goodness of fit. It is based on the concept that the scale of the variance between the experimental data points and the prediction curve is a good measure of how well the curve fits the data. Previously, nonlinear data would be transformed into a linear form and accordingly analyzed the data by the least squares fit method. However, linearization analysis was reported to yield inherent bias (Han *et al.*, 2007). The error functions are calculated and used to measure the goodness of fit and their standard equations are described in Table two, (Allen *et al.*, 2003). The best fit of the data is influenced by the error deviation and the smaller the error function value for the better the data fits the model. The coefficient of determination, R^2 , is practical as it gives the proportion of the variance of one variable that is predictable from the other variable. The coefficient of determination is such that $0 < R^2 < 1$, and indicates the strength of the linear association between experimental data. As already mentioned in this chapter, conventional water treatment methods are not efficient to reduce the toxicity of the organic and inorganic pollutants. They involve high operating costs and could generate toxic byproducts into the ecosystem. As a results, heterogeneous photocatalysis among AOPs employing TiO_2 semiconductor photocatalysts has revealed its efficiency in degrading a wide range of recalcitrant contaminants. Though TiO_2 alone has been used by many researchers as photocatalyst under UV radiations and solar light due to its photocatalytic activity to degrade

different pollutants. It was also reported an additional practice step would need to be entailed for post-separation of the photocatalyst. This separation practice is important to avoid the loss of catalyst particles and thus means that an addition cost would be required. Hence in this work, low cost material such as zeolite and silica were used to overcome this problem of the photocatalyst recovery.

Table 2.2. The list of error functions (Repo, 2011)

Error Functions	Equation
The coefficient of determination, correlation coefficient (R^2)	$R^2 = 1 - \frac{\sum_{n=1}^n (q_{e,exp} - q_{e,calc})^2}{\sum_{n=1}^n (q_{e,exp} - \bar{q}_{e,calc})^2}$
Marquardt's percent standard deviation (MPSD)	$MPSD = \sum_{n=1}^n \frac{(q_{e,exp} - q_{e,calc})^2}{(q_{e,exp})^2}$
The sum of the square of the errors (ERRSQ)	$ERRSQ = \sum_{n=1}^n (q_{e,exp} - q_{e,calc})^2$
The average relative error (ARE)	$ARE = \sum_{n=1}^n \left \frac{q_{e,exp} - q_{e,calc}}{q_{e,exp}} \right $
The sum of absolute errors (EABS)	$EABS = \sum_{n=1}^n q_{e,exp} - q_{e,calc} $
Mean error (ME)	$ME = \frac{100}{n} \sum_{n=1}^n \left \frac{q_{e,exp} - q_{e,calc}}{q_{e,exp}} \right $
Residual root mean square error (RMSE)	$RMSE = \sqrt{\frac{1}{n-1} \sum_{n=1}^n (q_{e,exp} - q_{e,calc})^2}$
Non-linear reduced chi-square (χ^2)	$\chi^2 = \frac{1}{n-p} \sum_{n=1}^n \left(\frac{q_{e,exp} - q_{e,calc}}{q_{e,calc}} \right)^2$

n = number of data observation, exp = experimental/measured, calc =calculated/estimated

CHAPTER 3

3. MATERIALS AND METHODS

Different materials and methods were used to synthesize the TiO₂ photocatalyst supported on adsorbent. The prepared composite photocatalyst were characterized using the different characterization techniques. The ultraviolet (UVC)-induced photocatalytic degradation of aqueous solutions containing the azo dye methyl orange, pesticide and metal ions alone as well as their mixtures on photocatalyst composite was investigated in a batch reactor. Analytical equipment such as Brunauer–Emmett–Teller (BET), Scanning Electron Microscopy and Energy Dispersive X-ray (SEM-EDX) Raman spectroscopy (RS) and zeta potential (ZP) were employed to characterize the prepared composite photocatalysts. Different isotherms and kinetic modelling were performed to find out which model described the data well. Gas chromatograph mass spectroscopy (GCMS) was used to determine the intermediate products and Fourier transform infrared (FTIR) was used to identify the surface groups on methyl orange and atrazine after photocatalysis treatment.

3.1 Materials

All chemical (analytical grade) used, were purchased from Sigma Aldrich company, Finland and used without further purification. Methyl orange, an azo dye (99%, purity), potassium dichromate (99.8% K₂Cr₂O₇) as the source of Cr(VI), Atrazine (97.4% purity), HA (98% purity) and arsenic trioxide as the source of As(III) were selected as model compounds co-existing in various industrial and municipal wastes. Titanium dioxide containing mainly anatase, with 30% rutile was used as photocatalyst with Ludox Hs-30 colloidal silica and zeolite (Turkey), as the supporting material. Diphenylcarbazide, sulphuric acid and absolute ethanol (Altia) were used to prepare the chromogenic agent for the determination of Cr(VI). Sodium chloride (>99.5% purity) and sodium sulphate (>99% purity) were used as inorganic salts during photocatalytic experiments. Commercial TiO₂ with an average particle size of 12 nm was used as reference.

3.2 Synthesis of TiO₂/zeolite and TiO₂/silica composite photocatalysts

The TiO₂ photocatalyst coated onto zeolite particles was prepared using the solid state dispersion (SSD) method modified by Nikazar *et al.* (2007). Zeolite (particle sizes 0.2-0.5, 0.5- 1.0 and 1.0-1.2 mm) was at first rinsed with Mill-Q water to remove any impurities and dried. In this method, absolute ethanol as a solvent was added into the mixture of TiO₂ and zeolite which was prepared using an agate pestle and mortar. The solution was stirred until the solvent was removed by evaporation. Subsequently, the sample was dried at 110°C and then calcined at 450°C for 5 h to produce TiO₂ supported zeolite catalyst. The TiO₂ supported-silica samples were prepared by adding Ludox Hs-30 colloidal silica solution to plain TiO₂ with proper mixing to ensure a homogeneous TiO₂ coating onto silica. After mixing, the mixture was dried at 110°C and screened to different particle sizes (particle sizes 0-38, 75-150 and 150-250 µm). The TiO₂/silica coated particles were then dispersed in Mill Q-plus water, till the pH of the suspension was close to 6.5. By this procedure, a sample of 3-20 wt.% of TiO₂ onto different silica and zeolite particles was prepared.

3.3 Characterization of composite photocatalysts

3.3.1 BET surface area

The BET surface area of the photocatalyst was determined by the physical adsorption of mono layer of nitrogen gas at 77K using a Micromeritics 2000 instrument. The photocatalyst was dried in oven at 200°C for 30 minutes prior to BET analysis.

3.3.2 SEM instrumentation

Surface morphology of the the successive composite photocatalyst was characterised by Hitachi S-4800 Ultra-High Resolution Field Emission SEM. Acceleration voltage 30.0 kV, emission current 20.0 µA, high current lens mode, signal type SE (upper detector), tilt angle 0 degree, working distance approximately 8 mm. Energy dispersive analysis of X-rays (EDAX) model S4800 (I) and detector type 7747/17-ME, Sapphire Si (Li). Active area, 10 mm² was used for EDX analysis. The examinations were carried out at 30 kV acceleration voltage, emission current 20.0 uA, tilt angle 0 degree, amplification time 102.4 µs, dead time 20-40%, spectrum acquisition time varies for each sample.

3.3.3 Raman Instrumentation

Raman spectra were obtained using a 632.818 nm red wave laser with an energy of 225 mW. The backscattered light was collected by a fiber optic probe (In Photonics) coupled to the entrance slit of 500-mm monochromator (Acton Research SpectraPro SP-500) using a 1200 groove/mm grating blazed at 1 μm . The slit width was set to 100 μm , and the band pass varied between 2.142 cm^{-1} (at 400 cm^{-1}) and 1.503 cm^{-1} (at 3300 cm^{-1}). The Raman spectra were collected in 10 min exposures to a liquid nitrogen cooled CCD camera (Roper Scientific LN400EB, 1340 x 400 pixel array, back-illuminated and deep depletion).

3.3.4 Zeta potential

Zeta sizer Nano Series model ZEN 3600 (Malvern, the UK) was employed to measure the isoelectric points before the degradation tests. The zeta potential measurements were performed in Milli Q water. The zeta potential measurements were performed using 0.1 M NaOH and 0.01 HCl as pH titrants (pH range 9 to 2 with a pH increment of 1).

3.4 Photocatalysis experiments

A 100 ml semi-batch reactor (Fig. 3.1) made of glass with dimensions of 9 cm in diameter and 15 cm in height was used for the photocatalytic experiments of methyl orange, atrazine and reduction of metal ions experiments. Aqueous solution volume of 80 ml containing either the dye alone, pesticides alone, metal alone or their mixture was used throughout. Milli Q-plus water (resistance = 18.2 M. Ω) was used for all experimental work and they were performed at room temperature ($25 \pm 3^\circ\text{C}$). The UVC lamp (low-pressure mercury lamp, wave length, 254 nm (Pen-Ray), with an intensity of 5.5 mW/m^2), protected by a quartz sleeve was used. For all experiments, the solution was left to equilibrate for 30 min in the dark before the lamp was switched on. This was sufficient to reach an equilibrated adsorption as deduced from the steady-state concentrations. Sample of 5 ml was taken at desired time interval and immediately filtered through a polypropylene syringe filter (0.45 μm). To determine the photodegradation efficiency at various pH, the pH of the dye/pesticides solutions was adjusted with 0.1 M HCl or 0.1 M NaOH aqueous solution.

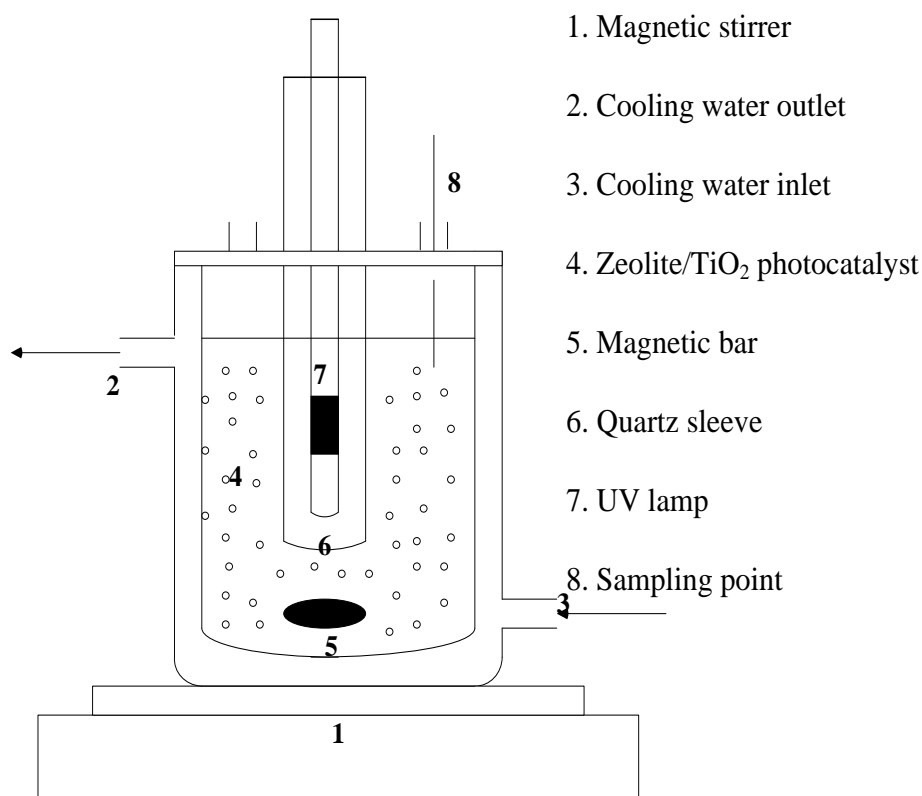


Figure 3.1. Experimental setup

3.5 Kinetics and Equilibrium modelling

Modeling of kinetics and isotherms on photocatalysis studies was conducted at varied concentration and pH. To illustrate the photocatalysis process and provide insights into possible reaction mechanisms, a pseudo-first-order and -second order kinetic model was used to fit the experimental data. Both linear and non-linear regression were applied using Solver function in MS Excel spreadsheet. Modeling of experimental isotherm data is important for predicting and comparing photocatalysis performance of the composite photocatalyst. Langmuir and Freundlich isotherm models were used to determine the proper isotherm for dye and atrazine photocatalytic degradation on TiO₂/zeolite and TiO₂/silica composite photocatalyst. The equations of the Langmuir and Freundlich models are expressed in section 2.7. A non-linear form of the isotherm and kinetics models need an error analyses and optimization techniques. Therefore the method was based on the minimizing of ERRSQ error function. Degree of fitness of predictions is also calculated so that the accuracy of fit could be measured. A function, named SOLVER in Microsoft Excel was used to fit non-linear functions.

The isotherm studies were carried out using single system containing either methyl orange alone or atrazine alone. The tests were performed in a semi-batch reactor at 25°C for 3.5 h, 6.25 g/L and 1.25 g/L of TiO₂/zeolite and TiO₂/silica composite photocatalysts, respectively; were added into 80 ml of target compound solutions. The initial concentration of methyl orange and atrazine were in the range of 5–50 mg/L and 5–25 mg/L, respectively. All the experiments were performed at pH = 6.5. The amount of the target compound adsorbed q_e (mg/g) was calculated according to the following equation:

$$q_e = \frac{(C_o - C_e)M}{V}$$

where V is the volume of target compounds solution (L), M is the mass of composite photocatalysts (g), C_o is the initial concentration (mg/L), and C_e is the equilibrium concentration (mg/L). Kinetic studies of methyl orange and atrazine in aqueous solution were performed by analyzing the compounds uptake with the initial concentration of about 25 mg/L (methyl orange) and 10 mg/L (atrazine) at different time intervals until the equilibrium was reached. The samples were taken at predetermined time intervals (from 30 min to 3.5 h).

3.6 Sample preparation

All glassware used was cleaned with an ammonium peroxydisulfate in sulphuric acid solution (0.08 M) to eliminate trace organics and rinsed with Milli Q-plus water (resistance = 18.2 M.Ω) six times. A 1000 ppm stock solution of dye, pesticides and metal ions were prepared using Milli Q-plus water (resistance = 18.2 M.Ω) and then an appropriate volume of stock solution was taken and diluted. The 1000 ppm As(III) stock solution was prepared by dissolving 0.1320 g of arsenic trioxide in 1 ml of 25% NaOH, immediately acidified with 2 ml concentrated HCl and diluted to 100 ml with deionized water. Sample solutions ranging from 1 to 10 mg/L were prepared from the stock solutions. Humic acid (HA) solution was prepared by dissolving 5 g of HA in 10 mL of a 0.025 M NaOH solution and after it was covered with foil and put in darkness overnight at 5°C an initial 100 mg/L HA solution was obtained. Then, dilutions were made in order to obtain 10, 15, and 20 mg/L HA solutions.

3.6.1 Sample preparation for chromogenic agent

Colorimetric technique (EPA Method) was used with a diphenylcarbazide solution for determination of Cr(VI) concentrations before and after the degradative treatment. To prepare the chromogenic agent for the Cr(VI) determination, diphenylcarbazide (0.1 g) was dissolved into 50 mL of absolute ethanol and then 200 mL of 10% (v/v) H₂SO₄ aqueous solution was added slowly into the diphenylcarbazide solution. The chromogenic agent was stored in the dark at 5°C prior to its use. The 10 ml filtered samples for Cr(VI) analysis after irradiation was diluted (1:10) with Milli Q-plus water up to 100 mL. Immediately afterwards, 95 mL of this dilution was taken, 2 mL of diphenylcarbazide solution was added, and the pH was adjusted to 2 with a 10% aqueous solution of H₂SO₄ in order to produce the colour development. Finally, the absorption spectra were recorded and the absorbance values at 540 nm were taken.

3.6.2 Sample preparation for FTIR and GC-MS analyses

Prior to GC/MS and FTIR analysis, a sample produced after degradative process was extracted using solid-phase extraction (SPE) columns (Chromabond C₁₈ ec (octadecyl—modified silica, end capped), Macherey-Nagel (Vilhunen and Sillanpää, 2009). Columns were first conditioned with 9 ml of methanol and 6 ml of 0.01M hydrochloric acid. The sample was treated with 0.2g of NaCl which was added for every 1 ml of sample and the pH was adjusted to 2 using HCl. The sample was transferred to SPE column and approximately 0.5 ml/min, aspirated through the column. Consequently the sample was cleaned twice with 500 µl of 0.01M HCl and dried under vacuum for 20 min. Elution was performed with 3×500 µl of methanol. This method was based on Macherey-Nagel Application-No. 301860. Vacuum chamber for extraction was from J. T. Baker (BAKER spe-12G). Before proceeding with the FTIR analysis, the potassium bromide (KBr) pellets were prepared by drying the KBr at 200°C overnight and then 200 mg was grounded to fine powder and placed on the die. The die containing the powder was placed on the press and the pump was turned on for 5 minutes. Finally, a uniform disk was formed at 60 MPa. The resulted disc was put in desiccator prior to its use.

3.7 Analysis of solutions

Before analysis, irradiated samples taken at desired time interval were filtered through a polypropylene syringe filter (0.45 μm) to remove TiO_2 agglomerates in suspension and to protect the various chromatographic columns. For the convenience of detection for the transformation products originated from the photocatalytic process, an extracted dye solution of 25 mg/L and 100 mgL^{-1} was applied. A UV/VIS spectrophotometer (Perkin-Elmer Lambda-45 spectrophotometer) recording the spectra over the 200–800 nm range was used for the determination of methyl orange concentration to follow its kinetics of disappearance. A Beer–Lambert diagram was established to correlate the absorbance at 466 nm to methyl orange concentration. Atrazine concentrations after degradation were determined by High Performance Liquid Chromatography (HPLC) (Agilent 1200, USA) equipped with reversed-phase C_{18} column (5 μm , 4.6 \times 200 mm) and a UV–vis photodiode array detector. The mobile phase was methanol/water (70/30, volume ratio) and the flow rate was 0.8 mL/min.

The Cr(VI) ion concentration was analysed by UV-VIS using diphenylcarbazide colorimetric method at 540 nm (GB 7466-87, Standards of China). The inductively coupled plasma optical emission spectrometry (ICP-OES), model iCAP 6300 (Thermo Electron Corporation, USA) was used to analyze As(III) concentration at wavelength of 189.042 nm before and after the process. The minimum detectable concentration of arsenic ions by ICP is 12.7 $\mu\text{g/L}$, respectively. Calibration was done using ICP standards and nitric acid at different metal concentration. Pure nitric acid was used as the reference. The relative standard deviation (RSD) of three replicate analyses was normally lower than 3%. All dishes used for this analysis were washed in accordance with the requirements for ICP analysis. Glasswares were washed as follows:

- a. Dishes were rinsed with distilled water (3 times)
- b. Soaked in 65% Suprapur HNO_3 for 5 hours
- c. And lastly they were rinsed with Mill Q water (6 times)

The solid-phase extraction permits concentration of the analytes and therefore it can be used to follow the transformation of products under current environmental concentration (at $\mu\text{g/l}$ level) (Konstantinou and Albanis, 2003). FTIR spectroscopy was used for the qualitative identification of the chemical groups present in the samples. Infrared spectra was measured

using an FTIR type Nicolet Nexus 8700 (USA) coupled to a PC with Omnic analysis software. The samples were examined within the range 350–4000 cm^{-1} using a Bruker Vertex 70 spectrophotometer equipped with a Spec Gol en Gate ATR (attenuated total reflection) device and the spectra were averaged over 64 scans. The KBr pellet technique was used for the dye and pesticides analysis. FT-IR spectral data were converted into ASCII files and the resulting data were imported into the Origin Pro software (version 8.0, Microcal, USA) for peak area integration. Chromatographic measurements were performed with a capillary column DB-5 MS (30.0m x 0.25mm x 0.25 μm). The gas chromatograph is interfaced to a mass selective detector. A split–splitless injector was used in splitless mode, with a split flow of 10 ml/min and a split time of 0.75 min. The injector temperature was 300°C and the injection volume was 1.0 ml. Carrier gas was helium with the flow of 1.2 ml/min. The column temperature program was as follow: 35°C (hold time: 2 min) \rightarrow 20°C/min to 260°C \rightarrow 15°C/min to 300 °C (hold time: 1 min).

The TOC concentration before and after the degradative process was analyzed by direct injection of the filtered samples to monitor the mineralization of organic chemical species using TOC-V_{CPH} Shimadzu Analyser. Prior to this analysis, vials were washed (24 h) with ammonium persulfate solution in order to minimize the concentration of inorganic or organic carbon in sample. This instrument is equipped with an ASI automatic sample injector and calibrated with standard solutions of potassium hydrogen-phthalate. The formation of anions during dye and pesticides degradation was followed using ion chromatography (Shimadzu LC-20) equipped with a conductivity detector (model: CDD-10A VP). Column: IC SE-50 4E (4.0 x 250 mm) was used for this analysis and its temperature was at 25°C. The injection volume was 10 μL . The mobile phase was 3.2 mM Na_2CO_3 and 1mM NaHCO_3 at a flow rate 0.7 mL/min. Calibration curves were obtained by using the pure standards of the related ions.

CHAPTER 4

4. RESULTS AND DISCUSSION

Material characterization was done using SEM-EDX, RS and ZP analysis techniques and the results showed that TiO₂ is supported onto zeolite and silica surface material. Control experiments conducted in the presence of composite photocatalyst without the UV light (dark reaction), showed a small decrease in the concentration of methyl orange. The degradation efficiency of TiO₂ supported on to zeolite and silica for the studied pollutants was found to be better than TiO₂ alone. Different operating parameters such particle size, composite photocatalyst concentration, initial pollutant concentration and pH on photodegradation were optimized and their findings were used in further experiments to identify intermediate products after photocatalysis process. The presence of inorganic ions and humic substances acting as photo generated holes scavengers hindered the dye and pesticide degradation, respectively. The photoreduction of metal ions was much faster in the mixed system than in the single one.

4.1 Material Characterization

Internal surface area plays a significant role in adsorption and catalysis process. This study reveals that TiO₂ loading into zeolite does not significantly alter the surface area. Meanwhile from SEM images, the zeolite presents porous flower-like surface whereas silica has a close packed cubic arrangement. The EDX and Raman spectras shows the presence of TiO₂ on zeolite and silica surface. The isoelectric point of the TiO₂/silica composite photocatalyst is found at pH 2.

4.1.1 BET Surface Area

Table 4.1 shows the BET surface area of different composition of the photocatalyst (wt. % TiO₂ in the mixture of TiO₂/zeolite composite, clinoptilolite. According to IUPAC classification, TiO₂/zeolite (clinoptilolite) are Type I isotherms and characteristic of microporous solids having relatively small external surfaces (Sing *et al.*, 1985). The surface area slightly increased with an increase in proportion of TiO₂ in the composite and decreased with a further increase of TiO₂. This could be due to deposition of TiO₂ particles on the zeolite surface and blocking of the pores. Since the pore sizes of clinoptilolite are between 0.4-0.7 nm (Nikazar *et al.*, 2007), there was no possibility of TiO₂ nanoparticles entering the zeolite pores

in the SSD method of preparation. Therefore, the TiO₂ nanoparticles were loaded onto the surface of zeolite not inside the internal pores of the zeolite. Gomez *et al.* (2013) and Nikazar *et al.* (2007) observed similar trends, and 10 wt.% TiO₂ was found to be the optimum loading on zeolite. Gomez *et al.* (2013) reported a surface area of 375 m²/g for 10 wt.%/TiO₂/zeolite. The difference between the observed values in the present study and that reported by Gomez *et al.* (2013) is attributed to the different methods used to prepare the composite photocatalyst and also the treatment method of the prepared composite photocatalyst prior to BET analysis. In addition, this could also be a result of synthetic zeolite used. In this study a hydrothermal crystallization method was applied. Similar BET results are provided in appendix (Table A1).

Table 4.1. Surface area of TiO₂ supported onto zeolite

Catalyst	BET surface area (m ² /g)
TiO ₂ on composite, wt.%	
0	20.08
3	21.31
10	22.93
15	20.44
20	19.92

4.1.2 SEM- EDX analysis

The morphology of the zeolite support alone and the prepared TiO₂/zeolite with different particle sizes was characterized by SEM technique coupled with EDS analysis. Figure 4.1a shows that the zeolite alone has porous flower-like surface which in turn could enhance the adsorption of organic compounds. The EDX spectra of zeolite alone (Fig. 4.1b) shows that the composition of the major building block of zeolite framework which is the tetrahedron, the centre occupied by a Si and Al atom. The surface morphology of the TiO₂/zeolite at zeolite particle size 0.2-05 mm (Fig. 4.1c) shows the porous flower characteristic of zeolite and TiO₂ spherical nanoparticles. This was observed for all TiO₂/zeolite morphologies. The EDX spectra of zeolite alone shows the tetrahedron occupied by a Si and Al atom reduced after supporting TiO₂ onto 0.2-0.5 mm zeolite surface (Fig. 4.1d). Similar trend is observed for the composition of other elements such as O, Mg, K, Ca and Fe. The low Ti composition shown in Fig. 4.1b increased significantly after supporting TiO₂ on zeolite material particle sized 0.2-0.5 mm

(Fig. 4.1d). This clearly shows that crystallites of TiO_2 is distributed on the surface of the zeolite supporting material.

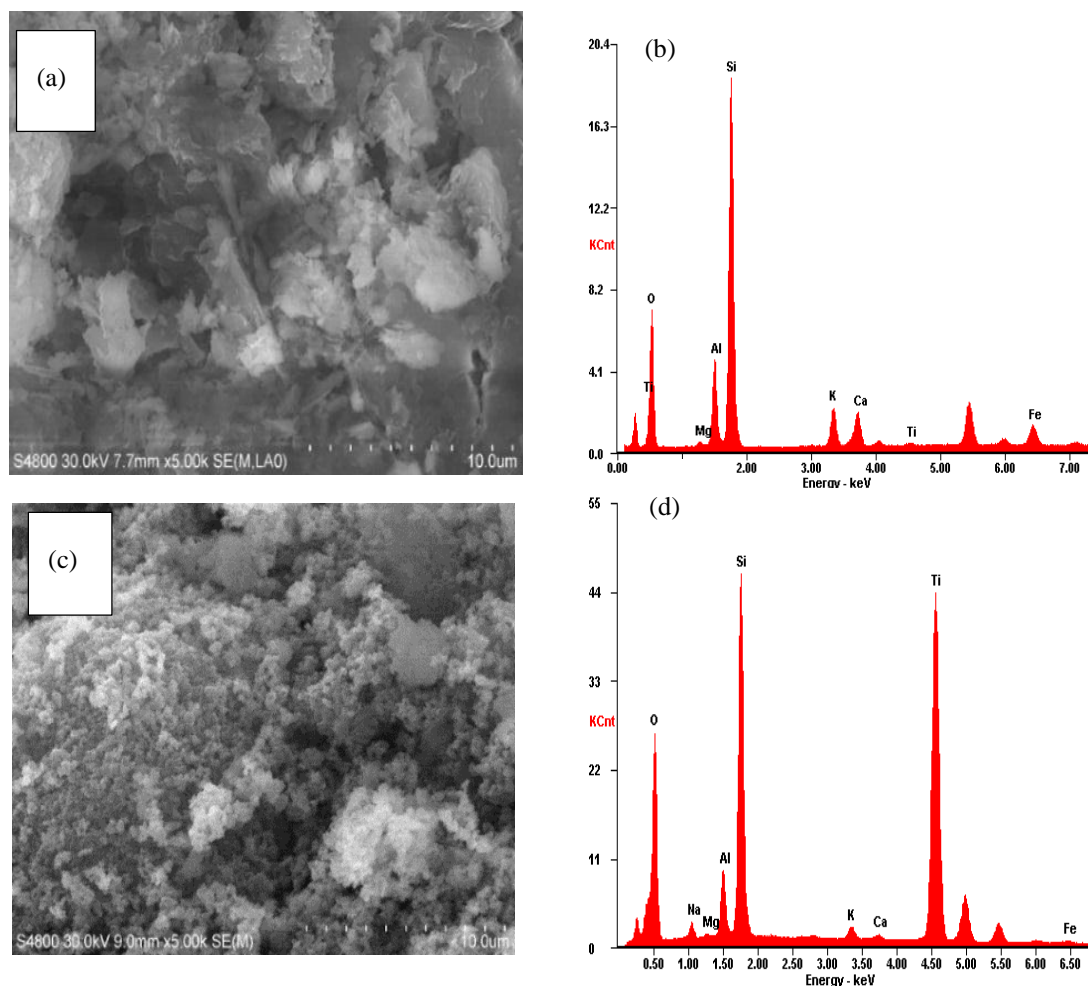


Figure 4.1. SEM images and EDX spectra of zeolite: (a and b) zeolite alone (c and d) 10% TiO_2 supported on 0.2-0.5 mm zeolite

When TiO_2 is supported onto 0.5-1.0 mm zeolite particle size, the composition of Si and Al atom decreased significantly (Fig. 4.2a) and this is noticed in all particle sizes. Ti appeared as the major constituent in all modified zeolite surface with different particle sizes, however, the Ti showed to be well distributed on 0.5-1 mm zeolite particle size (Figs. 4.2a and b) than onto 0.2-0.5 mm and 1.0-1.2 mm (Figs. 4.2c and d) zeolite particle sizes. Zeolite particle size of 0.2-0.5 mm (Fig. 4.1) and 1.0-1.22 mm indicate that some of the TiO_2 might have fallen or detached from zeolite surface during the synthesis process. The 0.2-0.5 mm seems to be small size particle for TiO_2 to be attached on its surface whilst 1-1.2 mm shows to be bigger size, hence TiO_2 is attached better on 0.5-1 mm zeolite particle. This is indicated by the low TiO_2

composition detected in 0.2-0.5 mm and 1-1.2 mm zeolite particle size as shown by EDX spectras (Fig. 2.1). The SEM images of the TiO₂/zeolite indicate that the TiO₂ particles were not aggregated in nucleus-like but rather present in agglutinated shape.

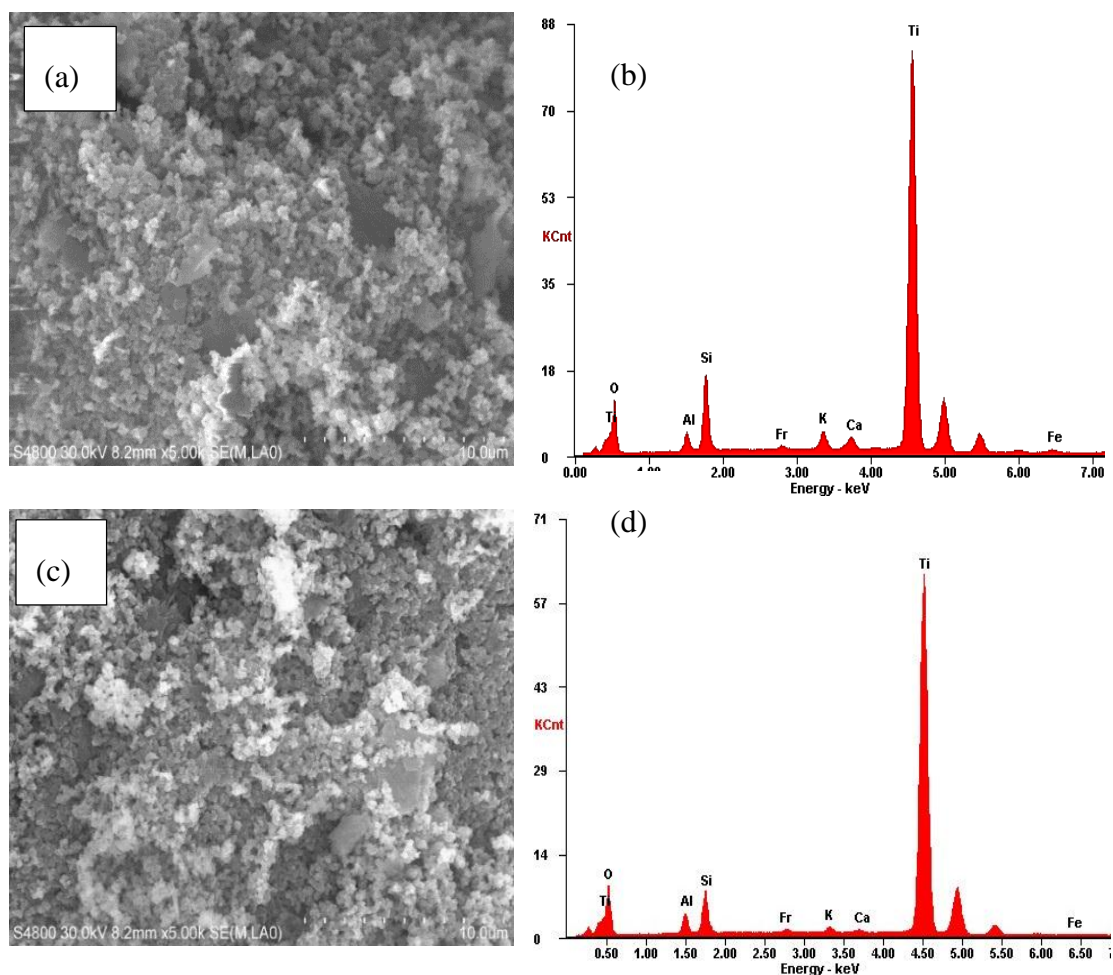


Figure 4.2. SEM images and EDX spectra of 10% TiO₂ supported on different zeolite particles: (a and b) 0.5-1.0 mm (c and d) 1.0-1.2 mm

The morphology of the silica alone and the prepared TiO₂/silica composite photocatalyst is shown in Figs. 4.3 and 4.4. From Fig. 4.3a, the morphology may be described as close packed cubic arrangement. This morphology remained the same even after supporting TiO₂ (Figs. 4.3c and 4.4) on silica with different size particles. Taking into account the EDX spectra of silica support material alone (Fig. 4.3b) this arrangement could be that of oxygen ions, with the silicon ions dispersed on tetrahedral interstices, since Si⁴⁺ is very much smaller than O²⁻ (Papirer, 2000). The main components of silica, O and Al were detected throughout the EDX spectrum analysis, however, their compositions reduced on after supporting TiO₂ on silica

surface. This was more evident on 38-75 μm (Fig. 4.3c) silica particle size. Interestingly, the composition of Si, O, and Al increased significantly when TiO_2 is supported on silica particle sized 75-150 μm (Fig. 4.3d) and reduced again on silica particle sized 150-250 μm (Fig. 4.4b). This shows that the silica particle sized 38-75 μm seemed to be inadequate to hold the TiO_2 on its surface while TiO_2 could not cover the surface of 150- 250 μm silica particle size. This suggests that some of the TiO_2 particles were lost during the synthesis process. The Ti-O interaction is observed after modifying the silica surface sized 75-150 μm (Fig. 4.4b) and 150-250 μm (Fig. 4.4d), however the interaction was stronger on 75-150 μm silica particle size.

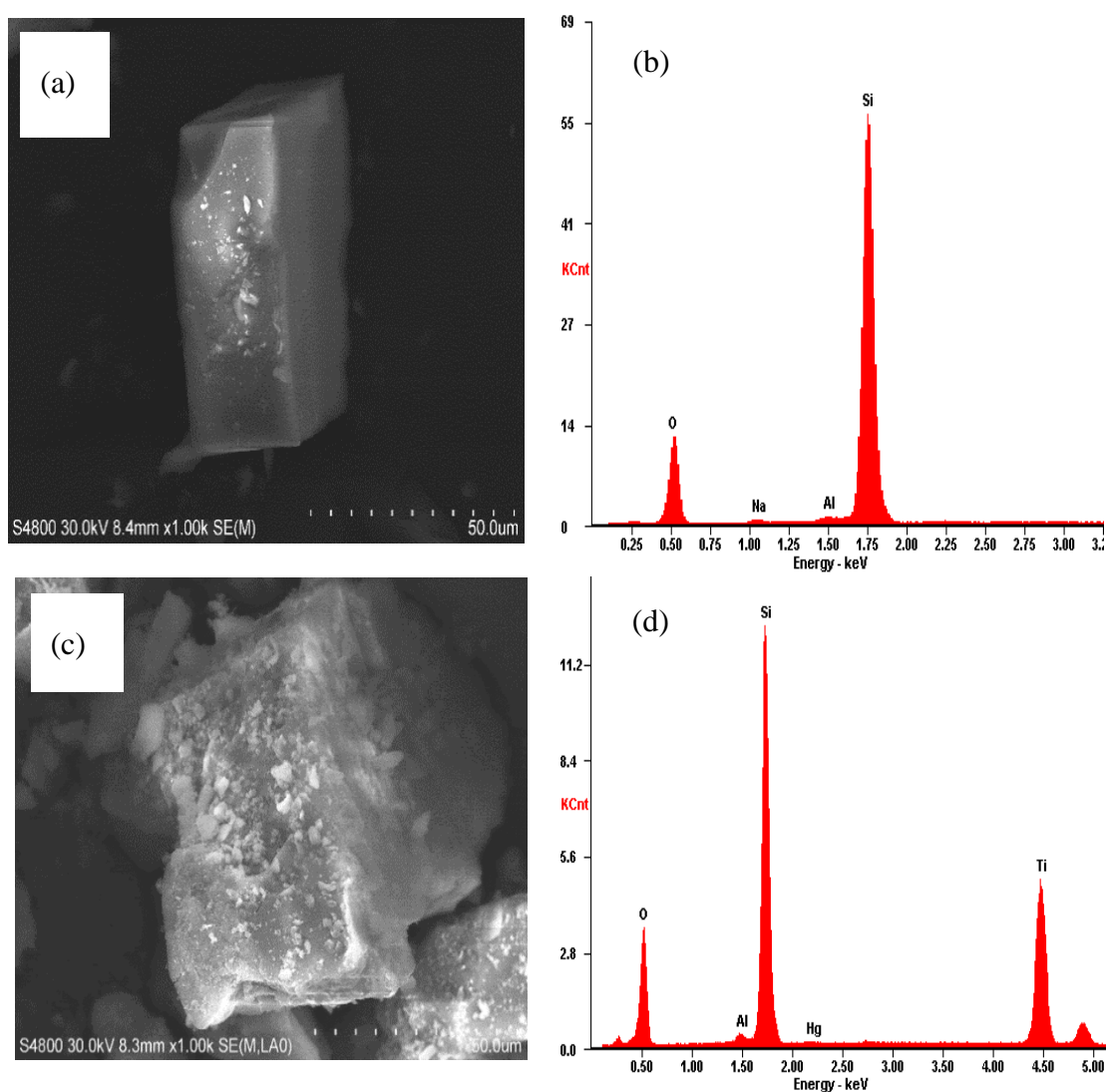


Figure 4.3. SEM images and EDX spectra: (a and b) silica alone (c and d) 38-75 μm 15% $\text{TiO}_2/\text{silica}$

It is noticed that Hg is detected on TiO₂/silica (38-75 μm) and thereafter disappeared completely as the particle size was increased (Fig. 4.4). This can be explained by a low atomic ratio of Hg/(Si+Ti) of 0.27% (Pitoniak, 2004). Unidentified peaks with different composition on both prepared composite photocatalysts were observed. Extra SEM-EDX analysis are given in appendix showing their EDX mapping also.

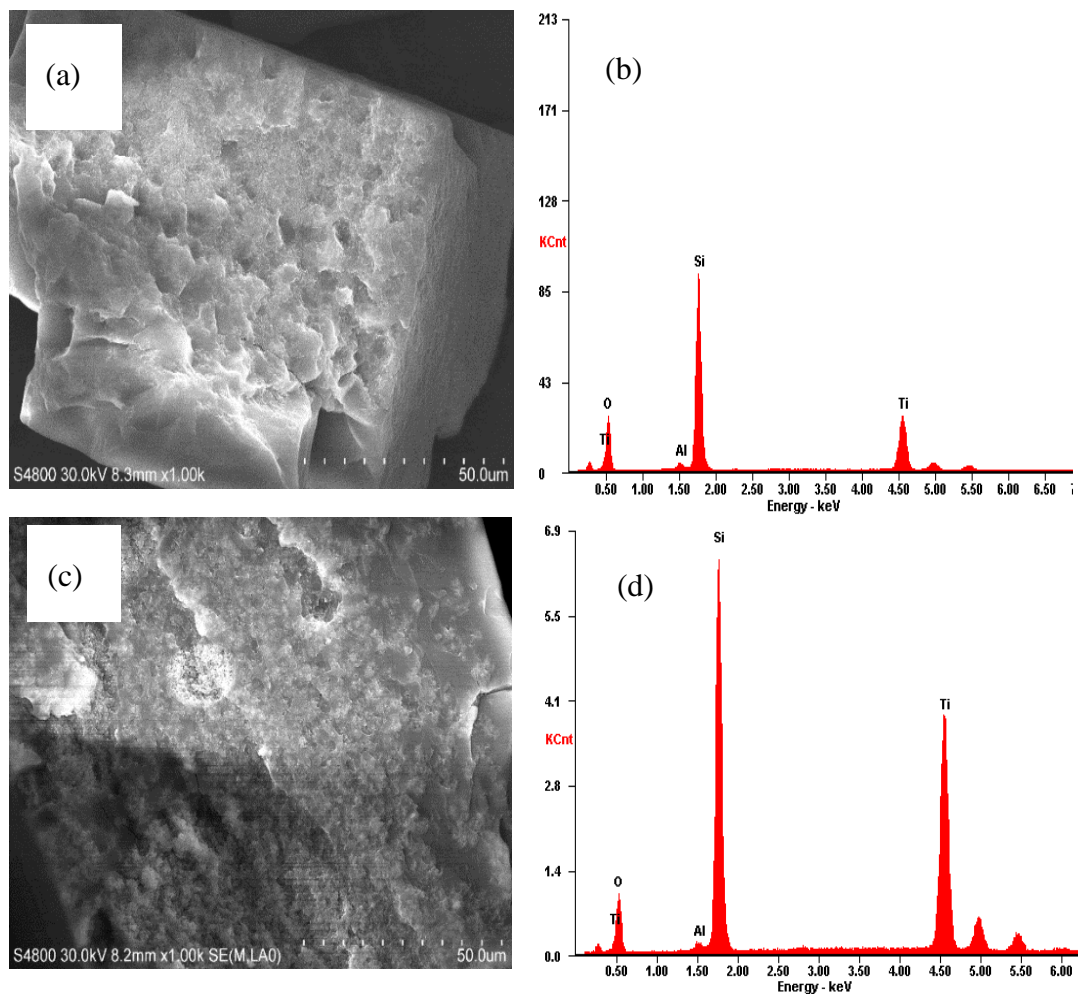


Figure 4.4. SEM images and EDX spectra of TiO₂/silica: (a and b) 75-150 (c and d) 150- 250 μm

4.1.3 Raman Spectroscopy

The Raman spectra of 10% TiO₂/zeolite and 15% TiO₂/silica composite photocatalyst before and after the photocatalytic treatment of methyl orange are displayed in Fig. 4.5. Two very strong sharp bands at 196.1 and 137 cm⁻¹, a medium band at about 638.5 cm⁻¹ and three small bands at 137, 396.4, 514.5 cm⁻¹ are observed in Fig. 4.5a. These well-defined bands observed indicate that anatase crystallites prevail in the structure of the prepared photocatalyst

composite. The peaks correspond well with those observed for a single-crystal anatase (640, 515, 400, 197, 144 cm^{-1}) (Beattie and Gilson, 1968). Further analysis of the Raman spectra unveil the existence of the other two Raman signals, close to 145 and 437.4 cm^{-1} that can be associated with the occurrence of rutile phase in TiO_2 structure. The Raman spectra indicated the presence of very small Raman signals in the 200–360 cm^{-1} range assigned to the vibration of Si-O bonds in zeolite. The presence of anatase on TiO_2 /zeolite composite photocatalyst surface can still be observed at the same bands as before even after the photocatalysis degradation of methyl orange (Fig. 4.5b). The bands did not shift to either higher or less wavenumbers however their intensities significantly shifted to lower values.

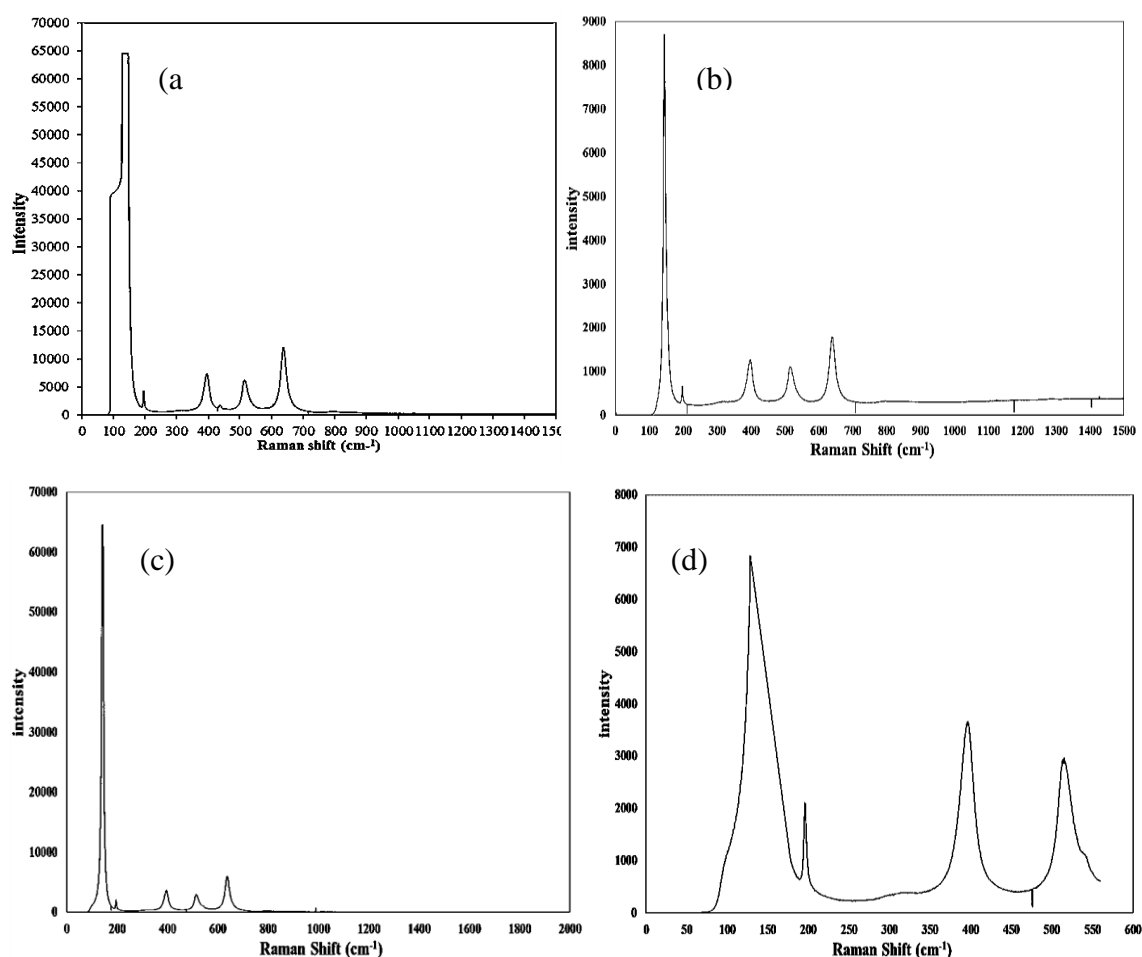


Figure 4.5. Raman spectra of (a) 10% TiO_2 /zeolite before and (b) after the treatment (c) 15% TiO_2 /silica before and (d) after photocatalysis treatment

In the Raman spectrum measured after the methyl orange degradation (Fig. 4.5b) a peak of the rutile band can still be discerned but much less pronounced than before the treatment. The presence of anatase crystallites in TiO_2 /silica composite are displayed at well-defined bands

198, 397.6, 517.4 and 641.2 cm^{-1} . These observed bands, indicating the presence of anatase on $\text{TiO}_2/\text{silica}$, are similar to the one observed on $\text{TiO}_2/\text{zeolite}$ composite photocatalyst. The rutile phase has Raman band at 143 cm^{-1} .

4.1.4 Isoelectric Point Measurements (IEP)

The IEP or point of zero charge (PZC) of $\text{TiO}_2/\text{silica}$ composite photocatalyst (diameter between 38-75 microns) composite was determined by zeta potential measurements (Fig. 4.6). The differences in acid-base properties of $\text{TiO}_2\text{-SiO}_2$ oxide composites have an impact on the obtained zeta potential values (Nowacka *et al.*, 2013). Upon evaluating the course of the electrokinetic curve for the $\text{TiO}_2/\text{silica}$ composite, it can be seen that its zeta potential is decreases with an increase in the pH values, which confirms that the zeta potential value strongly depends on the pH value. The IEP for the $\text{TiO}_2/\text{silica}$ particles is found at the pH value of 1.5 and reaches zeta potential values from 10 to -34 mV in the studied pH range. In addition, the stability of $\text{TiO}_2\text{-silica}$ composite photocatalyst is high in the pH values from 4 to 6, as indicated by high zeta potentials. The IEP for TiO_2 was reported to be around 6 (Londeree, 2002). The differences in the electrokinetic properties of the studied composite photocatalyst and that of TiO_2 are a result of the proposed synthesis method and the percent composition of a given oxide. Lower IEP value of the prepared synthetic composite photocatalyst is most likely caused by a higher percent composition of silica, which is characterized by an isoelectric point at a pH value of 2.

These results were consistent with the findings revealed by Papirer (2000) where the silica's point of zero charge ranged between 2 and 3. In addition, the surface charges were changed from positive to negative as a function of pH due to the deprotonization of the surface groups. At a pH less than the IEP, the $\text{TiO}_2/\text{silica}$ surface was positively charged due to the formation of Si-OH_2^+ . At a pH above the IEP, the surface of the $\text{TiO}_2/\text{silica}$ had a negative charge due to the deprotonation of the silanol group resulting in Si-O^- . As the pH approached 6, the Si-O^- become dominant (the pK_a for $\text{SiOH} = \text{Si-O}^- + \text{H}^+$ is around 6 and 7) (Cox, 1993). Londeree (2002) reported that these Si-O^- sites react with cations in solution and an increase in pH would significantly improve the adsorption of organic and inorganic compounds on composite surface. For nonionic compounds in solution, adsorption could take place at the silanol groups by either Van der Waals forces or hydrogen bonding. It was further reported (Londeree, 2002) that for anionic compounds, adsorption could occur at a pH above the PZC of silica, but instead it would be occurring at the TiO_2 surface which is positively charged at $\text{pH} < 6.0$.

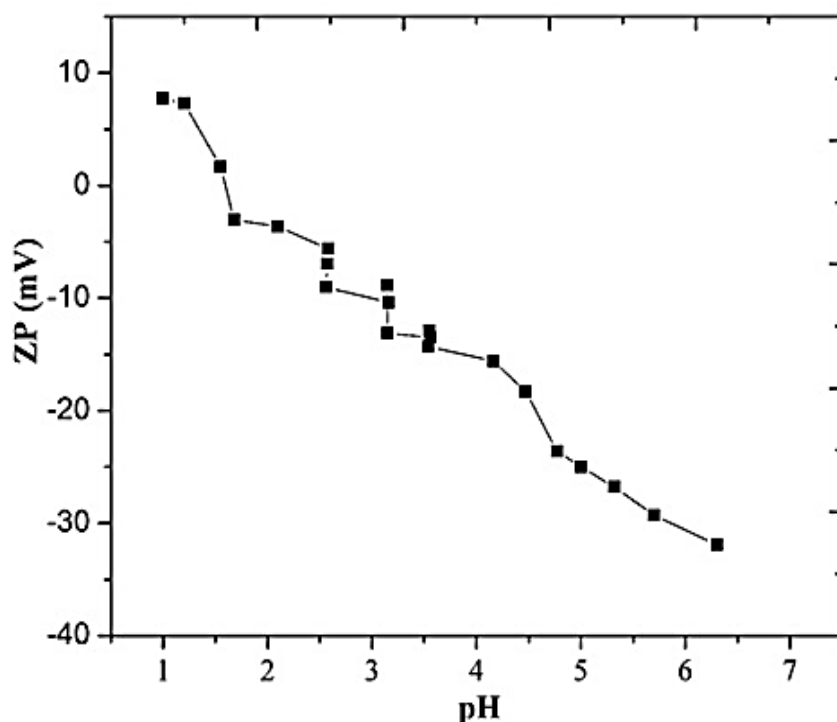


Figure 4.6. Zeta potential of TiO₂/silica as a function of pH

4.2 Photocatalytic degradation of dye by TiO₂/zeolite and TiO₂/Silica photocatalyst

Experiments were conducted at two different conditions, dark adsorption over composite photocatalysts and photolysis under UV light only at pH 6.5 (Fig. 4.7). Dark experiment was carried out to saturate the composite photocatalysts surface by dye adsorption so that during the reaction under UV light no more adsorption of dye occurs. From the result it was noticed that there is a small change in concentration of methyl orange in absence of light (dark reaction) and in presence of photocatalyst composites. This can be attributed to the adsorption of methyl orange onto the surface of the TiO₂/zeolite and TiO₂/silica composite. This indicates that the role played by adsorption is minimal and hence, for all experiments, the solution was left to equilibrate for 0.5 h in the dark. Since some dyes can be degraded by direct UV irradiation without the assistance of photocatalysts (Chakrabarti and Dutta, 2004), it was important to find out the extent of direct photolysis of methyl orange with respect to photocatalysis. From Fig. 4.7, it can be seen that photolysis played an important role in degrading the dye since 58% degradation was achieved in 3.5 h irradiation time by the assistance of light. To recognize the role of support material during the photocatalytic degradation of methyl orange, the 10 wt.% TiO₂/zeolite and 15 wt.% TiO₂/silica composite was compared with unsupported TiO₂ amount

equivalent to the one available on both photocatalyst for the degradation efficiency. It can be clearly seen from Fig. 4.7 that over 90% degradation of methyl orange was achieved over supported system ($\text{TiO}_2/\text{zeolite}$ and $\text{TiO}_2/\text{silica}$), whereas the degradation over TiO_2 alone only reached 45% degradation even after 3 h. The enhanced photodegradation of methyl orange by $\text{TiO}_2/\text{zeolite}$ could be attributed to the fact that zeolite possesses high ion exchange capacity, sorption and relatively large pore size that exhibits the highest photoactivity. Furthermore, as reported in section 2.7.3; the zeolite plays a positive influence in the processes of charge and electrons transfer during the photocatalytic reaction, which subsequently decreases the recombination of the charge carriers (Dubey *et al.*, 2006).

Silica-modified TiO_2 was noticed to exhibit a better photocatalytic performance also than TiO_2 itself. This could be explained in terms of the existed strong interaction between SiO_2 and TiO_2 , and Ti–O–Si bonds formed during the preparation process. Moreover, the transparency of silica allows the penetration of photons to the TiO_2 catalyst surface. It can be seen that the TiO_2 supported on zeolite and silica material demonstrated a more efficient use of the TiO_2 sites than for TiO_2 alone. Apart from that, hydroxyl radicals ($\bullet\text{OH}$), on the surface of TiO_2 , are easily transferred onto the surface of zeolite and silica support material. That means the methyl orange pollutant, which has already been adsorbed on the non-photo active zeolite and silica, has a chance to be degraded due to the appearance of $\bullet\text{OH}$, resulting in the enhancement of the photodegradation performance of the prepared composite photocatalysts. Nikazar *et al.* (2007) reported that 97.4% of Azo Dye Direct Yellow 12 was degraded at the irradiation time of 2 h in the supported system while 63.2% was achieved for unsupported TiO_2 . This is attributed to the fact that when TiO_2 is illuminated with the light of $\lambda < 390$ nm, electrons are promoted from the valence band to the conduction band of the semi conducting oxide to give electron-hole pairs. The valence band (h_{VB}) potential is positive enough to generate hydroxyl radicals at the surface, and the conduction band (e_{CB}) potential is negative enough to reduce molecular oxygen. The hydroxyl radical is a powerful oxidizing agent and attacks organic pollutants present at or near the surface of TiO_2 . It causes photo-oxidation of dye according to the reactions equations given in section 2.5 and the mechanism summarized in Fig. 2.1.

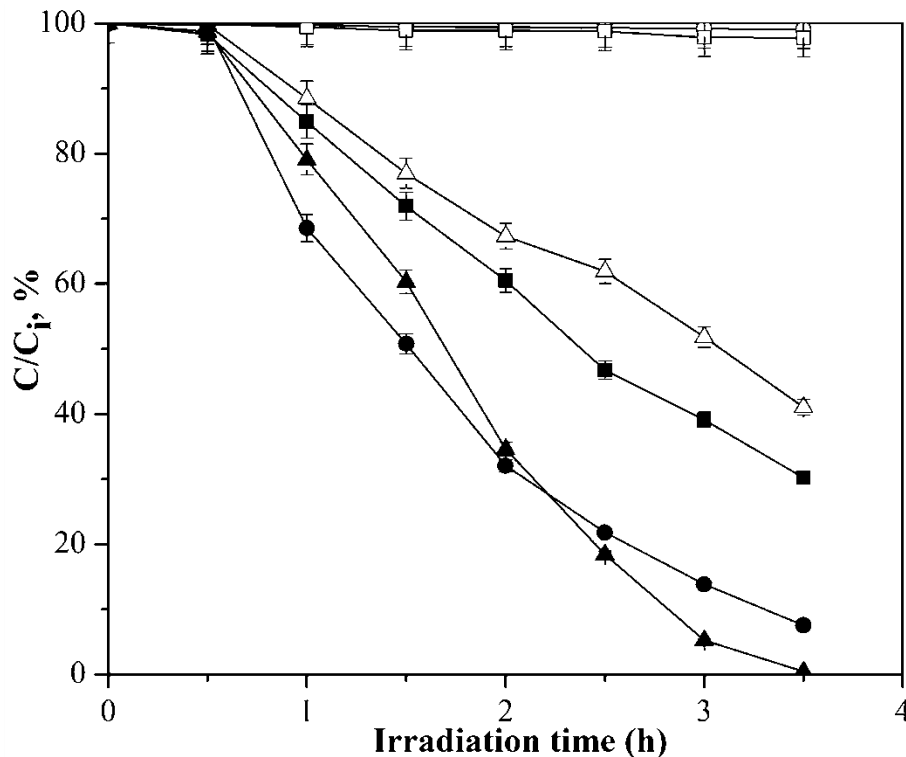


Figure 4.7. Adsorption of methyl orange over TiO₂/zeolite (□) and TiO₂/silica (○); photocatalytic degradation of methyl orange over UV (Δ); UV-TiO₂ (■); UV-TiO₂/zeolite (▲); UV-TiO₂/silica (●) (C₀ = 25 mg/L, TiO₂/zeolite = 6.25 g/L TiO₂/silica = 1.25 g/L)

Figure 4.8 shows the box and whiskers plot of degradation of methyl orange over treatment methods applied in Fig. 4.7. Adsp 1 represents the adsorption of methyl orange on TiO₂/zeolite while Adsp. 2 denotes adsorption over TiO₂/silica in the dark. The box and whiskers plot reveals valuable information about the distribution of the continuous variable and each distribution is presented by a box and protruding lines (called whiskers). The line across the inside of the box represents the median value. Any data points that statistical analysis considers are outliers which appear as little circles indicating data points that are quite different from the remainder of the sample, either higher or lower (Pallant, 2007). According to the box and whiskers plot, the distribution for UV, UV/TiO₂ and UV-TiO₂/zeolite treatment processes are positively skewed with no outliers. This is attributed to the large mean values (indicated with □ inside the box) than the median values. This was more observed for adsorption treatment method. The distribution of the data on UV-TiO₂/silica is symmetrical and unimodal, as indicated by the close mean value (almost equal) to the median (mean = 50.1 and median = 50). The distribution on adsorption experimental data is not clearly indicated since no significant degradation of methyl orange took place. Figure 4.8 shows there is a significant

difference in degradation efficiency when comparing all the treatment methods applied for the degradation of methyl orange. This results correspond well with the scatter plot in Fig. 4.7.

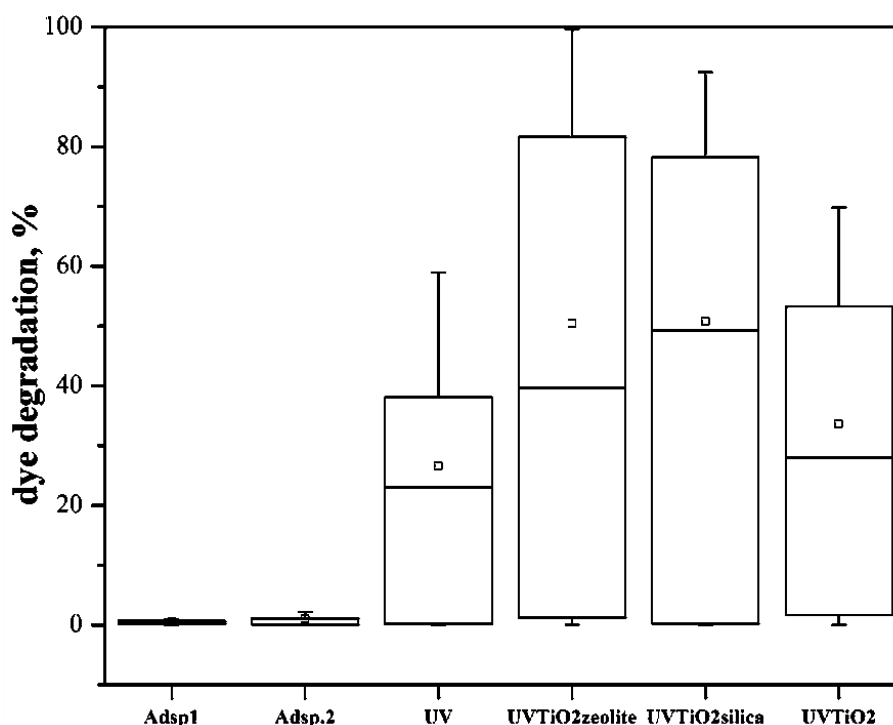


Figure 4.8. Boxplots built up with data values obtained at different treatment processes

4.2.1 Effect of particle size of the supporting material

The effect of both support material particle size on methyl orange degradation was evaluated. To study the effect of zeolite particle size on the photodegradation of dye, 10 wt.% TiO_2 was supported on 0.2-0.5 mm, 0.5-1.0 mm, and 1.0-1.2 mm. From Fig. 4.9, it can be seen that 0.5-1 mm achieved better degradation efficiency than 0.2-0.5 mm and 1.0-1.2 mm zeolite particle sized. As the particle size increased from 0.5-1.0 mm to 1.0-1.2 mm, the degradation efficiency decreased. It has been reported by Almquist and Biswas (2002) that the larger sized particles decrease the available surface area for the reaction to take place. Hence, the degradation efficiency decreased for TiO_2 supported on 1.0-1.2 mm zeolite. Conversely, smaller particles sized are known to have higher degradation performance than larger ones due to their higher surface area to volume ratio, however this was not the case for 0.2-0.5 mm zeolite particle size. The better degradation efficiency for TiO_2 supported on zeolite particle sized 0.5-1.0 mm is attributed to the SEM images coupled with EDX spectra (Figs. 4.2a and b), showing that the

TiO₂ is well attached/distributed on 0.5-1.0 mm zeolite surface than the other two particle sizes. Therefore, in further experiments, TiO₂ was supported onto 0.5-1.0 mm zeolite particle size.

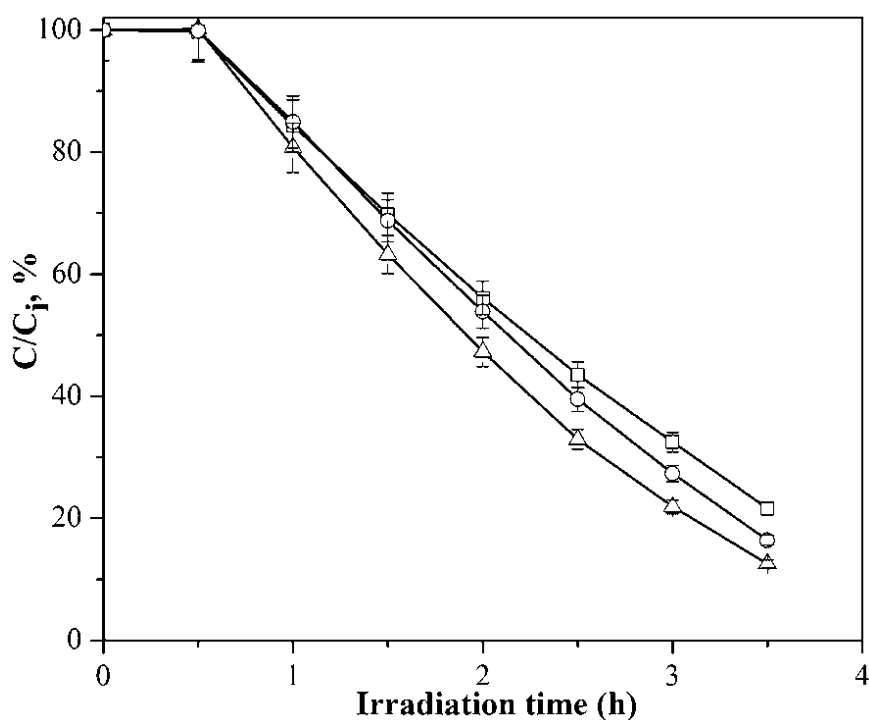


Figure 4.9. Effect of zeolite particle size: 0.2-0.5 mm (□); 0.5-1.0 mm (Δ); 1.0-1.22 mm (○)

The prepared 15 wt% TiO₂/silica composite photocatalyst, after being dried (section 3.2), was screened to different particle sizes (particle sizes, 38-75 μm, 75-150 μm, and 150-250 μm) and their effect on photocatalytic degradation on dye was evaluated. Figure 4.10 shows a contrasting trend as compared to the one observed in Fig. 4.9, in this set of experiments, better degradation performance was achieved at smaller particle size (38-75 μm). Similar trends have been reported by other researchers (Almquist and Biswas, 2002), however, their studies were based on the effect of particle size on the photoactivity of TiO₂ only without the supporting material. It was concluded in their studies that the optimum particle size observed was due to the off-setting contributions of high surface area and changes in the structural and electronic properties of the TiO₂ as the particle size decreases.

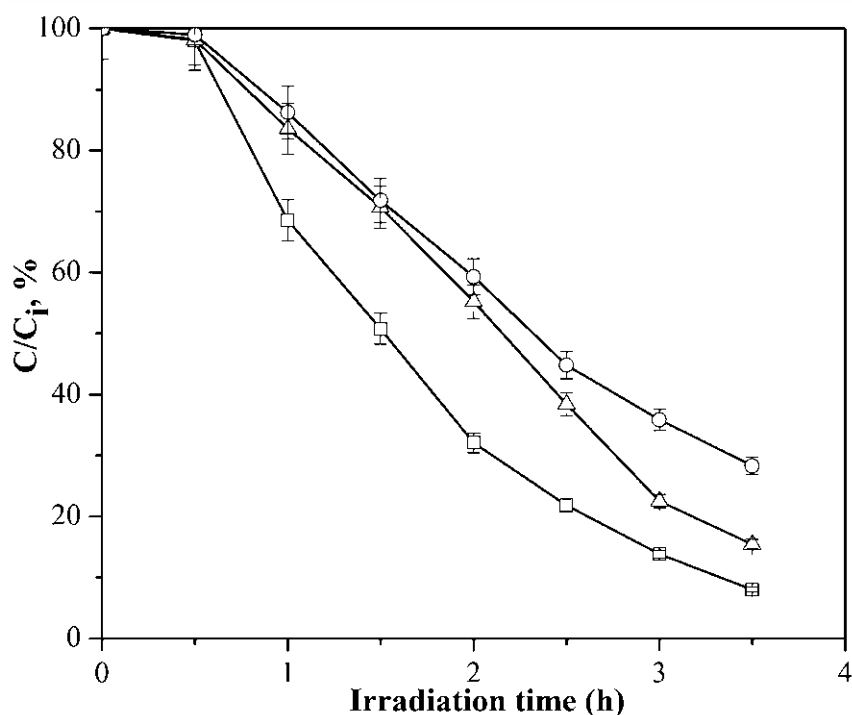


Figure 4.10. Effect of silica particle size: 38-75 μm (\square); 75-150 μm (\circ); 150-250 μm (Δ)

4.2.2 Effect of TiO_2 composition on supporting material

To determine the effect of TiO_2 loading onto zeolite and silica, different proportion of TiO_2 were functionalized on zeolite and silica (Figs. 4.11 and 4.12). Figure 4.12 shows that effective degradation of methyl orange dye after 3 h irradiation time is observed when the composite photocatalyst contained 10 wt.% TiO_2 and 90 wt.% zeolite. The photodegradation efficiency increased with an increase in the proportion of TiO_2 and then decreased when the TiO_2 composition increased to 20 wt.%. This trend can be explained by the fact that when all dye molecules are adsorbed on the photocatalyst, the addition of higher quantities of TiO_2 would have no effect on the degradation efficiency. Normally, an increase in TiO_2 composition increases the degradation rate of the dyes. However, in this study, TiO_2 composition did not significantly affect the extent of dye removal by the modified photocatalyst, as they had similar surface area. This is indicated by the BET surface area measurement of TiO_2 /zeolite composite as a TiO_2 loading (Table 4.1). A paired-samples t-test is conducted to check whether there was a statistically significant difference in degradation efficiency in the TiO_2 composition for 15 wt.% and 20 wt.%. The test statistic is found to be 2.92 with a p-value of 0.0249 at 1% level of significance (99% confidence interval) (Table 4.2). This shows there was no statistically decrease when TiO_2 is increased from 15 wt.% to 20 wt.%.

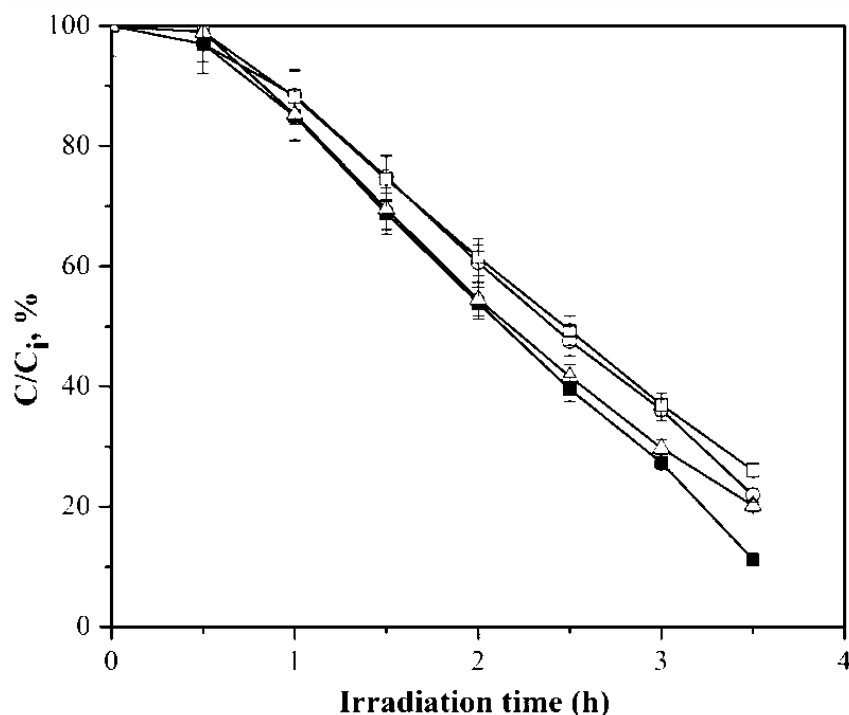


Figure 4.11. Photocatalytic degradation of methyl orange over different loading of TiO₂ supported on zeolite: 3 wt.% (□); 10 wt.% (■); 15 wt.% (○); 20 wt.% (Δ)

Table 4.2. Paired T-test on the difference of TiO₂ Composition supported on zeolite

TiO ₂ Composition difference	N	Mean	Std Dev	Std Err	95 % CL Mean	Std Dev	95 % CL Dev
15 wt.%-20 wt.%	7	3.7	3.2938	1.2449	2.6649 6.7463	3.29	2.1225 7.2531
T-Tests Difference	DF	t value	Pr > t				
15 wt.%-20 wt.%	6	2.97	0.0249				

Figure 4.12 shows that the photodegradation efficiency of methyl orange decreased significantly on 20 wt.% TiO₂ and 80 wt.% silica. In view of these, 10 wt.% and 15 wt.% of TiO₂ with respect to zeolite and silica were the best condition to achieve the synergism between TiO₂ and the applied supporting material. This synergic effect may be due to the fact that the presence of zeolite and silica maintains the molecules of methyl orange dye near the composite photocatalyst. Hence, 10 wt.% TiO₂ /zeolite and 15 wt.% TiO₂/silica may be covering the monolayer surface completely and efficiently resulting in better methyl orange degradation efficiency.

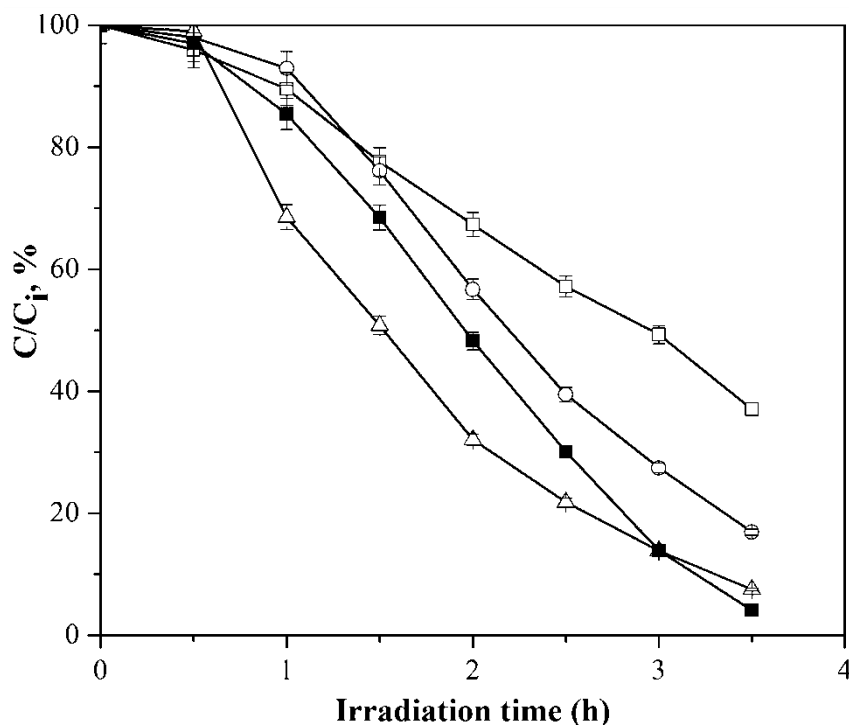


Figure 4.12. Photocatalytic degradation of methyl orange over different loading of TiO₂ supported on silica: 3 wt.% (□); 10 wt.% (○); 15 wt.% (■); 20 wt.% (Δ)

Table 4.3 shows a test statistic of 2.34 with a p-value of 0.059 at 1% level of significance implying that when there is a statistically decrease in dye degradation when TiO₂ was increased from 15 wt.% to 20 wt.%. Furthermore, the Eta squared which determines the effect size of paired-sample t-test is calculated using Eq.4.1. The guidelines proposed by Cohen (1988) for interpreting this value are: 0.01 = small effect, =0.6 moderate effect, 0.14=large effect. In this study, eta squared value of 0.47 is found and can be conclude that there is a large effect, with a substantial difference in the degradation efficiency achieved at 15 wt.% TiO₂ and 20 wt.% TiO₂ supported on silica material. Eta squared (θ) can be obtained using the following formula:

$$\theta = \frac{t^2}{t^2 + N - 1} \quad 4.1$$

where t is the t-value, N is the number of observation.

Table 4.3. Paired T-test on the difference of TiO₂ Composition supported on silica

TiO ₂ Composition difference	N	Mean	Std Dev	Std Err	95 % CL Mean	Std Dev	95 % CL DeV
15 wt.%-20 wt.%	7	8.012	9.063	3.425	-0.369 16.395	9.063	5.8405 19.9584
T-Tests							
Difference	DF	t value	Pr > t				
15 wt.%-20 wt.%	6	2.34	0.0579				

4.2.3 Effect of composite photocatalyst concentration

The TiO₂/zeolite composite photocatalyst concentration was varied from 1.25-18.75 g/L at 25 mg/L initial concentration of methyl orange and solution pH 6.5. Figure 4.13 shows that the degradation of methyl orange initially increased with photocatalyst concentration and then decreased. This can be explained by the fact that as the photocatalyst concentration increases, the turbidity of the solution increases, resulting in a decrease in UV light penetration. When the composite photocatalyst concentration exceeded 6.25 g/L, the degradation efficiency decreased thus causing light scattering and a screening effect while reducing the photocatalytic activity of the composite photocatalyst. The results suggested that an optimal concentration of the composite photocatalyst is necessary for efficient degradation. In this study, the optimum composite photocatalyst concentration was found to be 6.25 g/L. The effect of TiO₂/silica composite photocatalyst concentration was determined from 1.25-12.75 g/L. It is observed in Fig. 4.14 that initially the degradation of methyl orange reduced significantly with an increase in composite photocatalyst concentration. This was more pronounced at 6.25 g/L (TiO₂/silica) composite photocatalyst concentration which can be due to the partial deactivation of activated molecules by collision with ground state molecules. Furthermore, the significant reduction in degradation percentage of methyl orange above 1.25 g/L TiO₂/silica photocatalyst

concentration can be explained in terms of the availability of active sites on TiO₂/silica surface and the light penetration of photoactivating light into the suspension.

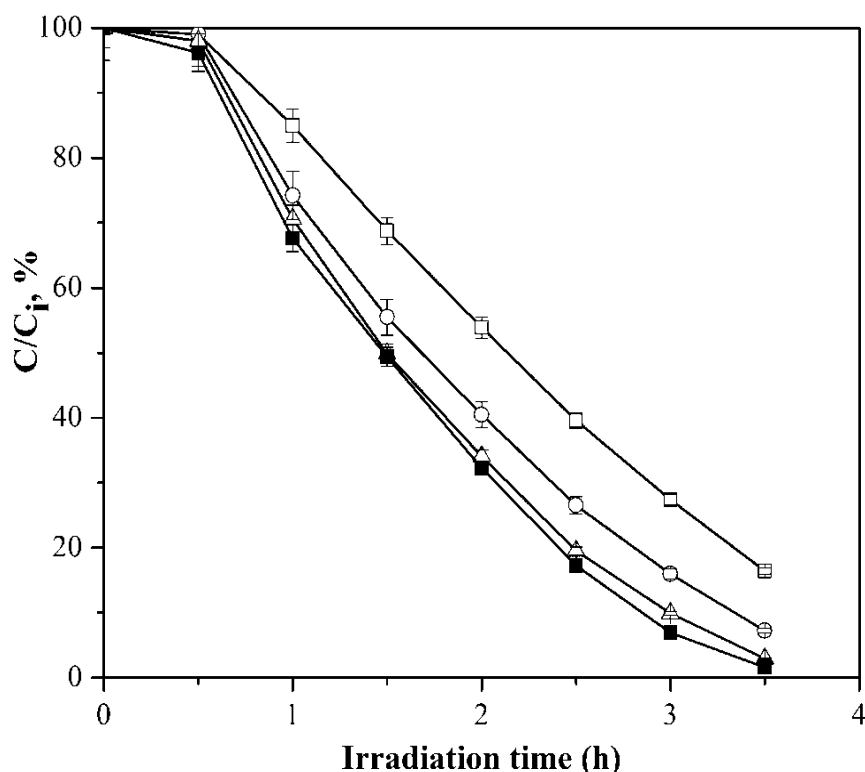


Figure 4.13. Effect of TiO₂/zeolite composite photocatalyst concentration on dye degradation: 1.25 g/L (□); 6.25 g/L (■); 12.25 g/L (Δ); 18.75 g/L (○). Condition: C₀= 25 mg/L; pH= 6.5

The availability of active sites increases with the suspension of photocatalyst loading (Neppolian *et al.*, 2002). When the amount of photocatalyst increases above an optimum level, the light photon absorption coefficient usually declines. The optimum concentration of 1.25 g/L TiO₂/silica composite photocatalyst was found and used in further experiments. Many studies have reported the effect of photocatalyst concentration on the process efficiency (Gaya and Abdullah, 2008; Herrmann, 1999). These results are mostly independent and a direct comparison cannot be made, as the photoreactor, radiation fluxes, intensity and wavelengths used were different.

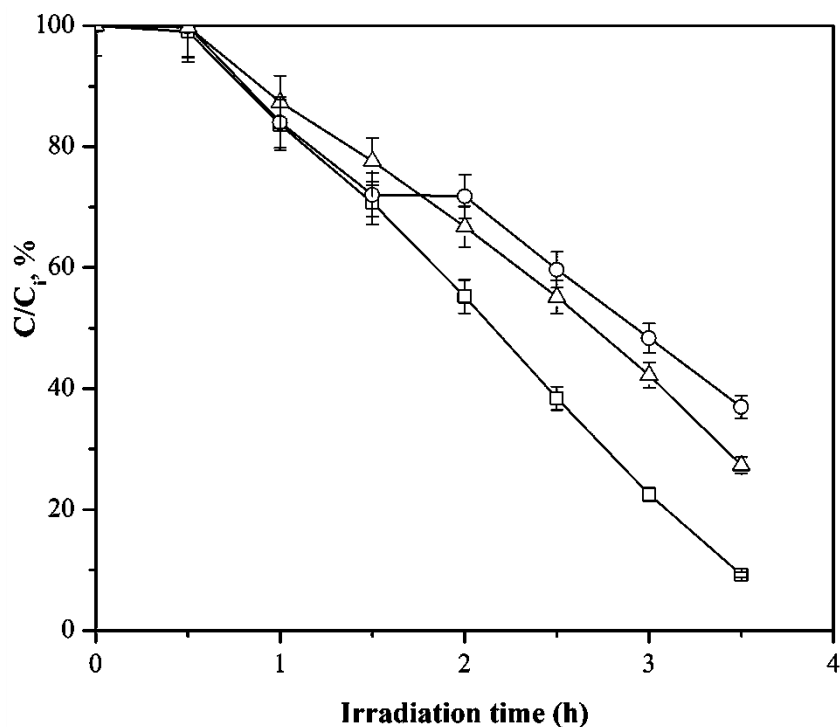


Figure 4.14. Effect of $\text{TiO}_2/\text{silica}$ composite photocatalyst concentration on dye degradation: 1.25 g/L (\square); 6.25 g/L (\circ); 12.25 g/L (Δ). Condition: $C_0 = 25$ mg/L; pH= 6.5

4.2.4 Effect of dye initial concentration

Efficient application of the photocatalytic oxidation system requires the investigation of the dependence of photocatalytic degradation efficiency on the substrate concentration. The characteristic of organic dye concentrations in wastewater from textile industry is usually in the range of 10-50 mg/L (Kansal *et al.*, 2007). Therefore, methyl orange solution concentrations were varied in the range 5-50 mg/L during the photocatalytic degradation experiments at solution pH 6.5 (Fig. 4.15). The degradation rate was found to increase up to an initial concentration of 35 mg/L and then declined significantly. An increase in substrate concentration can lead to the generation of intermediates which may adsorb on the surface of the photocatalyst (Papadam *et al.*, 2007). The cationic dye radicals readily interacts with $\text{O}_2^{\cdot-}$ and HO^{\cdot} species to generate intermediates as shown in Eq. 2.7. Slow diffusion of the generated intermediates from the composite photocatalyst surface can result in the deactivation of active sites of the photocatalyst, and consequently result in a reduction in the degradation rate.

The limited number of surface sites on zeolite/ TiO_2 and silica/ TiO_2 particles may have an impact on dye photodegradation. When the concentration of methyl orange pollutant increases

more molecules of the compound get adsorbed onto the surface of the composite photocatalyst. At high dye concentrations the generation of $\cdot\text{OH}$ radicals on the surface of composite photocatalyst was reduced since the active sites were covered by dye ions. This could also be explained by the UV-screening effect of the dye itself. At a high dye concentration, a significant amount of UV may be absorbed by the dye molecules rather than the TiO_2 particles and that reduces the efficiency of the catalytic reaction due to decreased concentrations of $\cdot\text{OH}$ and $\text{O}_2\cdot^-$. In addition, the major part of degradation occurs in the region near to the irradiated side (known as reaction zone) where the irradiation intensity is much higher than in the other side. Thus at higher dye concentration, degradation decreases at sufficiently long distances from the light source or the reaction zone due to the retardation in the penetration of light. Hence, it is concluded that as initial concentration of the dye increases, the active sites on composite photocatalyst surface needed for the degradation also increases (Konstantinou and Albanis, 2004).

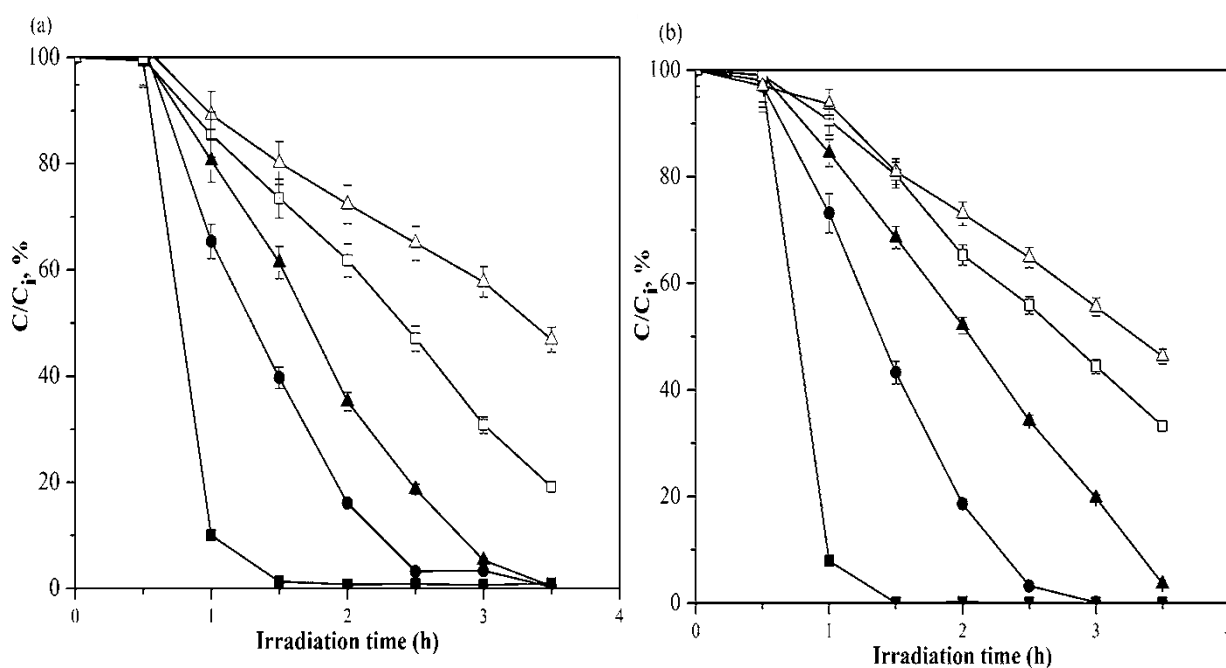


Figure 4.15. Effect of initial concentration on (a) $\text{TiO}_2/\text{zeolite}$ and (b) $\text{TiO}_2/\text{silica}$ photocatalyst 5 mg/L (■); 15 mg/L (●); 25 mg/L (▲); 35 mg/L (□); 50 mg/L (Δ)

4.2.5 Effect of solution pH

The solution pH does not only affect the surface charge of a photocatalyst, but also the degree of ionization or speciation (pK_a) of an organic pollutant during the reaction. Electrostatic interaction between semiconductor surface, substrate and charged radicals formed during

photocatalytic oxidation is profoundly dependent on the pH of the solution (Saien and Khezrianjoo, 2008). Therefore, the pH of the solution plays a key role in the photocatalytic oxidation of pollutants. To study the effect of H^+ concentrations on dye degradation, comparative experiments were conducted at three pH values: 3, 7 and 9 and results are shown in Fig. 4.16. The methyl orange degradation efficiency on $TiO_2/zeolite$ were 99.8%, 82.6% and 93.8% at pH 3, 7 and 9, respectively, after 3 h irradiation. The observed trend can be attributed to two important roles. First, it is related to the surface charge properties of the composite photocatalysts and can be explained based on the isoelectric point (IEP). The IEP of the $TiO_2/zeolite$ composite photocatalyst was found to be around 6 (Liu *et al.*, 2014) which is nearly identical to that of TiO_2 consistent with the successful deposition of the TiO_2 particles onto the zeolite surface. Thus, the $TiO_2/zeolite$ surface is positively charged in acidic media ($pH < 6$), whereas it is negatively charged under alkaline conditions ($pH > 6$).

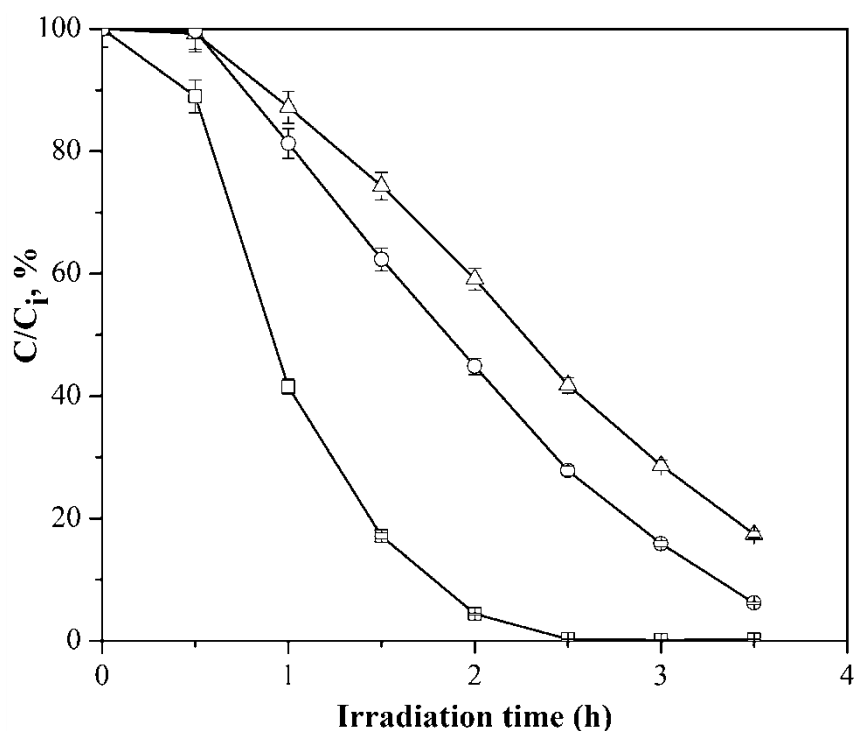


Figure 4.16. Effect of solution pH on dye degradation over $TiO_2/zeolite$: pH 3 (□); pH 7 (Δ); pH 9 (○). Condition: $C_0 = 25$ mg/L; $TiO_2/zeolite = 6.25$ g/L

The highest degree of photocatalytic degradation of methyl orange was observed at pH 3 and is attributed to the electrostatic attraction between the positively charged composite photocatalyst surface and negatively charged anions of methyl orange, which led to the increase of degree of adsorption of dye molecules onto the $TiO_2/zeolite$ surfaces and photodegradation.

At pH 7 and 9 opposite phenomenon was observed and it can be seen that the degradation efficiency decreased (Fig. 4.16). This can be attributed to the negative charge of the composite photocatalyst resulting in methyl orange intermediates products being repelled away from the composite photocatalyst surface and thus opposes the adsorption of substrate molecules on the surface of the composite photocatalyst. As a result, methyl orange degradation declines in alkaline medium. Secondly, hydroxyl radicals can be produced by the reaction between hydroxide ions and positive holes. The positive holes are considered as the major oxidation species at low pH whereas hydroxyl radicals are considered as the predominant species at neutral or high pH levels (Konstantinou and Albanis, 2004). It can be seen from Fig. 4.16 that the photodegradation of methyl orange increased from 82.6% at pH 7 to 93.8% at pH 9. This is due to the fact that in alkaline solution $^{\circ}\text{OH}$ are easier to be generated by oxidizing more hydroxide ions available on $\text{TiO}_2/\text{zeolite}$ surface, thus the efficiency of the photocatalysis is enhanced. Similar results are reported in the photocatalysed degradation of acidic azo dyes, although it should be noted that in alkaline solution there is a Coulombic repulsion between the negative charged surface of photocatalyst and the hydroxide anions (Neppolian *et al.*, 2002). This fact can prevent the formation of $^{\circ}\text{OH}$ and thus decrease the photooxidation. In the study conducted by Mills and Morris (1993), high pH values were found to be favorable even when anionic azo dyes should hinder adsorption on the negatively charged surface.

The effect of H^+ concentrations on dye degradation over $\text{TiO}_2/\text{silica}$ composite photocatalyst was also evaluated at three pH values: 3, 7 and 9 and results are shown in Fig. 4.17. The methyl orange degradation efficiency on $\text{TiO}_2/\text{silica}$ after 3.5 h are 99.8%, 96.4% and 91.56% at pH 3, 7 and 9, respectively. It should be noted that the IEP of $\text{TiO}_2/\text{silica}$ was found to be around pH 2 which is very close to that of silica (Fig. 4.6). However, high degradation of methyl orange was observed at pH 3 where the azo dye molecules is expected to inhibit the adsorption on the positively charged surface. This indicates that there may be some methyl orange molecules adsorption at a pH 3 which is above the IEP of silica; however, it would be occurring at the TiO_2 surface due to the TiO_2 having a positive charge at pH 3. It can be seen in Fig. 4.17 that the degradation of the dye at pH 7 and 9 decreased. This can be attributed by the fact that at high pH values the hydroxyl radicals are rapidly scavenged and they do not have the chance to react with dye molecules. It is then presumable that at a pH greater than 6, the silica surface becomes more concentrated with SiO^- groups, thus repelling the negatively sulfonic group of methyl orange. When the pH is 3, the silica has less of a negative charge and would allow the

penetration of methyl orange into the pores. Hence, acidic conditions would increase the ability of methyl orange to get within the vicinity of the TiO_2 . The interpretation of pH effect on the efficiency of dye photodegradation process is a very difficult task due to its multiple roles. The influence of the pH is dependent on dye type and on properties of the composite photocatalyst. Therefore, this effect on the photocatalytic efficiency must be accurately studied before any application.

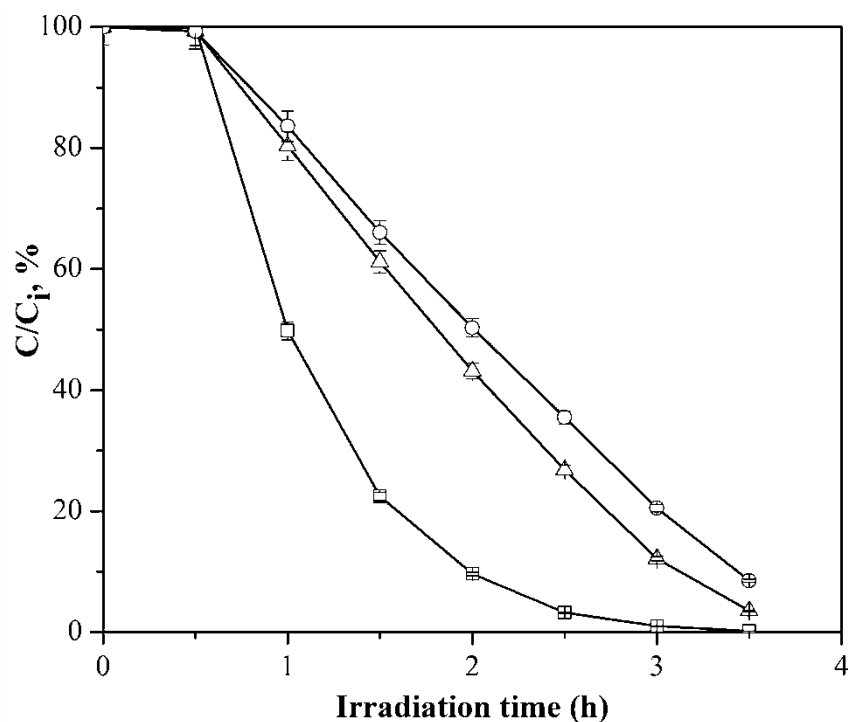


Figure 4.17. Effect of solution pH on dye degradation over $\text{TiO}_2/\text{silica}$; pH 3 (□); pH 7 (Δ); pH 9 (○). Condition: $C_0 = 25 \text{ mg/L}$; $\text{TiO}_2/\text{silica} = 1.25 \text{ g/L}$

4.2.6 Effect of inorganic salt

Inorganic salts form a major part in the application of numerous dyes during textile wet processes. They are usually used as retarding agents for applying leveling dyes on wool and basic dyes on acrylic. Hence, textile effluents contain large volumes of inorganic salts and dyes. The common applicable salts for this purpose are sodium chloride (NaCl) and sodium sulphate (Na_2SO_4). Moreover, NaCl performs the function of shielding the surface charge of the fiber allowing the dye to achieve improved bonding onto the fiber (Muthukumar and Selvakumar, 2004). In further experiments, the effect of the NaCl and Na_2SO_4 on methyl orange degradation at the concentration of 5 g/L over the prepared composite photocatalysts was evaluated and the

obtained results are shown in Figs. 4.18 and 4.19. It is observed that the presence of NaCl and Na₂SO₄ led to a decrease in methyl orange degradation on TiO₂/zeolite. It is important to note from Fig. 4.18 that Na₂SO₄ exhibited the strongest inhibition effect followed by NaCl. The degradation efficiency of methyl orange decreased from 99.5% to 93.7% and 59.69% for NaCl and Na₂SO₄, respectively. The decrease in the degradation of the dye in the presence of chloride and sulphate ions is due to the capturing of the photogenerated valence band hole and hydroxyl radicals by the respective anions (Eqs. (4.1)– (4.3)). According to Hu *et al.* (2003), the adsorbed anions compete with the dye for the photo-oxidizing species on the composite photocatalyst surface and prevent the photocatalytic degradation of dyes. Alternatively, they may act as light screens, thus reducing the photon receiving efficiency.

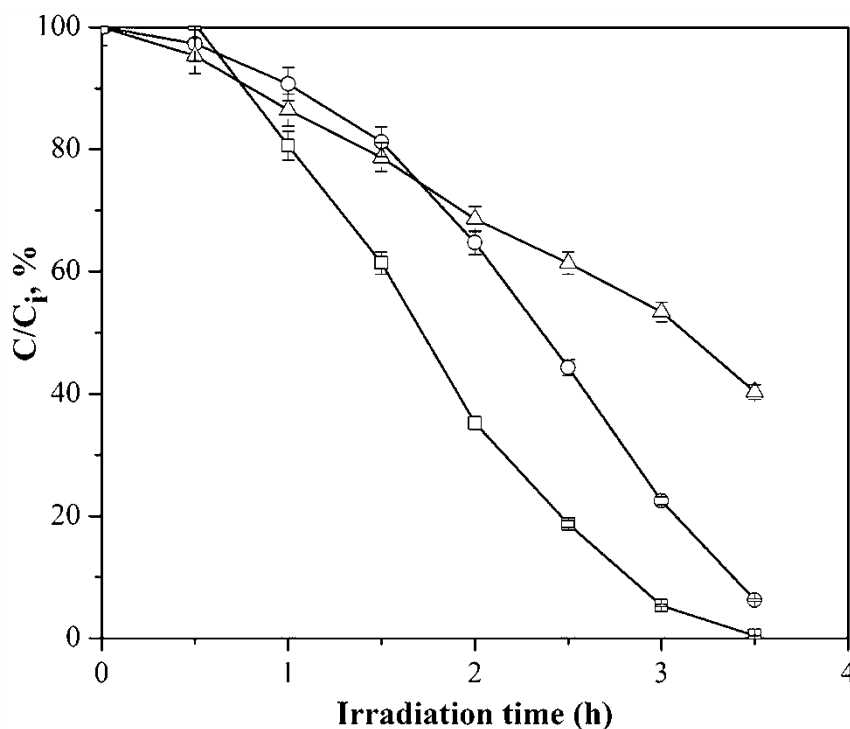


Figure 4.18. Effect of ions on methyl orange dye over TiO₂/zeolite: No ion (□); NaCl (○); Na₂SO₄ (Δ). Condition: C₀ = 25 mg/L; TiO₂/zeolite = 12.25 g/L, pH = 6.5

In addition, the formation of inorganic radical anions (Cl[•] and SO₄^{•-}) under these circumstances is possible to occur according to the following reaction (Chen *et al.* 2007):





The reactivity of these radicals may be considered, however, they are not as reactive as h^{+} and $^{\circ}\text{OH}$ (Hu *et al.*, 2003) and thus the observed retardation effect is thought to be related to the strong adsorption of the anions on the $\text{TiO}_2/\text{zeolite}$ surface. While chlorine radicals are forming slowly, they are instantaneously converted into chloride radical anion (Eqs. 4.1 and 4.2). The sulphate ions can react with hydroxyl radicals (Eq. 4.3) and thus the hydroxyl radical scavenging effect of these ions could result in decrease in degradation of the dye. Alternatively, surface sites normally available at the $\text{TiO}_2\text{-zeolite/dye}$ solution interface for adsorption and electron transfer from the dye can be blocked by anions such as chloride and sulphate which are very effective inhibitors for the degradation process. The Cl^{-} and SO_4^{2-} adsorbed on the composite photocatalyst surface may cause considerable inner-sphere surface complexes $\equiv\text{Ti}-\text{Cl}$, making the hole scavenging become more significant. Moreover, the oxidation potential of sulphate radical anion is 2.01 V which is higher than the oxidation potential of chlorine (1.36 V). Their oxidation potentials are lower than that of hydroxyl radicals, 2.8 V, hence, there was a reduction in the dye degradation (Kiwi *et al.*, 2000). Similar trends were observed in the photocatalytic degradation of methyl orange on $\text{TiO}_2/\text{silica}$ composite photocatalyst (Fig. 4.19).

The degradation efficiency of methyl orange decreased from 96% to 82.3% and 70.8% for NaCl and Na_2SO_4 , respectively. It is clear to note that Na_2SO_4 showed the strongest inhibition effect than NaCl as reported for the photocatalytic degradation of methyl orange on $\text{TiO}_2/\text{zeolite}$. It is also important to note that the inhibition effect of Na_2SO_4 was more pronounced on $\text{TiO}_2/\text{zeolite}$ than on $\text{TiO}_2/\text{silica}$ composite photocatalyst (Fig. 4.19). For instance, the degradation efficiency on $\text{TiO}_2/\text{silica}$ declined by 26% while that of $\text{TiO}_2/\text{zeolite}$ declined by 39%. This is related to the ionization state of the composite photocatalyst surface as well as to that of reactant dye. $\text{TiO}_2/\text{silica}$ surface is negatively charged (Fig. 4.6) at pH 6.5, so there is an electrostatic repulsion to the negatively charged sulfonic group of methyl orange. It can be seen that the type of composite photocatalyst has a huge impact of the dye degradation especially in the presence of inorganic salts.

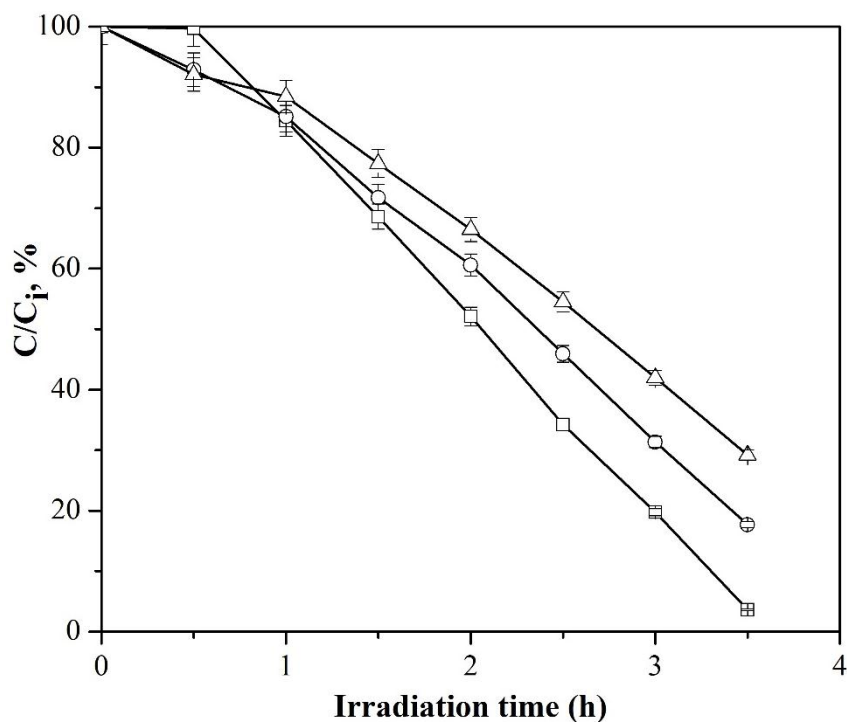


Figure 4.19. Effect of ions on methyl orange dye over $\text{TiO}_2/\text{silica}$: No ion (\square); NaCl (\circ); NaSO_4 (Δ) Condition: $C_0 = 25$ mg/L; $\text{TiO}_2/\text{silica} = 1.25$ g/L pH = 6.5

4.2.7 Equilibrium modelling of methyl orange degradation

An isotherm represent the equilibrium relationship between the substrate concentration in the liquid phase and that on the composite photocatalyst surface at a given condition. The parameters obtained from the different models provide important information on the surface properties of the composite photocatalyst and its affinity to the substrate. Several isotherm equations have been developed and employed for such analysis and the two important isotherms, the Langmuir and Freundlich (linear and non-linear forms) are applied in this study. For nonlinear form, error functions such as the residual root mean square error (RMSE) and chi-square test (χ^2) were used to evaluate the equilibrium model with the optimal magnitude. The linear plots for Langmuir and Freundlich models (Eqs. 2.12 and 2.15) are shown in Fig. 4.20 and the correlation coefficient R^2 values along with other parameters for Langmuir and Freundlich models are given in Table 4.4.

Clear deviations are observed in the Langmuir and Freundlich isotherm models. Figs. 25a and b show a straight line with a correlation coefficient (R^2) of 0.999 and 0.999 for $\text{TiO}_2/\text{zeolite}$ and $\text{TiO}_2/\text{silica}$, respectively, which indicates that the linear form of Langmuir isotherm could

fit the experimental data well than that of Freundlich isotherm model. Although, the R^2 values for linear regression of Langmuir models for both composite photocatalysts are high, both plots showed an influential point far away from the others (Fig. 4.20). Influential point is a point in the data set that is far away from the rest of the point and when this point is in accordance with the other point, it means it has a positive impact however when it pulls the regression line towards it, thus a negative impact since the regression line can have a different slope if obtained without this point (Belsley *et al.*, 1980). In this investigation, its effect was positive, implying that the influential point is in accordance with the other points and therefore strengthens the experimental data in the linearity of the regression line (Figs. 4.20a and b).

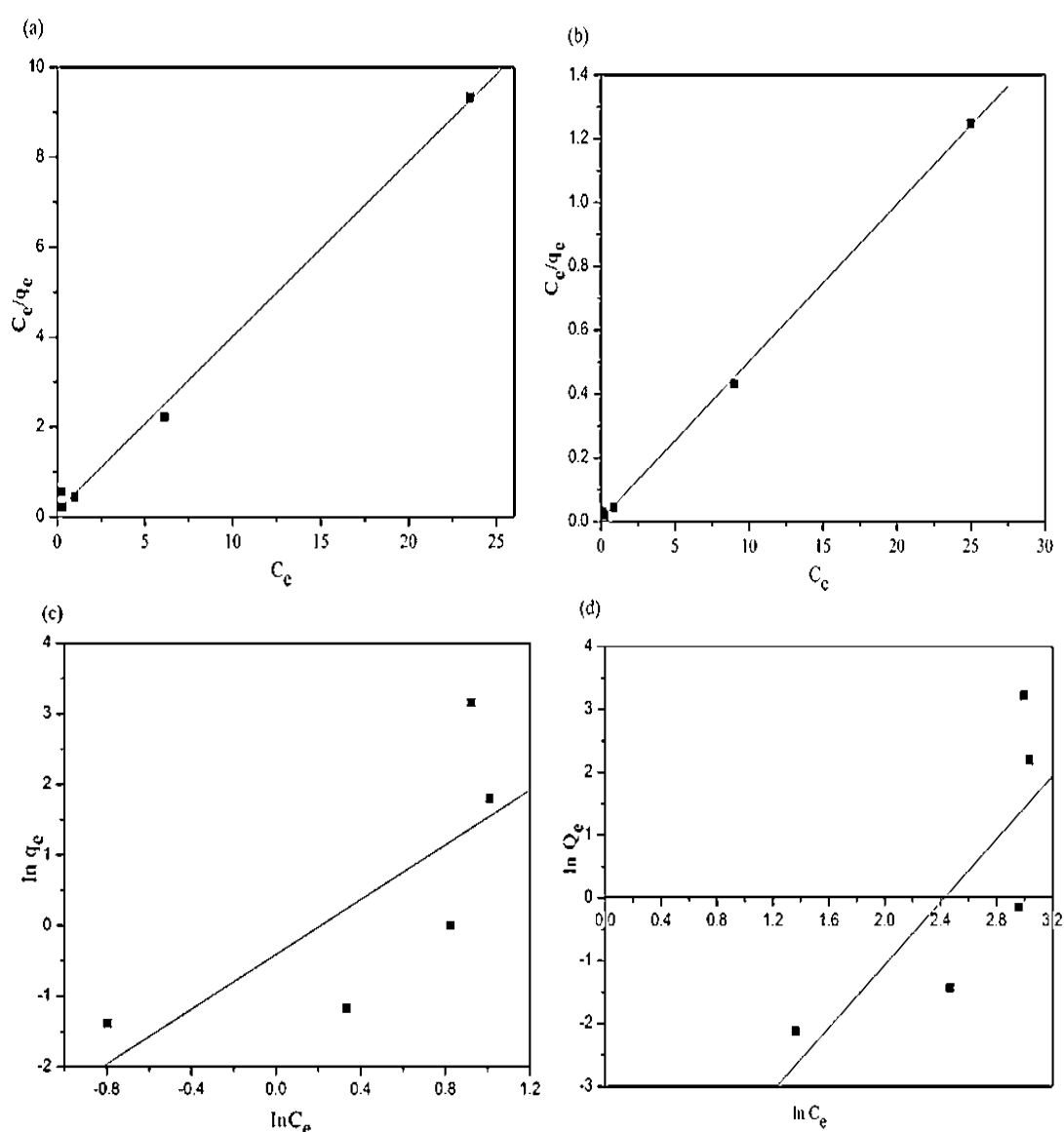


Figure 4.20. Linear transform of Langmuir isotherm over (a) $\text{TiO}_2/\text{zeolite}$ (b) $\text{TiO}_2/\text{silica}$ and Freundlich isotherm (c) $\text{TiO}_2/\text{zeolite}$ (d) $\text{TiO}_2/\text{silica}$

In the case of linear form of Freundlich model (Figs. 4.20c and d) low values of R^2 0.549 and 0.599 for TiO₂/zeolite and TiO₂/silica, respectively, shows a poor fitting in comparison to the linear form of Langmuir model (Figs. 4.20a and b). This observation is also reflected by the low ' n_f ' values which are less than 1 (Table 4.4) indicating that the Freundlich model is not representative enough to fit the equilibrium data. This implies that heterogeneous adsorption might not have occurred on the surface of both composite photocatalysts. In addition, the important characteristics of the Langmuir isotherm can also be expressed in terms of the dimensionless constant separation factor (R_L), which is defined by Weber and was applied earlier by Gupta *et al.* (2006). Equation 2.13 was used to calculate the R_L value and results are shown in Table 4.5. The R_L value is to be favorable at ($0 < R_L < 1$); unfavorable ($R > 1$), linear ($R_L = 1$) and irreversible ($R_L = 0$). Since all the values of R_L for both composite photocatalysts were less than 1 but greater than 0 at a concentration range of 5-50 mg/L, it can be confirmed that the linear form of Langmuir isotherm model suggesting that adsorption occurs at specific homogeneous sites within the substrate without any interaction between the adsorbed substances provide a good fit to the experimental data.

Table 4.4. Linear Fitting results of Langmuir and Freundlich isotherms for the degradation of methyl orange on composite photocatalysts.

Composite photocatalyst	Langmuir isotherms			Freundlich isotherms		
	qm (mg/g)	K (L/mg)	R^2	n_f	K_f (L/mg)	R^2
TiO ₂ /zeolite	2.574	2.9	0.999	0.516	0.665	0.549
TiO ₂ /silica	20.24	6.5	0.999	0.399	2.3×10^{-3}	0.599

Table 4.5. Values of R_L obtained for linear regression of Langmuir isotherm

Initial dye concentration (mg/L)	R_L (TiO ₂ /zeolite)	R_L (TiO ₂ /silica)
5	0.064	0.029
15	0.022	0.01
25	0.014	0.006
35	0.009	0.004
50	0.007	0.003

Figures 4.21 and 4.22 show the plot obtained by applying the nonlinear form of Langmuir and Freundlich model (Eqs. 2.11 and 2.14) and their output are given in Table 4.6. The Langmuir model showed a moderate fit with R^2 of 0.889 and 0.949 for $\text{TiO}_2/\text{zeolite}$ and $\text{TiO}_2/\text{silica}$, respectively. However a high R^2 of $\text{TiO}_2/\text{silica}$ was supported by low values of the RMSE and χ^2 than the $\text{TiO}_2/\text{zeolite}$ composite photocatalyst. In the case of nonlinear Freundlich model, the 'n' values were higher than 1, suggesting that the adsorption is possibly favorable. Thus, the adsorption of methyl orange on both composite photocatalyst represents a favorable uptake. However, the Freundlich model was not representative enough (especially for $\text{TiO}_2/\text{zeolite}$ composite photocatalyst) to estimate the equilibrium data, as reflected by the low R^2 (0.59) and high values of RMSE and χ^2 . Furthermore, a moderate Freundlich fit with R^2 value of 0.929 and low values of RMSE and χ^2 for $\text{TiO}_2/\text{silica}$ composite photocatalyst (Fig. 4.22) were obtained. This demonstrate that the nonlinear Freundlich model could be able to fit the experimental data as supported by the value of 'n_f' as 7.7186 which lies between 1 and 10.

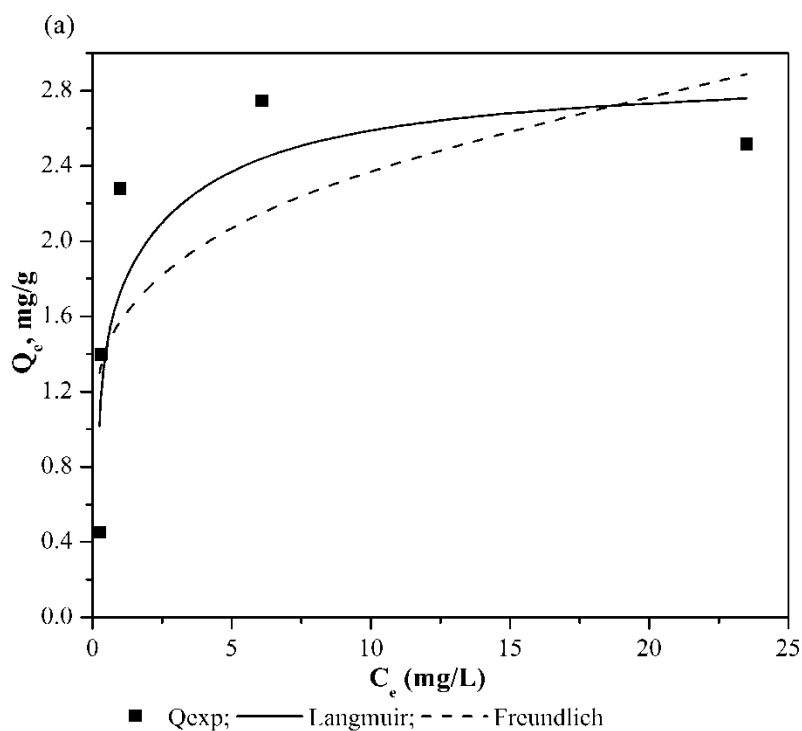


Figure. 4.21. Photodegradation isotherms of methyl orange on $\text{TiO}_2/\text{zeolite}$

However, the Freundlich model was found not to be representative enough to describe the data, as reflected by the low correlation coefficients as compared to the Langmuir model. Hence, the linear regression of Langmuir model suggesting homogeneous distribution of

active sites on composite photocatalyst surface was found to be the best fit. In addition, for TiO₂/silica composite photocatalyst, the linear regression of Langmuir model gave a better value of the maximum adsorption capacity of 20.24 mg/g for methyl orange without significantly affecting the quality of the fit, as the experimental values were close to the estimated values obtained by the model.

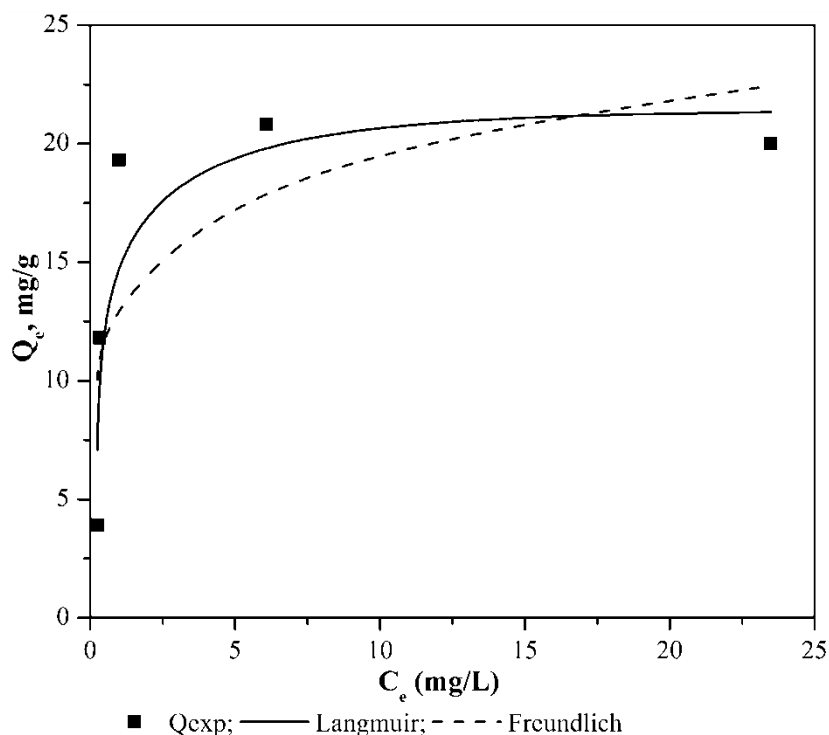


Figure 4.22. Photodegradation isotherms of methyl orange on TiO₂/silica

Table 4.6. Nonlinear Fitting results of Langmuir and Freundlich isotherms for the degradation of methyl orange onto composite photocatalysts.

Photocatalyst	Langmuir isotherm						Freundlich isotherm			
	Q _m	K	R ²	χ ²	RMSE	n _s	K _f	R ²	χ ²	RMSE
TiO ₂ /zeolite	2.811	2.266	0.889	0.132	0.282	5.676	1.655	0.59	0.796	0.639
TiO ₂ /silica	2.559	4.072	0.949	0.054	0.194	7.718	1.680	0.929	0.044	-4.413

Residual root mean square error (RMSE); chi-square test (χ²)

4.2.8 Kinetics modelling of methyl orange degradation

To determine the photodegradation kinetics of methyl orange, linear and nonlinear regression of the two kinetic models (pseudo first order and pseudo second order) were applied. The pseudo first order kinetic model is frequently used to predict photodegradation kinetics. This model proposes that the rate of change of solute uptake with time is directly proportional to difference in saturation concentration. The pseudo first order and pseudo second order equations are presented in section 2.8. These models are based on accumulation in the solid phase. The upper and lower confidence limits (95%) of the model prediction was also calculated. The goodness of fit of the nonlinear regression analysis to the experimental data were assessed by the R^2 , sum of the squares of the errors (SSE), sum of the absolute errors (SAE), average relative error (ARE) and average relative standard error (ARS).

Figures 4.23a and b show the linear regression of pseudo first order (Eq. 2.18) and pseudo second order kinetic models (Eq. 2.20), respectively. It can be seen that pseudo first order kinetic model was not applicable for the degradation of methyl orange by $\text{TiO}_2/\text{zeolite}$ composite photocatalyst, as indicated by the low R^2 than those of pseudo-second-order kinetics (Table 4.7). The kinetic data of methyl orange degradation by the $\text{TiO}_2/\text{zeolite}$ composite photocatalyst were also simulated by nonlinear regression of pseudo first order (Eq. 2.17) and pseudo second order (Eq. 2.19) models and results are shown in Fig. 4.23c and d. It is clear that nonlinear regression for both kinetic models was suitable for predicting the dynamic behavior of the semi-batch reactor with respect to inlet methyl orange concentration (25 mg/L). The results demonstrated that the values of q_e obtained by nonlinear regression are almost all consistent and have similarity with the linear transform values, which are also close to those obtained experimentally (Table 4.7). In most cases, however, non-linear fitting presented rate constants around two times higher than the linear ones. However, the pseudo second order predicted the photocatalysis kinetics better than pseudo first order. Considering the determined coefficients at the same condition, the value of R^2 from nonlinear regressive (pseudo second order) method was larger than that from nonlinear form of pseudo first order regressive method. In addition, nonlinear pseudo second order model provided lower error values of SSE, ARE and ARS at all experimental conditions. Similar findings are reported for the degradation of methyl orange on $\text{TiO}_2/\text{silica}$ composite photocatalyst (Fig. 4.24).

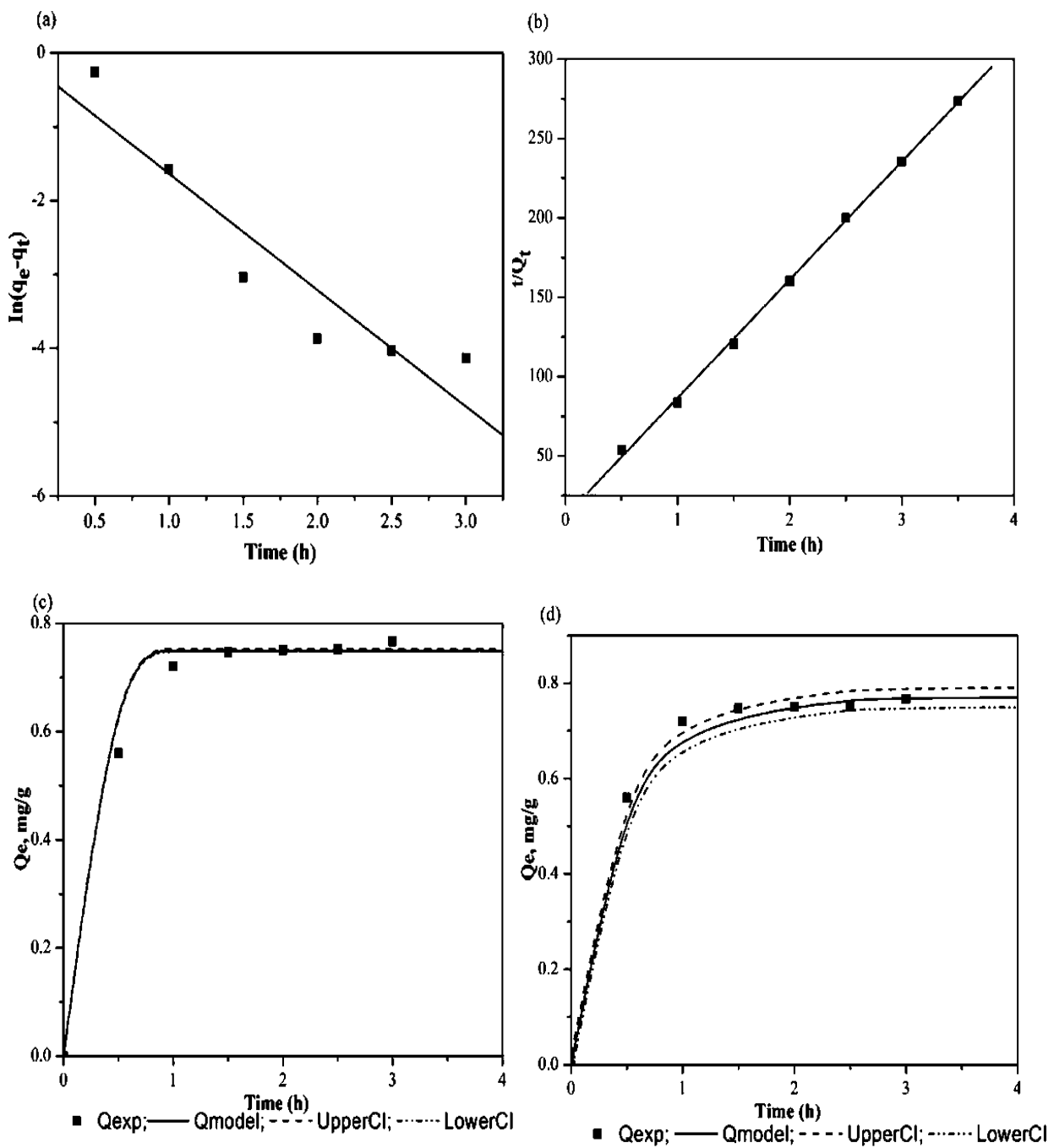


Figure 4.23. Linear regression of pseudo first order (a) and pseudo second order (b) model; nonlinear regression of pseudo first order (c) and pseudo second order (d) for dye degradation by $\text{TiO}_2/\text{zeolite}$ composite photocatalyst.

Table 4.7. Kinetic parameters for methyl orange photodegradation over TiO₂/zeolite composite photocatalyst

Pseudo first order kinetic model									
Linear			Nonlinear						
q_e (mg/g)	k_2 (min ⁻¹)	R ²	q_e (mg/g)	k_2 (g/ mg min)	R ²	SSE	SAE	ARE	ARS
0.499	0.029	0.9169	0.74974	1	0.997	0.037	-0.184	0.003	0.133
Pseudo second order kinetic model									
0.807	0.128	0.932	0.827	0.097	0.999	0.007	0.217	0.003	0.016

Sum of the squares of the errors (SSE), sum of the absolute errors (SAE), average relative error (ARE) and average relative standard error (ARS).

Figures 4.24a and b indicate that linear regression of pseudo-first-order model is not representative to describe the experimental data. This is also indicated by the low R² than those of pseudo-second-order kinetics (Table 4.8). This could be due to the fact that pseudo-first-order do not fit well with the whole range of contact time and is applicable only for the initial stage of degradation (Repo, 2011). It is evident that the pseudo second order gave the best fit to the experimental data since $q_{e,exp}$ and $q_{e,model}$ are close to each other (Figs. 4.24c and d). Furthermore, with respect to the R² and SSE, ARE and ARS values, the pseudo second order seems to describe well the experimental data. According to the Azizian's theory (2004), when the initial concentration value of the pollutant is not high the sorption fits better to the pseudo-second-order model than to the first-order model, which was also the case in this study since the kinetics models studies were conducted under the condition of dye initial concentration of 25 mg/L. The values of the pseudo-second-order rate constants showed faster degradation kinetics for TiO₂/silica and TiO₂/zeolite composite photocatalysts (Table 4.8). Therefore the dye degradation system is a second order reaction, based on the assumption that the rate limiting step may be chemi-adsorption, involving valence forces through sharing or exchange of electron (Gupta *et al.*, 2013).

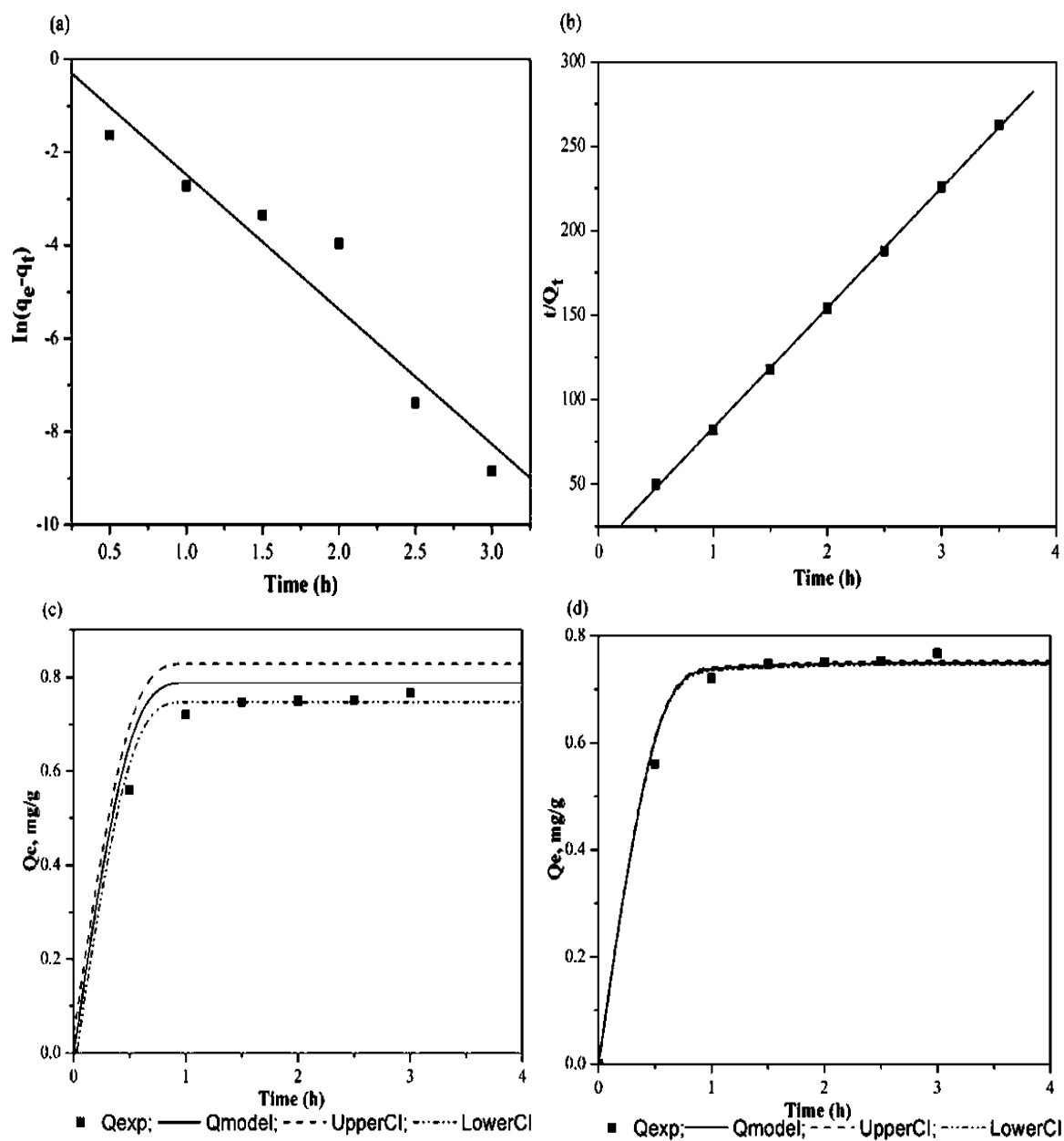


Figure 4.24. Linear regression of pseudo first order (a) and pseudo second order (b) model; nonlinear regression of pseudo first order (c) and pseudo second order (d) for dye degradation by $\text{TiO}_2/\text{silica}$ composite photocatalyst.

Table 4.8. Kinetic parameters for methyl orange photodegradation over TiO₂/silica composite photocatalyst

Pseudo first order kinetic model									
Linear			Nonlinear						
q _e (mg/g)	k ₂ (min ⁻¹)	R ²	q _e (mg/g)	k ₂ (g/ mg min)	R ²	SSE	SAE	ARE	ARS
0.95	0.122	0.936	0.7878	1	0.89	0.037	0.218	0.011	0.016
Pseudo second order kinetic model									
0.844	0.118	0.999	0.755	0.999	0.999	0.026	-0.14	0.003	0.01

Sum of the squares of the errors (SSE), sum of the absolute errors (SAE), average relative error (ARE) and average relative standard error (ARS).

4.2.9 Photocatalytic reduction with single substrate: Cr(VI)

In this study, photocatalytic reduction of Cr(VI) alone was conducted with solution containing 5 mg/L Cr(VI) and 6.25 g/L and 1.25 g/L of TiO₂/zeolite and TiO₂/ silica respectively, for 3.5 h illumination at pH 3 and 6.5. Figures 4.25a and b show a substantial photocatalytic reduction of Cr(VI) at pH 3 and this can be explained by the positively charged surface of the composite photocatalyst attracting the largest amount of negatively charged anions of Cr(VI). When the solution pH is low, negatively charged CrO₄²⁻ can associate with hydroxyl groups on composite photocatalyst surface via electrostatic attraction with positively charged Ti-OH leading to a better reduction (Asuha *et al.*, 2010). As the solution pH was increased from 3 to 6.5, the photoreduction decreased significantly. This is due to the electrostatic repulsion between negatively charged CrO₄²⁻ and the negatively charged surface of the composite photocatalyst, resulting in decrease in the reduction. Moreover, at high pH value, Cr(OH)₃ can cover the surface active position of TiO₂ due to the Cr(III) deposits on TiO₂ hindering the photocatalytic activity (Chen and Cao, 2005). Photocatalytic reduction of Cr(VI) has been investigated by several researchers using CdS and WO semiconductor catalyst (Chen and Ray, 2001). The general results showed that Cr(VI) can be easily reduced photocatalytically under UV irradiation and this was not in agreement with the results found in the present study.

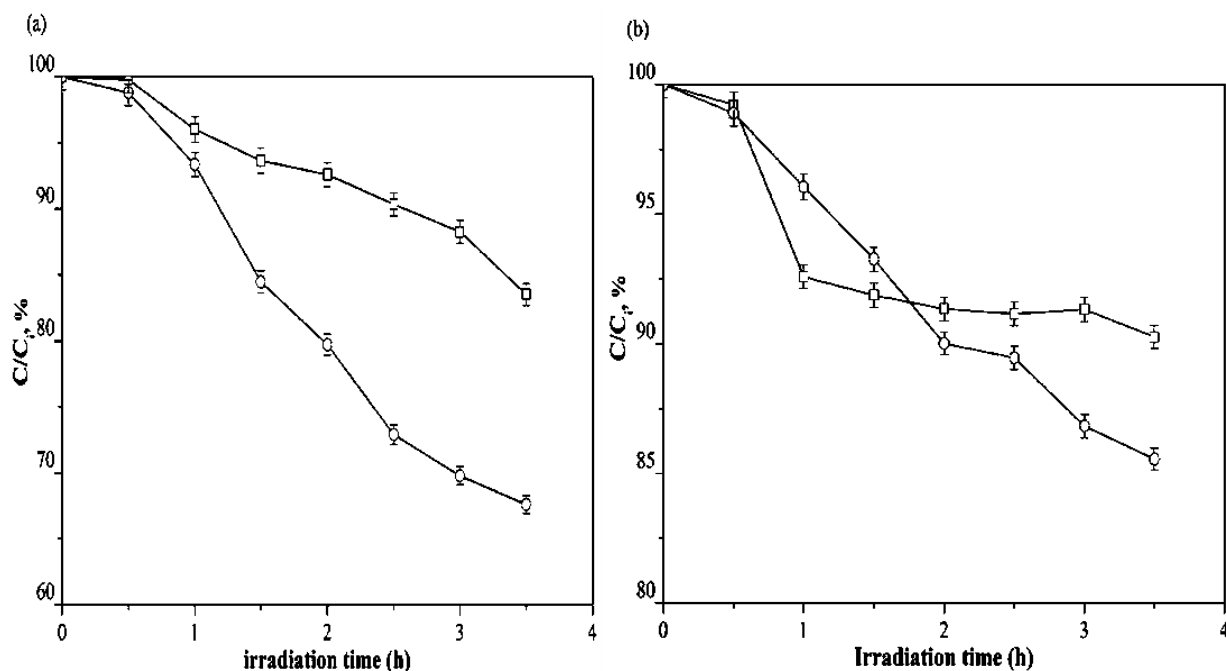


Figure 4.25. Photocatalytic reduction of Cr(VI) over (a) TiO₂/zeolite and (b) TiO₂/silica pH 6.5 (□); pH 3 (○)

4.2.10 A comparison of method analysis of Cr(VI) reduction in the mixed system

Metal ion Cr(VI) concentration in solution at different irradiation time intervals was determined by two different analytical methods, namely; direct monitoring the absorbance at its characteristic 348 nm band using UV-vis spectrophotometer and diphenylcarbazide colorimetric method (GB 7466-87, Standards of China) and results are shown in Fig. 4.26. When the Cr(VI) concentration was analyzed at 348 nm band by UV-vis spectrophotometer, the reduction of Cr(VI) in the presence of methyl orange was 29.3% even when the illumination was performed for as long as 3.5 h. The diphenylcarbazide colorimetric method revealed a contradictory observation. The reduction of Cr(VI) increased considerably when diphenylcarbazide colorimetric (56.2%) method was used. The decreased reduction by UV-vis spectrophotometer at 348 nm is ascribed to the deactivation of the photocatalyst which could be possibly due to the accumulation of metal complexes arising from the aromatics intermediate products on active sites (Papadam *et al.*, 2007). Considering the characteristic absorption band of Cr(IV) at 348 nm band as shown in Fig. 4.27, it can be seen that its band is not well separated from that of the methyl orange at 466 nm and the absorption spectrum of their mixture (curve c) is exactly the sum of their separate spectra.

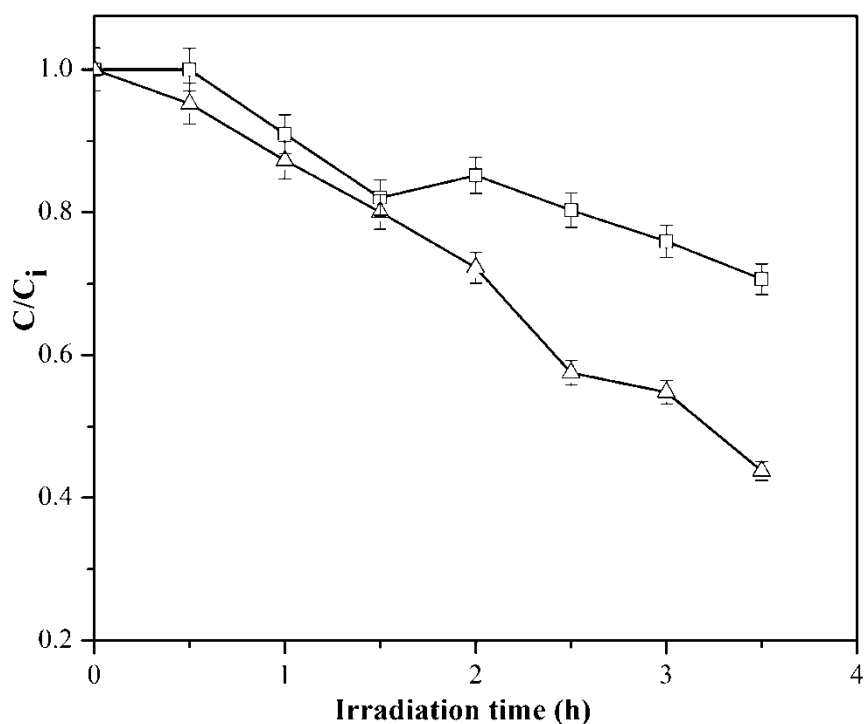


Figure 4.26. Photocatalytic reduction of Cr(VI) in the presence of methyl orange. Concentration of Cr(VI) were determined by UV-vis at 348nm (□), at 548 nm using the EPA method (○)

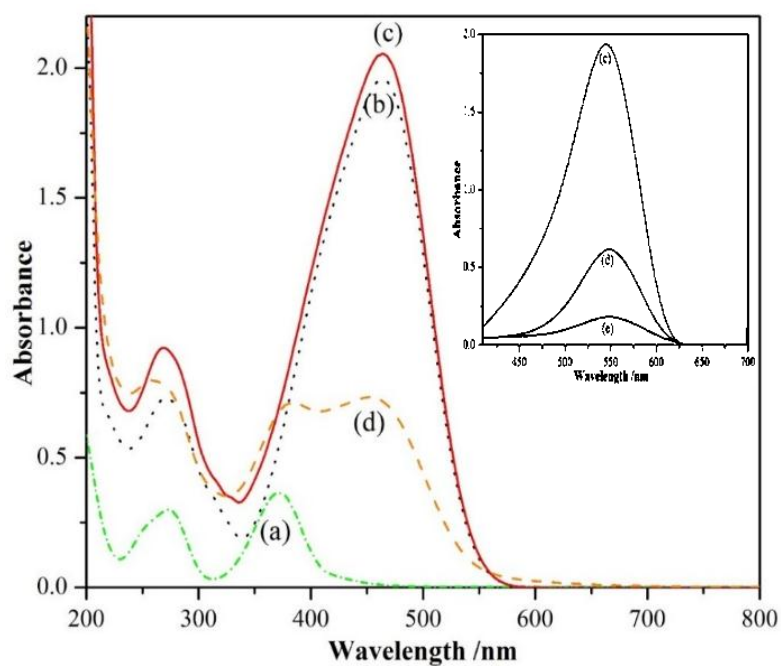


Figure 4.27. UV-vis absorption spectra of (a) Cr(VI), (b) methyl orange, (c) Cr(VI) + methyl orange before illumination, and the solution of (c) after being UV irradiated for (d) 2 h and (e) 3 h; inset; spectra of the Cr(VI) determination obtained using diphenylcarbazide colorimetric system

This demonstrated that the UV-vis spectrophotometer at 348 nm cannot be fully a reliable analytical method for Cr(VI) in the presence of methyl orange dye due to the possible absorption of the intermediate products that can interfere with the analysis. To overcome the interference of the intermediate products from the photocatalytic degradation of methyl orange on the Cr(VI) determination, the concentration of Cr(VI) can be determined by using the diphenylcarbazide colorimetric method (GB 7466-87, Standards of China). The diphenylcarbazide colorimetric method correspond well with the ion chromatographic measurement as defined in EPA method 218.6, which is similarly based on the fact that Cr(VI) reacts with diphenylcarbazide to form a colored product being far from the absorption peaks of the possible intermediate products as shown in the insets in Fig. 4.27. It is clear that this method explicitly gives the information on ion concentration whereas that of Uv-vis at 348nm is implicit and thus prone to intermediate compounds effect.

4.2.11 Photocatalytic degradation of the dye and reduction of Cr (VI), binary system

The effect of Cr(VI) on the photocatalytic degradation of methyl orange, an azo dye was studied at various experimental conditions in further experiments. Figures 4.28 and 4.29 show the degradation-time profiles as well as the final Cr(VI) reduction at different composite photocatalyst concentration which was conducted at pH 6.5 and 3. The initial dye concentration was kept constant at 25 mg/L. It can be seen that photocatalytic dye degradation efficiency on TiO₂/zeolite decreased with an increase composite photocatalyst concentration at pH 6.5 and pH 3 compared to the preliminary experiment of dye alone. It is remarkable to note from single dye/TiO₂-zeolite and dye/TiO₂/silica system (Fig. 4.15) that dye removal continuously proceeded faster than that of the respective binary dye/Cr(VI)/composite photocatalysts system, irrespective of the composite photocatalyst concentration and solution pH. This was more evident for the experiments executed at pH 6.5 and 6.25 g/L (TiO₂/zeolite) photocatalyst loading, for instance, the extent of color removal at 3.5 h of irradiation was 99.5% (Fig. 4.15a) and 80% (Fig. 4.28a) for the single and binary systems, respectively, with the values at pH 3 being 99.75% and 92.7% for the single and binary systems, respectively. Considering the effect of composite photocatalyst concentration at pH 6.5 and 3, the optimum TiO₂/zeolite concentration remained the same at 6.25 g/L for the methyl orange degradation in the presence of Cr(VI). The achieved optimum TiO₂/zeolite concentration is the same as the one in the absence of ion (Fig. 4.13). The dye degradation at 3.5 h of irradiation was 96.4% (Fig. 4.15b)

and 72.8% (Fig. 4.29a) for the single and binary systems, respectively, with the values at pH 3 being 99.8% and 76.17% for the single and binary systems, respectively. At pH 6.5, high photodegradation efficiency was observed with 1.25 g/L and 12.5 g/L for the single and binary systems, respectively.

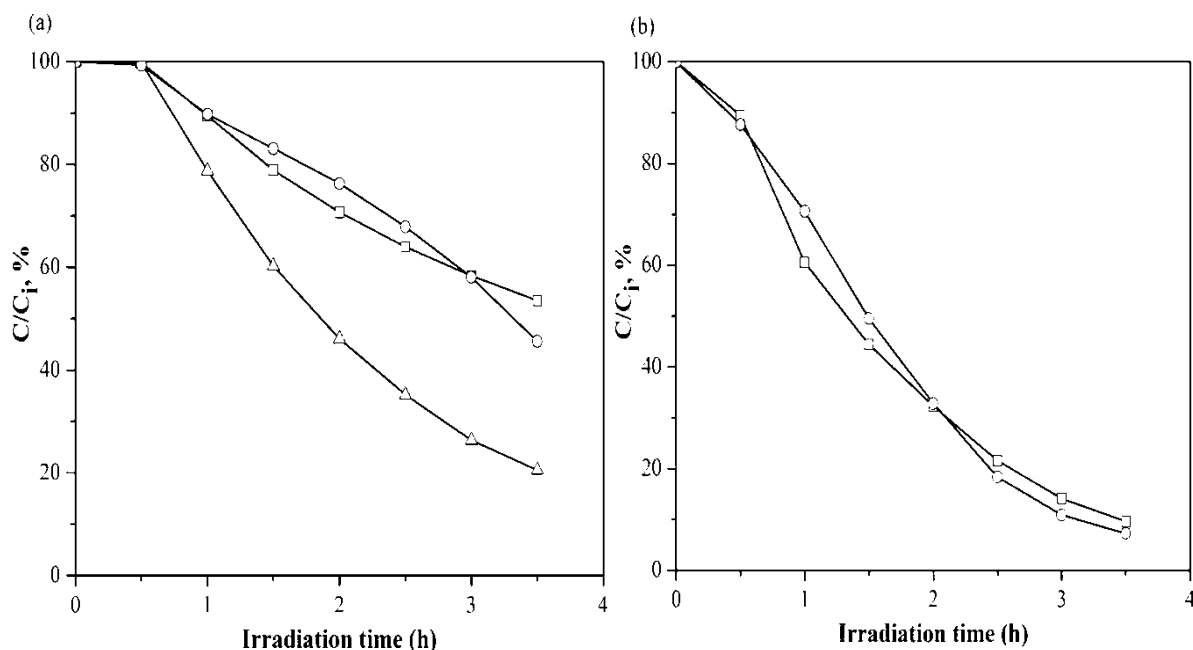


Figure 4.28. Effect of $\text{TiO}_2/\text{zeolite}$ concentration on dye degradation in the presence of Cr(VI) at (a) pH 6.5: 1.25 g/L (□); 6.25 g/L(Δ) 12.5 g/L (○)and (b) pH 3: 6.25 g/L (○); 12.5 g/L(□).

However, the maximum dye degradation was achieved with 12.5 g/L at pH 6.5 and pH 3. This clearly indicates that the dye degradation in the presence of Cr(VI) needed more active sites on $\text{TiO}_2/\text{silica}$ composite photocatalyst surface compared to the dye degradation alone (Fig. 4.14). This is due to the competition between the dye and metal ion for the active sites on $\text{TiO}_2/\text{silica}$ composite photocatalyst surface. It is clear that the degradation of methyl orange was more favoured at acidic conditions even in the presence of Cr(VI) , however the degradation of dye/composite photocatalysts system continued much faster than that of the respective binary dye/ Cr(VI) /composite photocatalyst system. Hypothetically, the photocatalytic reduction of Cr(VI) is expected to be more efficient in the Cr(VI) –dye system than in the single system due to the promoter effect by photocatalytic degradation of the dye. It is important to note that high metal reduction on $\text{TiO}_2/\text{zeolite}$ and $\text{TiO}_2/\text{silica}$ composite photocatalyst was achieved at 6.25 g/L and 12.5 g/L respectively, in spite of the pH solution.

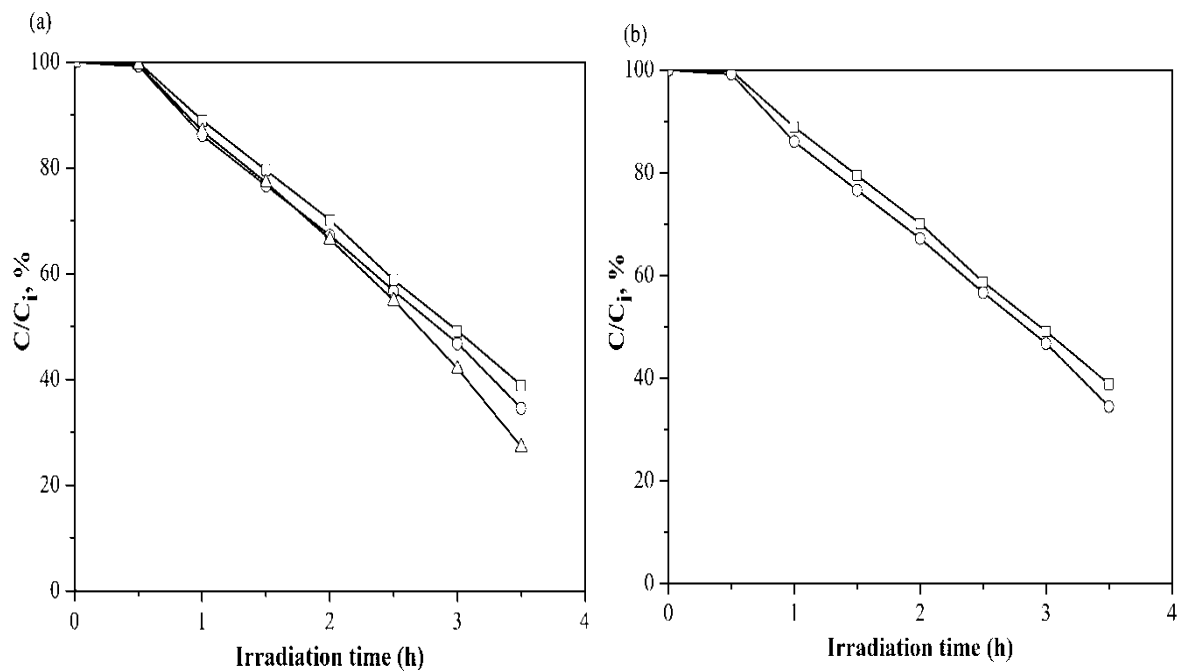


Figure 4.29. Effect of $\text{TiO}_2/\text{silica}$ photocatalyst concentration on dye degradation in the presence of Cr(VI) at (a) pH 6.5: 1.25 g/L (□); 6.25 g/L(Δ) 12.5 g/L (○) and (b) pH 3: 6.25 g/L (○)12.5 g/L (□)

This clearly indicates that during the binary system, an extent of Cr(VI) reduction and methyl orange degradation was achieved at the same optimum composite photocatalyst concentration. In such organic and metal ion compound coexisting systems, the dye receives holes from the electrons band directly or indirectly and is oxidized (Papadam *et al.*, 2007). This explains the fact that the photoreduction of Cr(VI) was much faster in the mixed system than in the single one. This fact can be attributed to the oxidation of dye consuming photo-excited holes quickly, which weakens electron–hole recombination promoting the photocatalytic reduction of Cr(VI) on the photocatalyst surface. The reduced photocatalytic efficiency in the mixed system can be due to the fact that both dye and dichromate anions compete for the equivalent composite photocatalyst active sites and, therefore, they have less probabilities to adsorb onto the photocatalyst surface and undergo photocatalytic reactions than in the individual single systems.

Moreover, the composite photocatalyst to some extent, becomes deactivated due to the formation of stable precipitates that hinder the active sites of the photocatalyst. For example, Chen and Cao (2005) reported that Cr^{3+} is likely to precipitate as Cr(OH)_3 at pH values beyond

4-5, therefore covering the photocatalyst surface. This agrees with the results obtained when Cr(IV) alone (Fig. 4.25) was photocatalytically reduced due to the slow reduction of Cr(IV) to Cr(III). Hence, the decline in photocatalytic activity was more distinguishable at near-neutral rather than acidic conditions. Furthermore, dye degradation intermediate products and chromic species can form complexes that also contribute to composite photocatalyst deactivation. Colon *et al.* (2001) investigated the simultaneous photocatalytic treatment of salicylic acid and Cr(VI) over various TiO₂ suspensions at pH 2 and reported that the conversion of both pollutants in the binary system was extensively lower than that in the corresponding single systems. This was due to the occurrence of photocatalyst deactivation as a result of trivalent chromium deposition on the active sites.

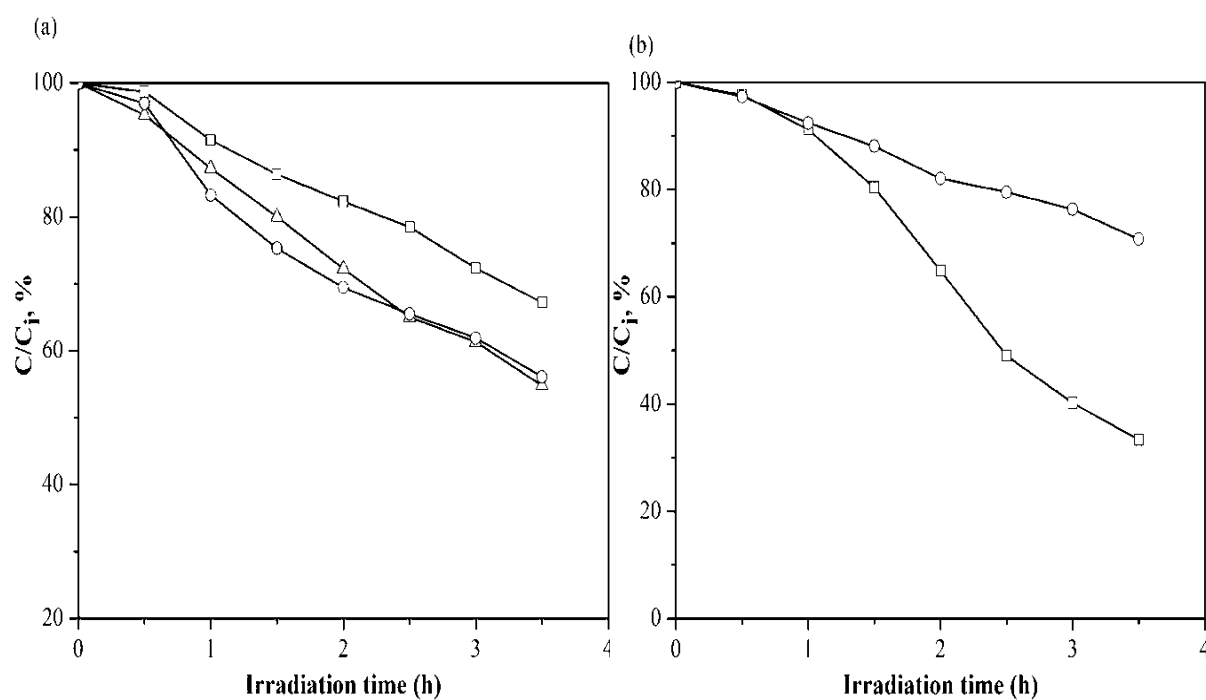


Figure 4.30. Effect of TiO₂/zeolite concentration on Cr(VI) reduction in the presence of dye; (a) pH 6.5: 1.25 g/L (□); 6.25 g/L (Δ); 12.5 g/L (○) and (b) pH 3: 6.25 g/L (○); 12.5 g/L(□).

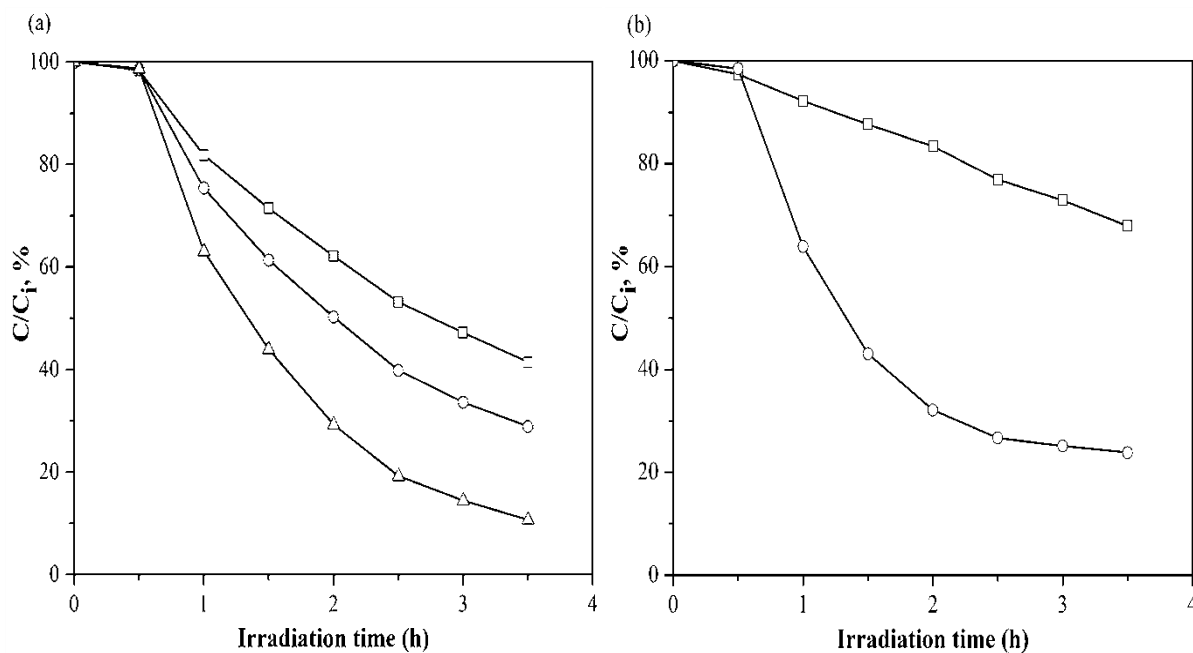


Figure 4.31. Effect of TiO₂/silica concentration on Cr(VI) reduction in the presence of dye; (a) pH 6.5: 1.25 g/L (□); 6.25 g/L (○); 12.5 g/L (Δ) and (b) pH 3: 6.25 g/L (□); 12.5 g/L (○).

In the final set of experiments, the effect of Cr(VI) concentration on the photocatalytic efficiency of methyl orange was evaluated at optimum conditions. Figure 4.32 shows that high photocatalytic degradation efficiency of methyl orange on TiO₂/zeolite composite photocatalyst was achieved with the increase of Cr(VI) concentration initially, however, decrease was observed when Cr(VI) concentration is beyond 2 mg/L. When the Cr(VI) initial concentration was increased from 2 mg/L to 5 mg/L and 10 mg/L, the degradation efficiency decreased from 93% to 79.5% and 75% for 5 mg/L and 10 mg/L, respectively. Similar trend was observed for dye degradation on TiO₂/silica composite photocatalyst, the degradation efficiency was 94.8% at 2 mg/L and decreased to 76.1% and 65.6% at 5 and 10 mg/L metal concentration, respectively (Fig. 4.33). The increase in degradation efficiency at low metal initial concentration can be due to the reaction in the hole photogenerated in the presence of Cr(VI) whose photoreduction is also favored in the presence of organic compounds. This aspect is important due to the high affinity of the dye to the composite photocatalyst surface as well as the production of more electrons in the conduction band. However, as the metal concentration increased, the dye degradation decreased and this may be attributed to more metal ions adsorbed onto TiO₂/zeolite and TiO₂/silica composite photocatalyst surface then block the adsorption of methyl orange molecules.

The reduction of Cr(VI) was found to increase up to an initial concentration of 5 mg/L and then declined significantly (Figs. 4.32 and 4.33). As the Cr(VI) initial concentration increases, available photons were inadequate to reach the composite photocatalyst surface due to light screening effect which may result in slower regeneration of the photogenerated pair hole/electron. Consequently, the photocatalytic activity decreased, since few electrons were available to reduce more Cr(VI) ions to Cr(III). The main part of degradation occurs in the area near the irradiated side (known as reaction zone) where the irradiation intensity is much higher (Konstantinou and Albanis, 2004). This indicates that the metal reduction declines at sufficiently long distances from the UV light or the reaction zone due to the obstruction in the penetration of light. Hence, it is clear that as the initial concentration of the Cr(VI) increases, the active species on composite photocatalyst surface needed for the reduction of the metal also increase.

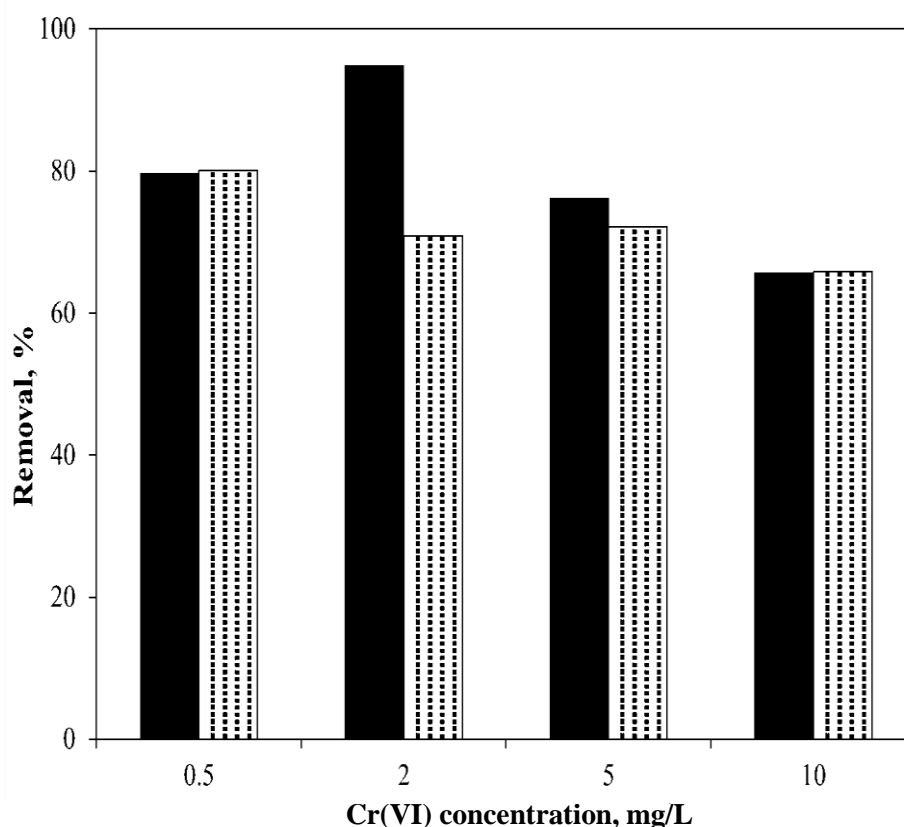


Figure 4.32. Effect of Cr(VI) initial concentration on dye degradation (black bars) over $\text{TiO}_2/\text{zeolite}$ and final Cr(VI) reduction (hatched bars). Condition: $C_0 = 25 \text{ mg/L}$; $\text{pH} = 3$

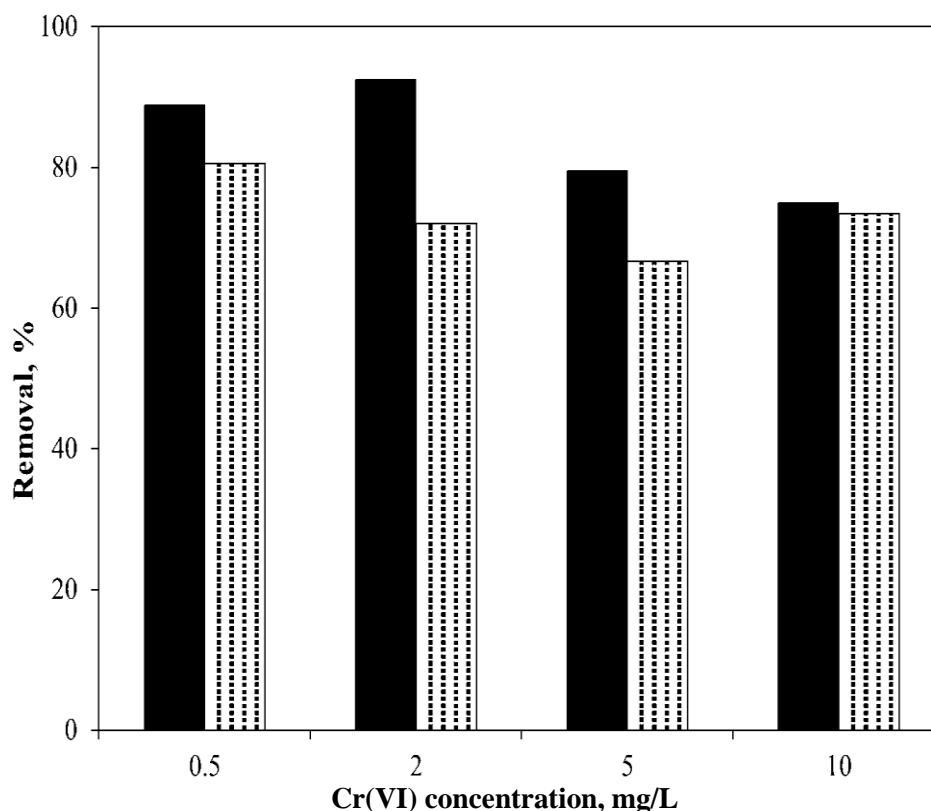


Figure 4.33. Effect of Cr(VI) initial concentration on dye degradation (black bars) over $\text{TiO}_2/\text{silica}$ and final Cr(VI) reduction (hatched bars). Condition: $C_0=25$ mg/L; pH= 3

4.3 Mineralization

A complete degradation of the target organic pollutant by photocatalysis treatment usually leads to the conversion of all its carbon atoms to gaseous CO_2 , and inorganic anions that remain in solution. In order to assess the degree of total mineralization of methyl orange over composite photocatalyst, TOC and inorganic ions formation, as a function of the irradiation time were evaluated. For this analysis, $\text{TiO}_2/\text{zeolite}$ composite photocatalyst was used for the experiment. The ion chromatography analysis allowed qualitative and quantitative monitoring of inorganic ions resulting from the photocatalytic treatment of methyl orange aqueous solution.

4.3.1 TOC analysis

Dye degradation takes place through the oxidative cleavage of the chromophore N=N bond resulting in the production of primary reaction by-products which are then oxidized and ultimately yielding carbon dioxide and water (MacKay and Pignatello, 2001). The TOC concentration is of importance as it is the best parameter to indicate the ultimate mineralization of the target compound. Figures 4.34 and 4.35 show the TOC reduction at different concentration of methyl orange solution and pH solution. As seen in Fig. 4.15, high colour removal was followed by low to moderate levels of TOC reduction. For instance, only 47% of TOC content was reached, while over 99% of the degradation efficiency was achieved at 5 mg/L. This means that the organic carbon initially present in the azo dye had been converted into other organic compounds that could not be easily mineralized and eventually accumulate in the reaction mixture. Augugliaro *et al.* (2002) observed a complete decolorization of methyl orange in few hours but mineralization occurred after a longer time with the formation of CO₂, nitrates and sulfates.

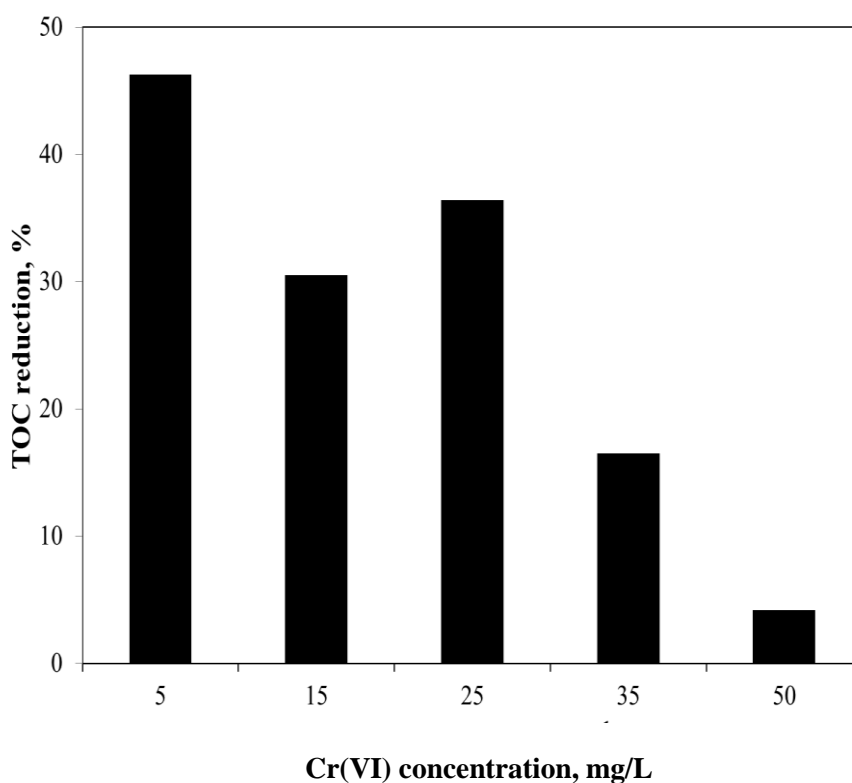


Figure 4.34. TOC reduction at different dye concentration. TiO₂/zeolite = 6.25 mg/L, pH = 6.5.

Although colour removal was achieved in less than 3 h irradiation, a high TOC reduction would require more time to achieve. At acidic conditions, the TOC reduction was more favored than at pH 7 and 9. At low pH values, the photocatalyst surface is positively charged and is simply effective in adsorbing the methyl orange having a negative charge, thus electrostatic attraction of the positively charged composite photocatalyst with the target dye. Due to the Coulombic repulsion at alkaline conditions, substrate is barely adsorbed. Hence, the reduced degree of mineralization was observed at high pH values. The TOC reduction was low, and a complete mineralization would need a long-time irradiation. This implies that in this case the heterogeneous photocatalysis is more suitable to be used as a pre-treatment method for reducing dye toxicity and improving the biodegradability of textile wastewaters.

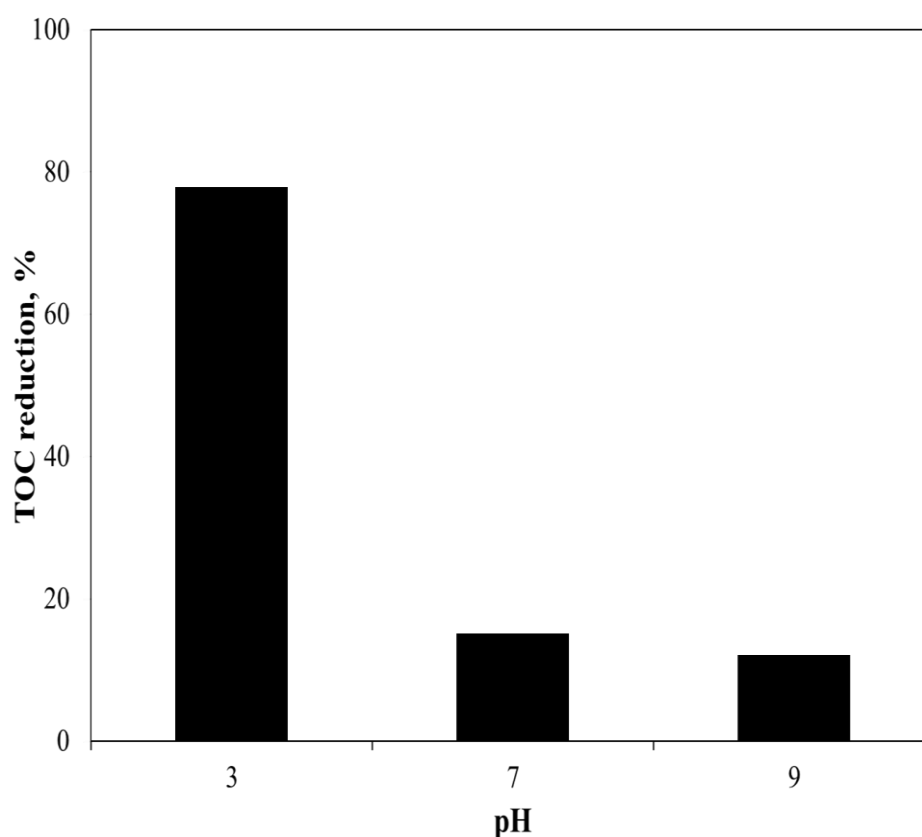


Figure 4.35. TOC reduction at different pH values. Condition: $C_0 = 25$ mg/L; $TiO_2/zeolite = 6.25$ mg/L

4.3.2 Identification and evolution of inorganic ions

The ion chromatography analysis allowed qualitative and quantitative monitoring of inorganic ions resulting from the heterogeneous photocatalysis treatment of 25 mg/L methyl orange aqueous solution using TiO₂/zeolite. Figure 4.36 presents the evolution of the released SO₄²⁻, PO₄³⁻, NO₂⁻ and NO₃⁻ ions concentration during heterogeneous photocatalysis. The concentration of SO₄²⁻ ions released from methyl orange mineralization reached the value of 0.133 mg/L in the first hour of photocatalysis. This showed that most of the sulfonyl group present in methyl orange structure were oxidized at the early stage of the treatment. The formation of SO₄²⁻ and PO₄³⁻ can be accounted by an initial attack by a photo-induced •OH radical. The cleavage of the chromophore N=N bond of methyl orange led to the formation of the intermediates containing (–NO₂) and (–NO₃) substituents (Guivarch *et al.*, 2003). These groups are oxidized to nitrate ions during the mineralization of corresponding intermediates by hydroxyl radicals.

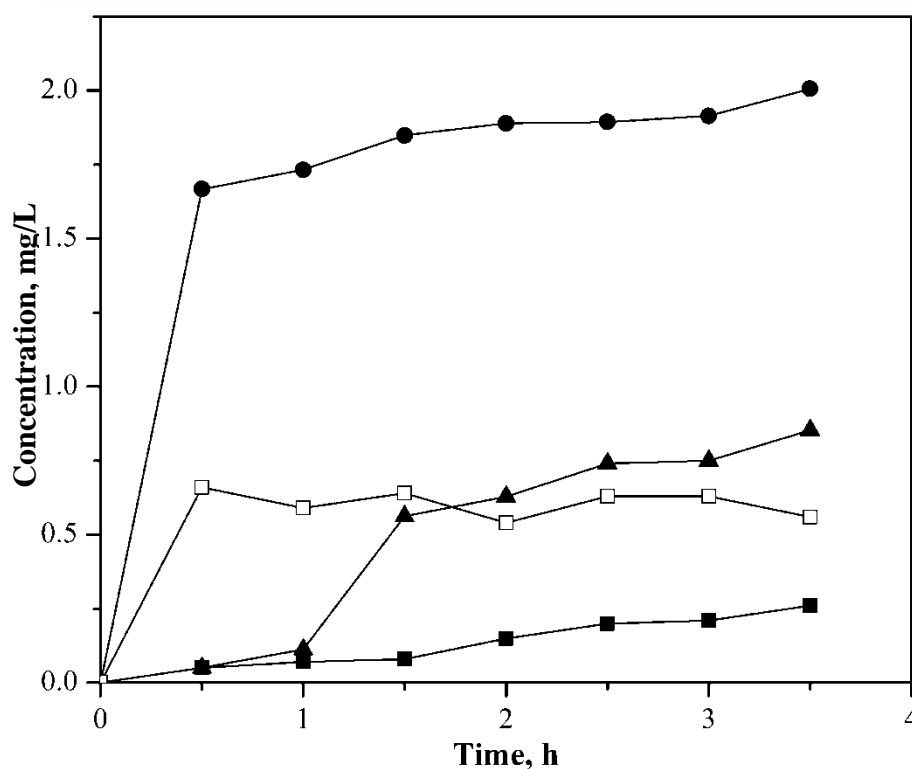


Figure 4.36. Time-course of inorganic ions concentration during heterogeneous photocatalysis treatment of an aqueous solution of methyl orange on TiO₂/zeolite:

NO₂⁻ (■); NO₃⁻ (●); SO₄²⁻ (▲); PO₄³⁻ (□)

4.3.3 Degradation of intermediate products

Identification of intermediate products is one of the keys to maximizing the overall photocatalysis process efficiency. Due to the fact that hydroxyl radicals react non-selectively, different by-products are released at low concentration levels. The intermediate organic products of photocatalysis were analyzed by gas chromatography coupled with mass spectrometry (GC/MS) operated in selected-ion- monitoring (SIM) mode and Fourier transform infrared (FTIR). Their GC retention times (t_R), molecular weights (M_w) and main spectrum are given in Table 4.9. N-Methylbenzenamine, N-Acrylonitril-2,2-dimethylaziridine and 5-Ethyl-2-methyl-pyridin-4-amine were identified by their mass spectra. The identified intermediate products showed that the heterogeneous photodegradation process took place through C–N cleavages. The intermediate products from the photodegradation of azo dyes have been reported for other oxidation treatment processes. In the photo-Fenton degradation of methyl orange, 4-dimethylamino aniline was detected by using gas chromatography/mass spectrometry (GC/MS), proposing an N–N bond cleavage of the azo linkage (Chen *et al.*, 2008). In the present work, different products from the ones reported were detected and this might have been due to the different degradation mechanisms involving different radicals as well as to the different experimental conditions and analytical techniques employed in various studies.

Table 4.9. GC/MS analytical results

Degradation intermediates	t_R (min)	M_w	Main fragment ions (m/z)
N-Methylbenzenamine	3.390	107	107, 106, 104, 79, 77, 51
N-Acrylonitril-2,2-dimethylaziridine	2.558	122	65, 93, 136, 66, 120, 137, 121
5-Ethyl-2-methyl-pyridin-4-amine	2.875	136	39, 42, 52, 66, 80, 94, 108, 121,136

Nevertheless identified intermediate products were confirmed by FTIR analysis. Figure 4.37 illustrates the FTIR spectra of methyl orange and the extract from the samples irradiated at a loading of 6.25 g/L TiO₂/zeolite composite loading for 3.5 h with an initial methyl orange

concentration of 25 mg/L. FTIR spectra of raw (control) methyl orange display peak at 2958.7 cm^{-1} , which correspond to the characteristic band of C–H stretching of methyl groups (Chen *et al.*, 2008). Comparison of the spectra of raw methyl orange and extract from the irradiated sample clearly showed that the band between 3000 and 3400 cm^{-1} , assigned for N–H bend and the bands of benzene rings at 1454.276 and 756.06 cm^{-1} significantly decreased in the spectrum of the extracted sample. It is interesting to note that no significant destruction of the aromatic components occurred on the composite photocatalyst after the photocatalytic treatment. This is evidenced by the persistence of the band associated to the aromatic C=C vibrations at 1454 cm^{-1} (Fig. 4.37a). However, from Fig. 4.37b, it is be noted that the band of aromatic groups reduced. This finding confirms that the sulfonate group of the dye were not present after the treatment, this shows a strong interaction of these groups of methyl orange with the composite photocatalyst surface. The C–N stretching signal is raised in the region of 1350 – 1000 cm^{-1} (Silverstein *et al.*, 1981). In the present compound, the C–N stretching vibrations are observed at 1924 and 1236.32 cm^{-1} . These results confirmed the degradation of methyl orange and the formation of intermediate products during heterogeneous photodegradation.

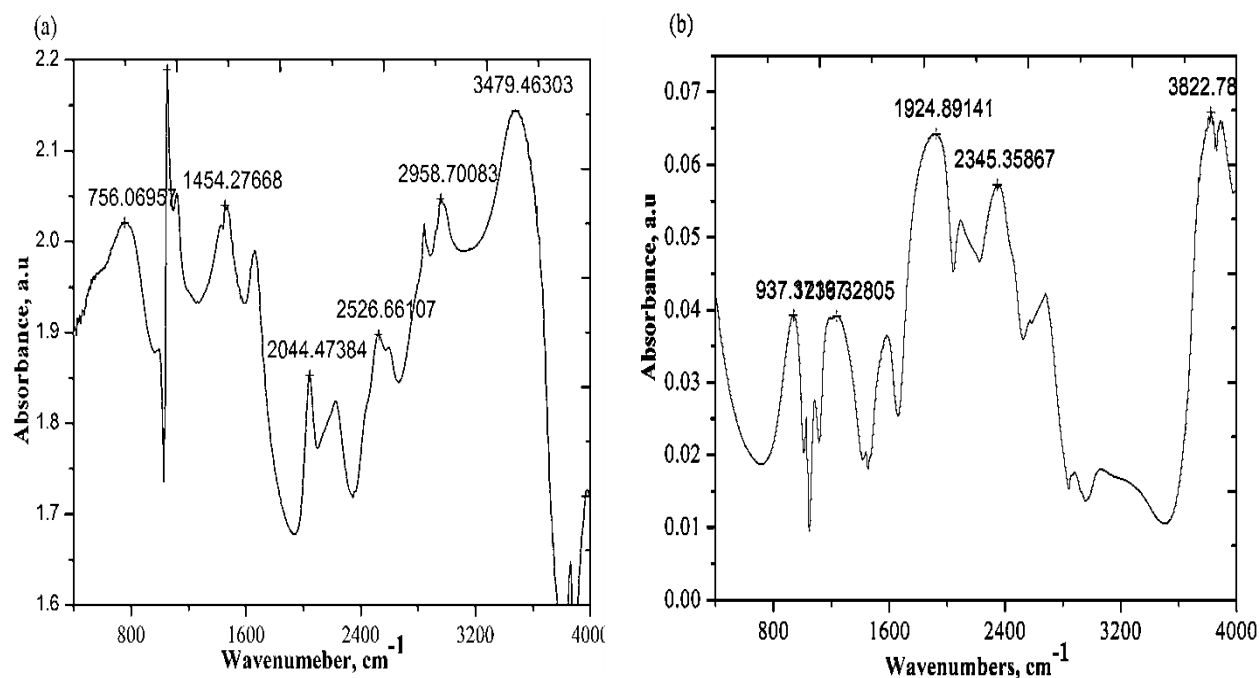


Figure 4.37. FTIR spectra of (a) raw methyl orange; (b) extracted methyl orange at 6.255 g/L $\text{TiO}_2/\text{zeolite}$ and 25 mg/L initial concentration after 3.5 h irradiation

4.4 Photocatalytic degradation of pesticides

Degradation of atrazine was carried out using the semi-batch reactor under UV light. In this study, TiO₂ supported on silica was used since the results reported on the degradation of methyl orange revealed that zeolite hinders light penetration despite its adsorption capability. As a result, silica was used as supporting material due to its light transparent nature which helps in attracting the pollutants to the vicinity of the TiO₂ surface and consequently leads to efficient degradation. An extensive characterization of the composite photocatalyst employed in the photocatalytic experiments is already reported in Section 4.1. Effects of different operating parameters on pesticide degradation by the prepared composite photocatalyst were determined.

4.4.1 Effect of composite photocatalyst size

To study the effects of particle size on atrazine degradation, the TiO₂/silica composite photocatalyst was prepared and crushed to different particle sizes and the results are shown in Fig. 4.38. It is noticed that the TiO₂/silica composite of 38-75 μm size was most effective for the degradation of atrazine, and was thus used for further studies. This behavior can be accounted for by considering that the smaller sized particles provide greater surface area, causing enhanced degradation rate. At 150-200 μm particle size, the photodegradation was slow, taking into account the SEM-EDX results, it was shown that though Ti was detected on 150-250 μm particle size surface, however, TiO₂ was not well supported as compared to other particle sizes. Similar trend was reported for the degradation of methyl orange on TiO₂/silica.

4.4.2 Effect of composite photocatalyst loading

Figure 4.39 presents the effect of TiO₂/silica concentration on the degradation of atrazine. The degradation efficiency is shown to increase with an increase in composite photocatalyst concentration up to 6.25 g/L and, on further increase in photocatalyst concentration lead to a decrease in degradation efficiency. This is attributed to the working conditions of the photoreactor where the surface reaction is initiated upon light photon absorption (Bamba *et al.*, 2008). When the composite photocatalyst concentration increases above an optimum level, the light photon absorption is reduced. However, such a light attenuation over the radial distance could not be well correlated with the Beer-Lambert Law owing to the scattering of light photons by the excess concentration of TiO₂/silica composite photocatalyst (Chong *et al.*, 2010).

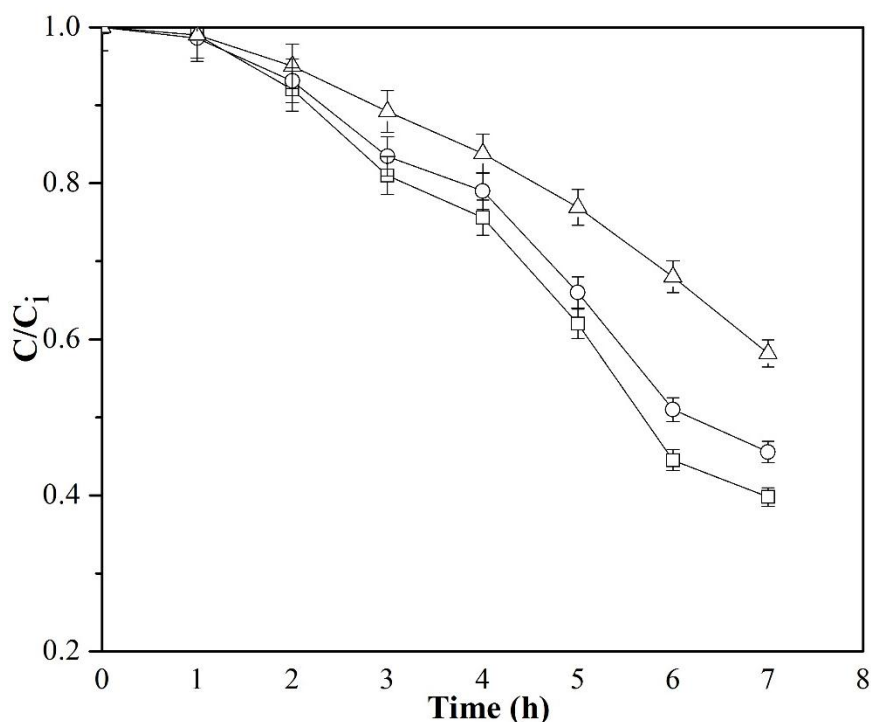


Figure 4.38. Effect of particle size for atrazine degradation on $\text{TiO}_2/\text{silica}$ at 1.25 g/L loading and 10 mg/L atrazine initial concentration 38-75 μm (\square); 75-150 μm (\circ); 150-250 μm (Δ)

The excess $\text{TiO}_2/\text{silica}$ particles can create a light screening effect that reduces the surface area of composite photocatalyst being exposed to light illumination and the photocatalytic efficiency. Although the number of active sites in solution will increase with catalyst concentration, a point appears to be reached where light penetration is compromised due to excessive particle concentration. A further increase in photocatalyst concentration beyond the optimum will result in non-uniform light intensity distribution, so that the reaction rate would indeed be lower with increased photocatalyst dosage. Similar trends were reported in section 4.2.3 for the photodegradation of methyl orange. The study conducted Sakthivel *et al.* (2003) also showed that above a 2000 mg/L of loading the reaction rate decreased. This was explained in terms of availability of active sites on photocatalyst surface and the light penetration of photoactivating light into the solution. Therefore, 6.25 g/L of $\text{TiO}_2/\text{silica}$ concentration was used in further experiments to avoid aggregation of $\text{TiO}_2/\text{silica}$ particles at high concentrations.

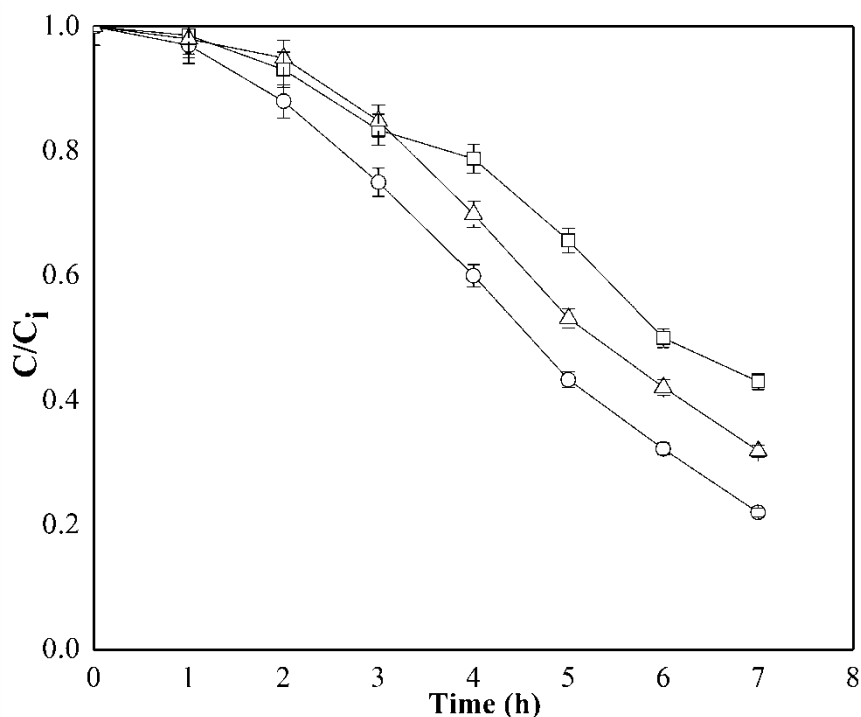


Figure 4.39. Effect of $\text{TiO}_2/\text{silica}$ concentration on pesticide degradation: 1.25 g/L (\square); 6.25 g/L (\circ); 12.25 g/L (Δ). Condition: $C_0 = 10$ mg/L; pH= 5.1

4.4.3 Effect of atrazine concentration

It is important both from a mechanistic and an application point of view to determine the dependence of the photocatalytic efficiency on the pollutant concentration. The effect of pesticides concentration on $\text{TiO}_2/\text{silica}$ was determined by varying the initial atrazine concentrations (Fig. 4.40). The degradation of atrazine proceeds in a shorter time period at lower concentrations, as anticipated. This can be accounted for by considering the availability of hydroxyl groups available at the $\text{TiO}_2/\text{silica}$ surface of the catalyst particles. The production of OH radicals on the composite photocatalyst surface is not adequate in comparison to the amount of atrazine adsorbed on the surface of the photocatalyst at higher concentrations. At high atrazine concentrations the production of OH radicals on the surface of composite photocatalyst is reduced since the active sites are covered by pesticides ions. Similar trend were observed from the studies conducted by Sakthivel *et al.* (2003). The major fragment of degradation occurs in the region near the irradiated side where the irradiation intensity is much higher than in the other side (Konstantinou and Albanis, 2004). Thus at higher atrazine concentration, degradation decreases at sufficiently long distances from the light source due to the hindrance in the penetration of light. As a result, there should be an equilibrium between

adsorption of reactant molecules and the generation of OH radicals from the TiO₂/silica active sites.

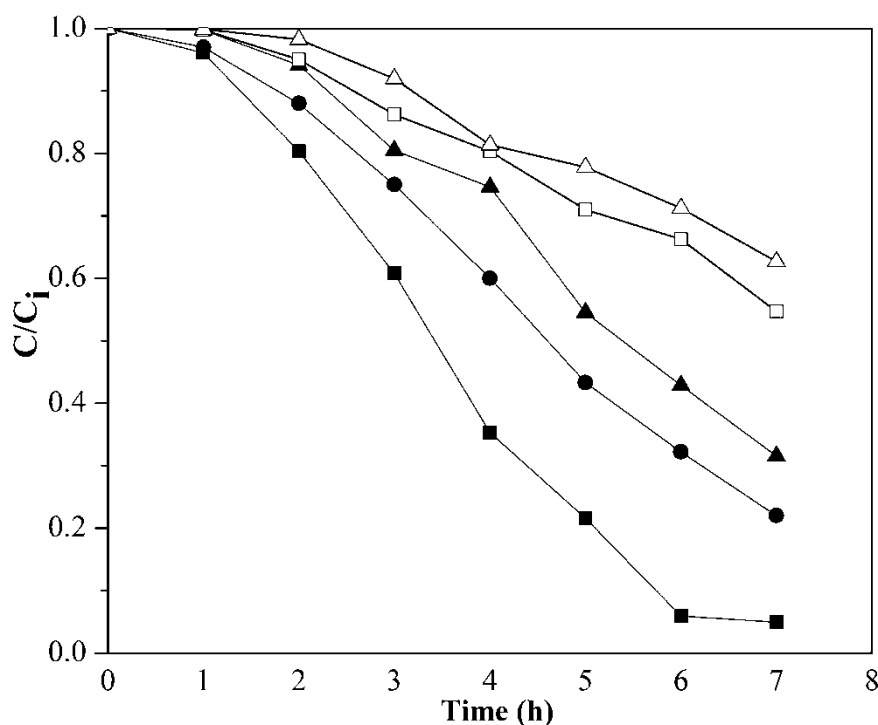


Figure 4.40. Effect of atrazine concentration on TiO₂/silica at pH 6.5 and 6.25 g/L loading 5 mg/L(■); 10 mg/L (●); 15 (▲); mg/L; 20 mg/L (□); 25 mg/L(Δ)

4.4.4 Equilibrium modelling of atrazine degradation

The linear plots for Langmuir and Freundlich modelling using (Eqs. 2.12 and 2.15) are shown in Figs. 4.41 and 4.42, the correlation coefficient R^2 values along with other parameters for these models are given in Table 4.10. Figure 4.41 gave a straight line with a correlation coefficient of 0.999 which indicates that the degradation of atrazine onto the TiO₂/silica fits the Langmuir isotherm reasonably well. The essential characteristics of the Langmuir isotherm expressed in terms of the dimensionless constant separation factor (R_L), is also applied in this study (Table 4.11). The values are found to vary between 0.062 and 0.012 with a maximum adsorption capacity (q_e) of 1.619 mg/g. Freundlich isotherm, from Fig. 4.42, the intercept and slope gave the values of K_f and n_s as 1.013 and 0.168, respectively (Table 4.10).

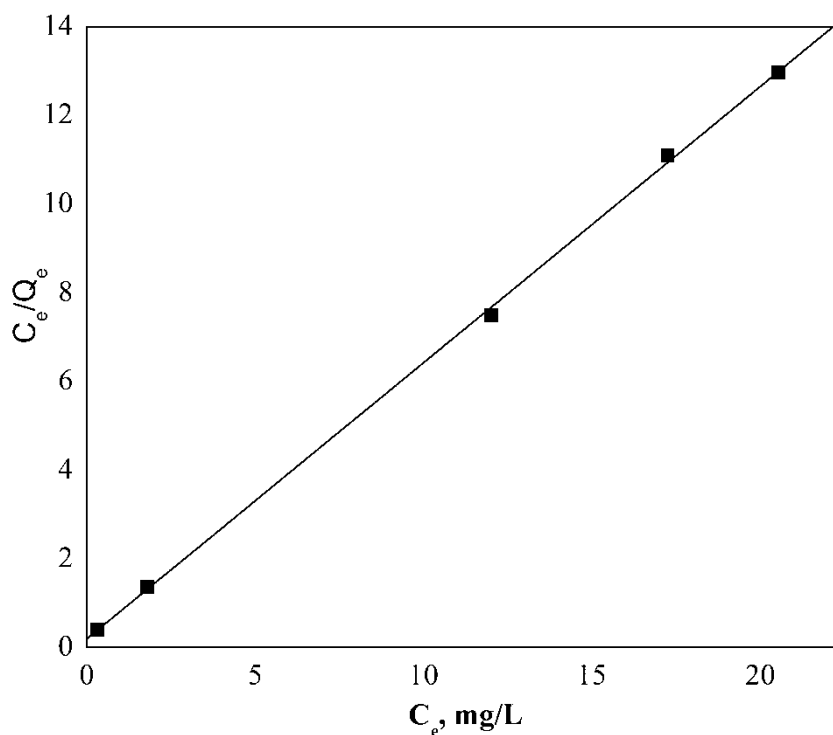


Figure 4.41. Linear transform of Langmuir isotherm over TiO₂/silica

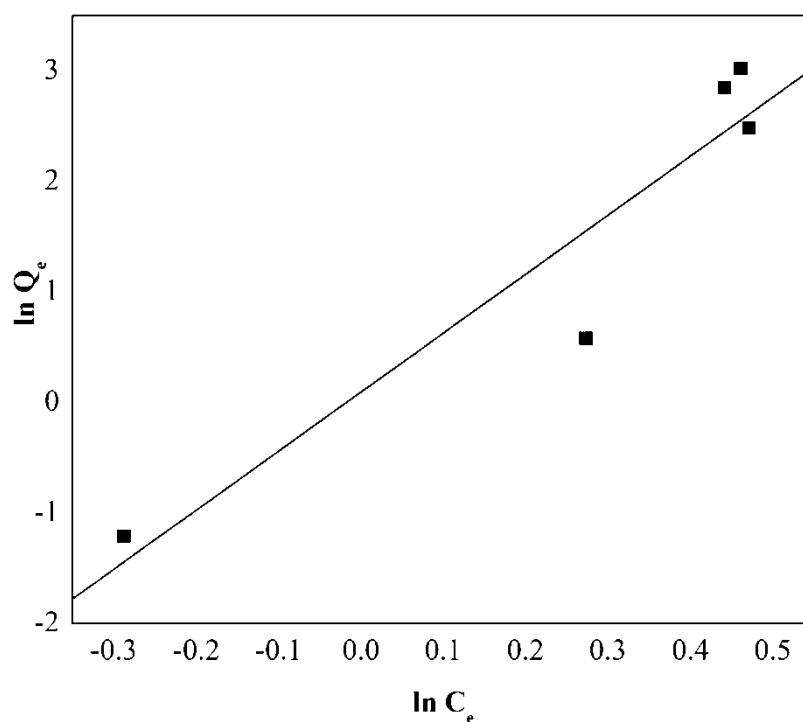
The parameters K_f and n_f indicated the adsorption capacity and the adsorption intensity of the system. The values of 'n' in the range of 1 to 10 represent high-quality adsorption (Freundlich, 1906). In this study, the exponent n indicates favorable adsorption, which is in agreement with the findings of moderate R^2 value of 0.8954. However, comparison of the correlation coefficients of both models suggests that the Langmuir model is suitable. The fact that the Langmuir isotherm fits the experimental data well may be due to homogeneous distribution of active sites on the composite photocatalyst surface.

Table 4.10. Linear Fitting results of Langmuir and Freundlich isotherms for the degradation of atrazine on TiO₂/silica composite photocatalyst.

Composite photocatalyst	Langmuir isotherms			Freundlich isotherms		
	qm (mg/g)	K (L/mg)	R^2	n_s	K_f (L/mg)	R^2
TiO ₂ /silica	1.619	3.06	0.999	0.167	0.0129	0.895

Table 4.11. Values of R_L obtained for linear regression of Langmuir isotherm

Initial dye concentration (mg/L)	$R_L(\text{TiO}_2/\text{silica})$
5	0.0613
10	0.0316
15	0.0213
20	0.016
25	0.012

Figure 4.42. Linear transform of Freundlich isotherm over $\text{TiO}_2/\text{silica}$

The Langmuir and Freundlich models using nonlinear least squares technique were further adopted to fit the experimental data. The isotherm parameters were evaluated by minimizing the two objective functions across the pesticide concentration range studied; the Derivative of Marquardt's Percent Standard Deviation (MPSD) and the Sum of the Squares of the Errors (ERRSQ). In addition, the difference between experimental and predicted variables was assessed by the standard deviation (σ), the coefficient of determination (R^2) and mean error

square (%). Figure 4.43 presents the graphical expressions of Langmuir (Eq. 2.11) and Freundlich (Eq. 2.14) modeling fits for atrazine pesticide on TiO₂/silica composite photocatalyst. The output parameters for Langmuir and Freundlich models along with the error functions calculated are listed in Table 4.12. It is shown in Fig. 4.43 that the Langmuir isotherm model correlated well with the experimental data by predicting similar data which were close to the data obtained experimentally. This is more demonstrated by the small value of the mean error obtained. In considering R², the Langmuir model gave a higher value of 0.994 compared to that of Freundlich model of 0.516, showing that the Langmuir model could describe the data better. Moreover, the minimum value of ERRSQ and MSPD achieved gave enough evidence to assure that the Langmuir model parameter values corresponded well to the global minimum of the objective function. Though the Freundlich model gave a low R² value in comparison to the Langmuir model, it also provided the high Freundlich parameter (n_f), suggesting there could be a possibility of some heterogeneity on the surface of the prepared TiO₂/silica.

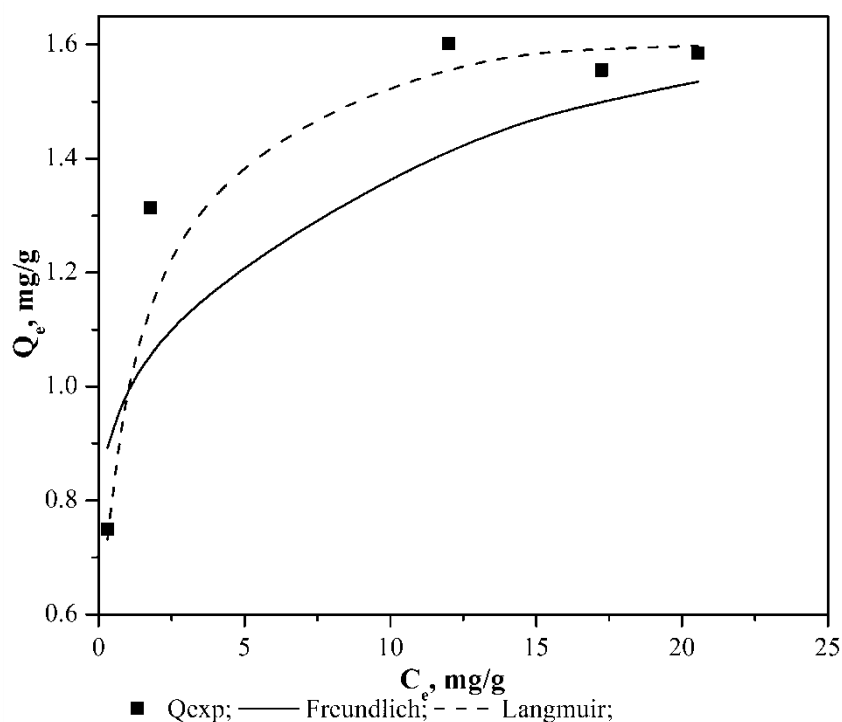


Figure 4.43. Isotherms modelling for degradation of atrazine on TiO₂/silica composite photocatalyst

Even though, Tang *et al.* (2012) reported that the Freundlich isotherms were more suitable than the Langmuir isotherms for the adsorption of atrazine on magnetic multi-walled carbon nano tube. In this study, experimental data could not be represented appropriately by Freundlich

model as it provided higher error functions. Hence, the Langmuir model suggesting the monolayer surface was the better model. Furthermore, an approach is adopted in this study to calculate the standard error of the data around the prediction curve. It is calculated by dividing the sum of the squares of the residuals by the degrees of freedom to obtain the variance of the experimental data. As a results, 95% confidence interval (CI) was calculated. This CI indicated the probability that the obtained experimental data lie within the range specified by the probability formula (Brown, 2001). From the results obtained, (Table 4.12), it is seen that the statistical measures to predict the real variance of probability of experimental data is well achieved.

Table 4.12. Isotherm parameters for Atrazine pesticides over TiO₂/silica composite photocatalyst

Model	q _m	K	R ²	Σ ERRSQ	MPSD	n _f	k _f	SE of Exp, q _e	Df	Ct	CI
Lang.	1.626	2.749	0.994	0.002	0.002			0.035	3	3.182	0.112
Freud.	0.174		0.516	0.333	0.262	7.808	1.042	0.174	3	3.182	0.554

4.4.5 Kinetics modeling of atrazine degradation

The experimental data sets were fitted to the linear form of pseudo first order (Eq. 2.18) and pseudo second order (Eq. 2.20). The slopes and intercepts of plots of the linear representations (Fig. 4.44) were obtained to determine the rate constants k and equilibrium adsorption amount q of the pseudo-first order and pseudo second order. The calculated kinetic constants are summarized in Table 4.13. A high R² value (0.9867) is observed for the pseudo first order model while pseudo second order model showed a low R² (0.7985). The pseudo first order adsorption ability of TiO₂/silica for atrazine degradation was greater than that of pseudo second order. Therefore the pesticide degradation system is a first order reaction based on the assumptions that the rate of change of solute uptake with time is directly proportional to difference in saturation concentration.

Table 4.13. Kinetic parameters for the degradation of atrazine onto composite photocatalyst.

Model	k (min^{-1})	q_e (mg/g)	R^2
Pseudo first order model	0.315	0.937	0.986
Pseudo second order model	3.484	0.156	0.799

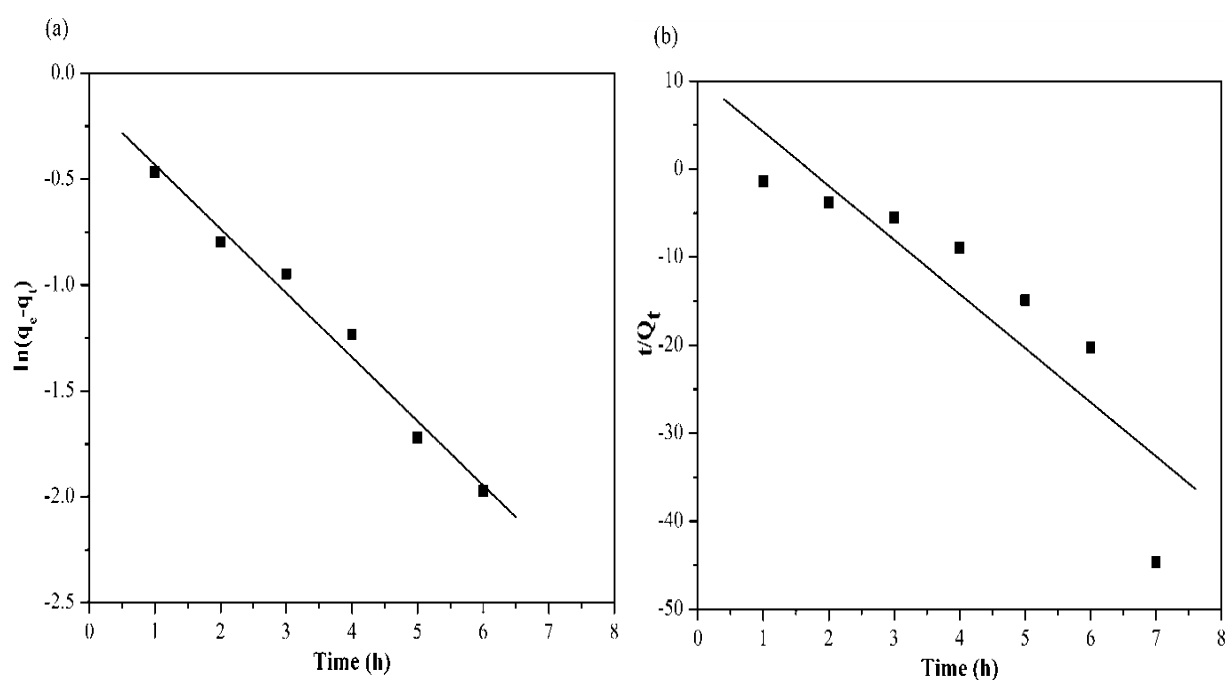


Figure 4.44. Pseudo first (a) and second order modelling (b) for pesticide degradation on TiO₂/silica composite photocatalyst

4.4.6 Effect of solution pH

The effect of pH on the degradation of atrazine was investigated at pH 3-9 over 6.55 g/L loading and 10 mg/L atrazine solution and results are shown in Fig. 4.45. It is noticed that the degraded amount of atrazine by TiO₂/silica is low at pH 3. Atrazine is protonized at pH 3, and as shown by the ZP measurement (Fig. 4.6), TiO₂/silica composite photocatalyst surface is positively charged, therefore the electrostatic repulsion between atrazine and TiO₂/silica surface lowers the atrazine degradation. Since atrazine is a weak base herbicide, it is found as uncharged molecule in the environment with pK_a values of 1.6 and 1.95 (Colombini *et al.*, 1998). As a result, when the pH value is near their pK_a , base molecules are adsorbed as protonated species.

Tao and Tang (2004) reported that the neutral form of atrazine could be adsorbed to catalyst surfaces by weak physical forces such as Vander Waals forces and hydrogen bonding through its nitrogen atoms. Furthermore, Parra *et al.* (2004) reported that at atrazine solution pH 2 and pH 10, the photocatalytic efficiency reduced considerably. It was further reported that the initial solution pH 7 and pH 10 changed to pH 5.1 and pH 6.5, respectively; during the photocatalytic reaction. It is proposed that the pH changes could be due to the production of NO_3^- and Cl^- during the photocatalytic treatment of atrazine herbicide. The optimum solution pH reported from Tao and Tang (2004) studies was 4.96 which is very close to the one found in the present study, pH 5.1.

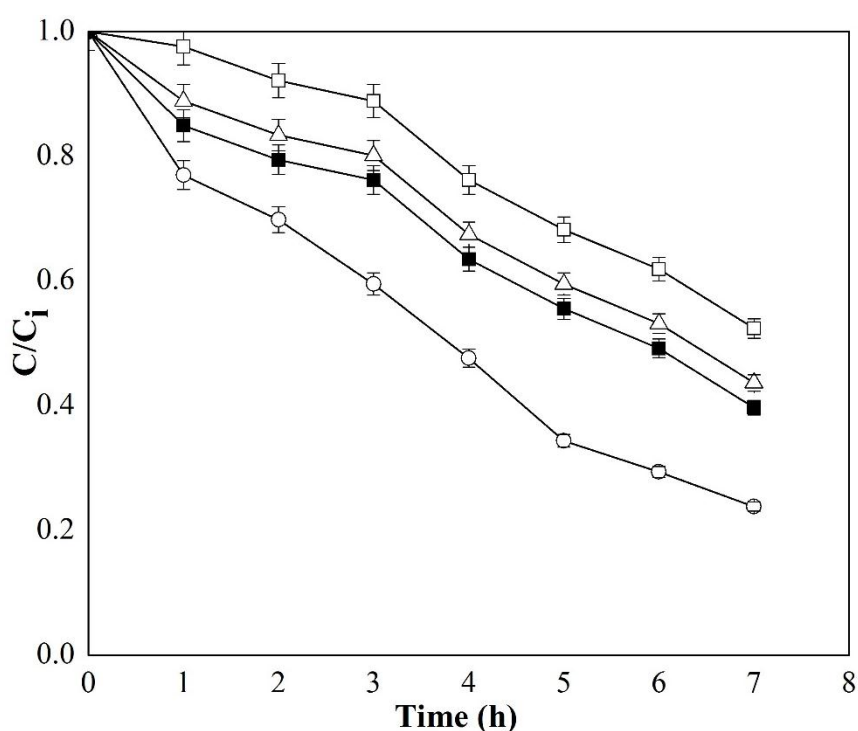


Figure 4.45. Effect of solution pH on atrazine degradation on $\text{TiO}_2/\text{silica}$; pH 3(□); pH 5.1 (○); pH 7(Δ); pH9 (■)

4.4.7 Photocatalytic reduction with single substrate: As(III)

It is well known that pH is one of the important critical parameters in the treatment of organic and inorganic pollutants. In further experiments, the photocatalytic reduction of As(III) in a single system was studied with 6.25 g/L loading and 5 mg/L initial As(III) concentration at different pH values. From Fig. 4.46, it can be seen that As(III) reduction was not significant especially at pH 3. Increasing pH from 3 to 6.4 showed an increase in the As(III) reduction,

however, the maximum As(III) reduction (65%) was obtained at pH 9.1. The decreased metal reduction at pH 3 could be due to the repulsion between the arsenic and the composite photocatalyst surface, since the PZC measurement (Fig. 4.6) showed that TiO₂/silica surface was positively charged. From the obtained results, As(III) was photocatalytically reduced better at pH 9, this could be described by the occurrence of As(III) as anionic species H₂AsO₃. It has been reported that at pH < than 9.1, the dominant specie of As(III) is the non-ionic H₃AsO₃ (Kuriakose *et al.*, 2004). Therefore, it was assumed that the van der Waals force was the only force acting between the H₃AsO₃ and the TiO₂/silica composite photocatalyst surface. Lee and Choi (2002) reported that the initial oxidation rate of As(III) at pH 9 was about twice as fast as the rate at pH 3. In their study, complete oxidation of As(III) took place in 2 h at 500 μM As(III) initial concentration and 1.5 g/L catalyst loading. In the studies completed by Manju *et al.* (1998), it was reported that As(III) adsorption on coconut husk carbon increased from 16 to 86% as pH was increased from 3 to 12.

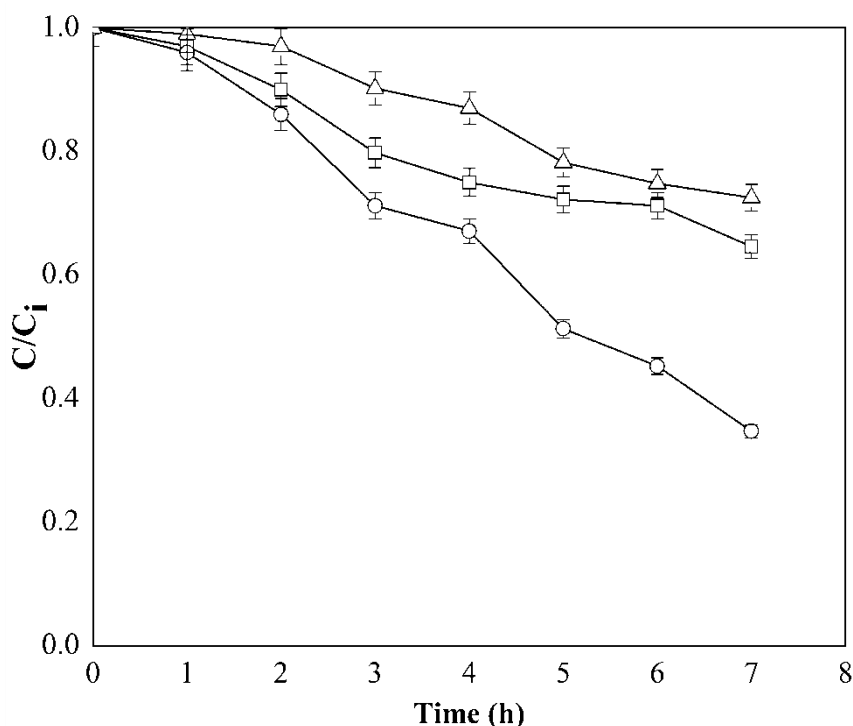


Figure 4.46. Effect of solution pH on atrazine degradation on TiO₂/silica composite photocatalyst: pH 3 (Δ); pH 6.4 (□); pH 9 (○)

Maji *et al.* (2007) reported that the removal of As(III) on laterite soil was possibly by physical adsorption rather than ion attraction. However, in the present study, a significant increase in metal reduction was observed at pH 9, As(III) was not completely reduced, this could be

affected by the slow oxidation of As(III) to As(V). It is suggested that the generated species such as $h_{\nu b}^+$, H_2O_2 , and $^{\circ}OH$ on composite photocatalyst were not enough to oxidize As(III) to As(IV). Therefore an extension of contact time or more composite photocatalyst loading would be required to achieve complete reduction of As(III).

4.4.8 Photocatalytic degradation of atrazine and reduction of As(III)

Agricultural wastewater may also contain metal ions due to metal containing pesticide used in the industry. The effect of initial concentration of As(III) on photodegradation of atrazine was evaluated and the results are shown in Fig. 4.48. The degradation of atrazine reduced slightly with an increasing concentration of As(III) during the simultaneous photocatalytic studies. The higher the As(III) concentration was, the less degradation for atrazine became, which suggested that As(III) had a suppression effect on photodegradation of atrazine. This could be due to the competition between the metal ion and the herbicide for the available photogenerated oxidizing species (i.e. valence band holes and hydroxyl radicals) on TiO_2 /silica composite photocatalyst surface. On the contrary, the reduction of As(III) (Fig. 4.48) at all different concentration was greatly favored. Tang *et al.* (2012) evaluated the effect of Cu(II) on magnetic multi-walled carbon nanotube (MMWCNT) in the presence of atrazine. It was reported that Cu(II) had a negative impact on the atrazine adsorption, which is a similar trend reported in this study. This was further ascribed to the formation of inner-sphere and outer-sphere complexes of Cu(II) through carboxylic groups and hydration on the surfaces of the adsorbent. Maji *et al.* (2007) evaluated the effect of atrazine and endosulfan compounds on the removal of arsenic metal ions, As(III) and As(V). It was found that the presence of organic contaminants had a negligible effect on As(III) while arsenate removal efficiency reduced from 95% to 90% for both organic pollutants. This was possibly due to the fact that these molecules being rather insoluble in water get adsorbed to the laterite soil thereby reducing As(III) reduction efficiency. The studies showed that the impact of As(III) on atrazine degradation could be neglected.

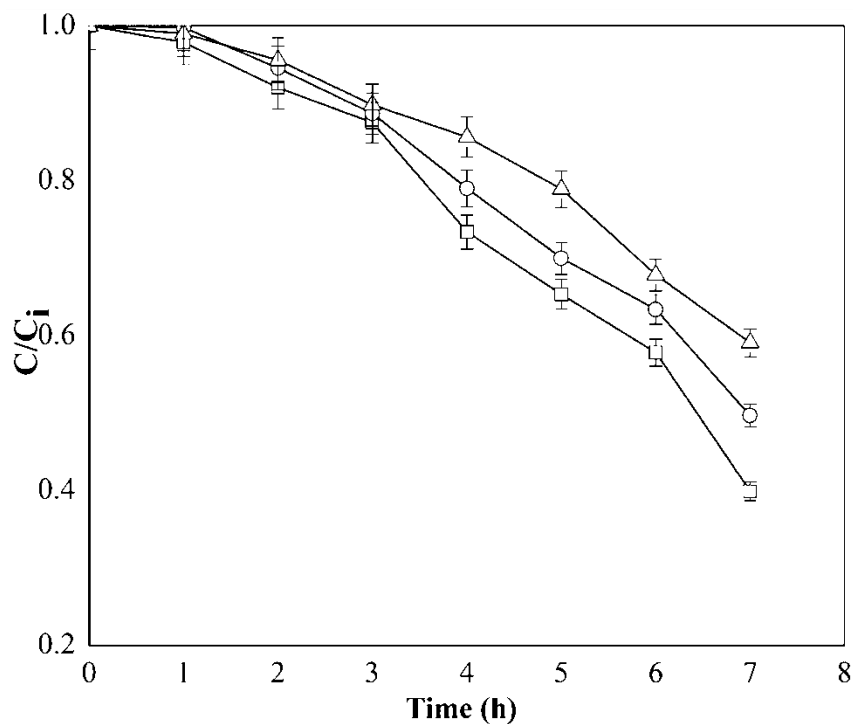


Figure 4.47. Effect of As(III) initial concentration on atrazine degradation over 6.25 g/L TiO_2 /silica concentration; 0.5 mg/L (□); 1 mg/L (○); 5 mg/L (Δ)

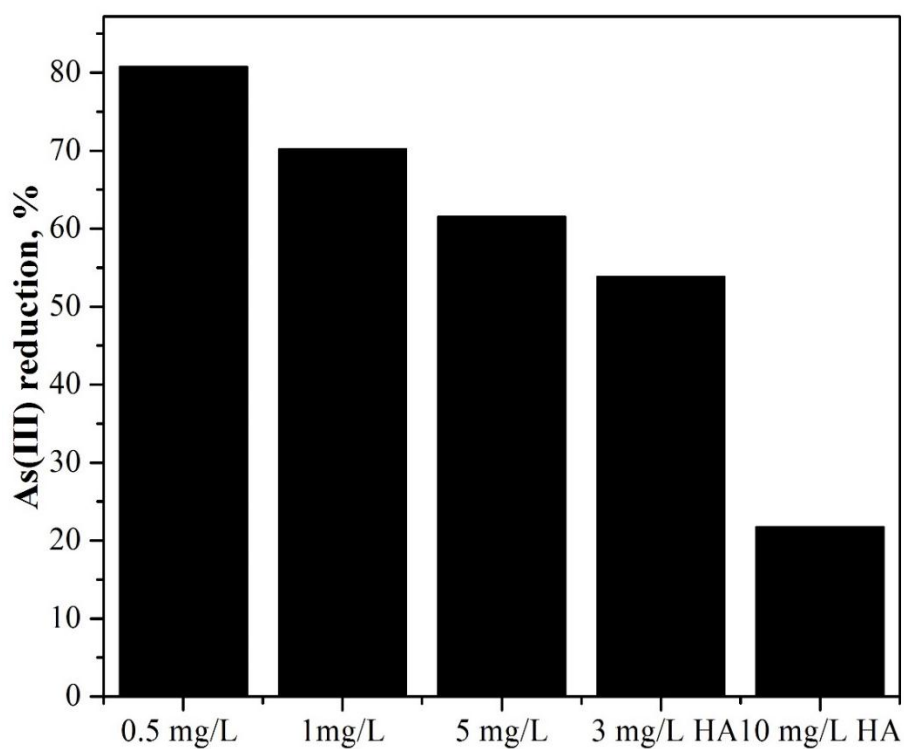


Figure 4.48. Final As(III) reduction in the presence of atrazine alone and atrazine/Humic acid mixture over 6.25 g/L TiO_2 /silica concentration after 6 h irradiation

4.4.9 Effects of As(III) and humic acid on the photodegradation of atrazine

Industrial wastewater does get contaminated with inorganic and organic compounds such humic acid. To understand the effect of As(III) on TiO₂/silica composite photocatalyst in the presence of humic acid, the effect of humic acid alone on the photodegradation of atrazine was investigated. Different concentrations of humic acid (3 and 10 mg/L) were added into atrazine solutions and the results are shown in Fig. 4.49. It can be seen that the photodegradation of atrazine decreased significantly with an increase in humic acid concentration. Humic acid was possibly adsorbed onto the composite photocatalyst surface of TiO₂/silica and occupied the active surface sites, thus leading to a decrease in atrazine degradation. For instance, after 4 h treatment time, atrazine photocatalytic degradation in the absence of humic acid system was about 65% and it was reduced to about 40% in the presence of 10 mg/L humic acid in the binary Atrazine/HA/TiO₂/silica system. The decreased photocatalytic degradation of atrazine in the presence of humic acid could be due to the competition between atrazine and humic acid for the available photogenerated oxidizing species which at a constant set of photocatalytic conditions, are produced at a constant rate. Such competition will result in decreased photocatalytic oxidation efficiency compared with the atrazine degradation in the absence of humic substance. Furthermore, humic acid is well-known as light absorbing substance and it is inevitable that it competed with atrazine for the available photons (Ou *et al.*, 2009). Therefore, an increase in HA concentration resulted in reduction in photodegradation, this could be due to the photons being consumed by increased humic acid concentration. Hua *et al.* (2000) reported that aromatic reticular formation of humic acid could also adsorb the herbicide, which led to the herbicide poorly absorbing light. It should be noted that such decreased photocatalytic activity of the binary system was also observed in the present study concerning the photocatalytic degradation of the azo dye methyl orange and Cr(VI) (section 4.3.9) on TiO₂/zeolite and TiO₂/silica composite photocatalysts.

The effect of coexisting As(III) and HA on the photodegradation of atrazine was determined and the results are also shown in Fig. 4.49. The photodegradation of atrazine moderately increased after 6 h irradiation when As(III) (5 mg/L) was added into the solution containing humic acid of 3 mg/L, for example the atrazine degradation increased from 40% to about 60%. Though the addition of As(III) concentration had a significant effect on pesticide degradation in the presence of humic acid, As(III) removal declined due to the addition of humic acid

substance. The retardation by humic substance may be ascribed to the combination effects of light attenuation and the competition between the As(III) and humic acid for the active sites on the TiO₂/silica composite photocatalyst resulting in a decrease in the metal reduction.

Sun *et al.* (2011) reported that the (electron spin resonance) ESR spectra analysis showed that there is no significant signal of OH radicals in the coexistence of humic acid and metal ion. Therefore in this study, it is likely that other active species are generated and improved photodegradation efficiency of atrazine in the presence of As(III) and humic acid. However, contradictory results were reported by Lee and Choi (2002) that the presence of humic acid improved As(III) oxidation at pH 3 but no effect was shown at pH 9. It was assumed that humic acid was first photosensitized and thereafter reacted with oxygen to increase the formation of superoxide radical. As a result, this ultimately enhanced As(III) oxidation at acidic conditions. It was also reported (Lee and Choi, 2002) that As(III) oxidation would be reduced in the presence of humic acid if hydroxyl radicals and valence band holes were the dominant oxidizing species rather than superoxide radicals and this is what is observed in the present study. In this study, UV-A light with irradiation intensity of 5.5 mW/m² was employed, while Lee and Choi (2002) employed a 300 W xenon arc lamp emitting in the UV-A/Vis region; this could possibly affect the photocatalytic efficiency of either As(III) or atrazine removal.

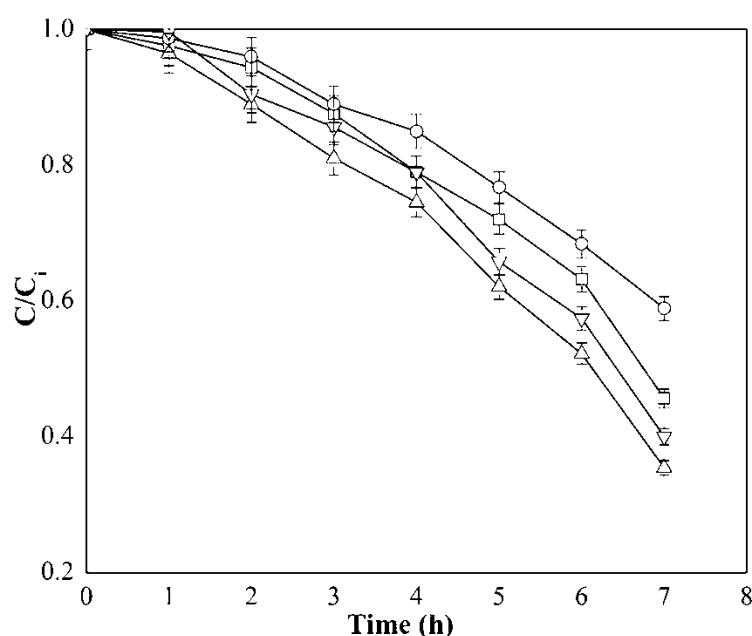


Figure 4.49. Effect of HA initial concentration on degradation of atrazine in the absence of arsenic 3 mg/L HA (□); 10 mg/L HA (○); and presence of 5 mg/L As(III): 3 mg/L HA (Δ); 10 mg/L HA (∇)

4.4.10 Identification of intermediate products

The FTIR spectra of atrazine before and after photocatalytic treatment was recorded using the KBr-pressed disk technique and the spectra is shown in Fig. 4.50. It was noted that the peak located at 3385 cm^{-1} is present in the spectra of the two samples. This peak was associated with hydrogen bonded OH stretching bands (Purcell *et al.*, 2001), however, it decreased in the spectrum of the treated sample after 6 h irradiation. This suggest that the water molecules interacts with the OH groups on the $\text{TiO}_2/\text{silica}$ composite photocatalyst surface, through hydrogen bonding. After atrazine was adsorbed onto $\text{TiO}_2/\text{silica}$ composite photocatalyst, new peaks appeared at 1014 cm^{-1} - 1113 cm^{-1} corresponding to vibrations of the TiO_2 surface hydroxyl groups. This phenomenon implies that the hydroxyl groups were the dominant oxidizing species during the atrazine degradation on $\text{TiO}_2/\text{silica}$ composite photocatalyst surface.

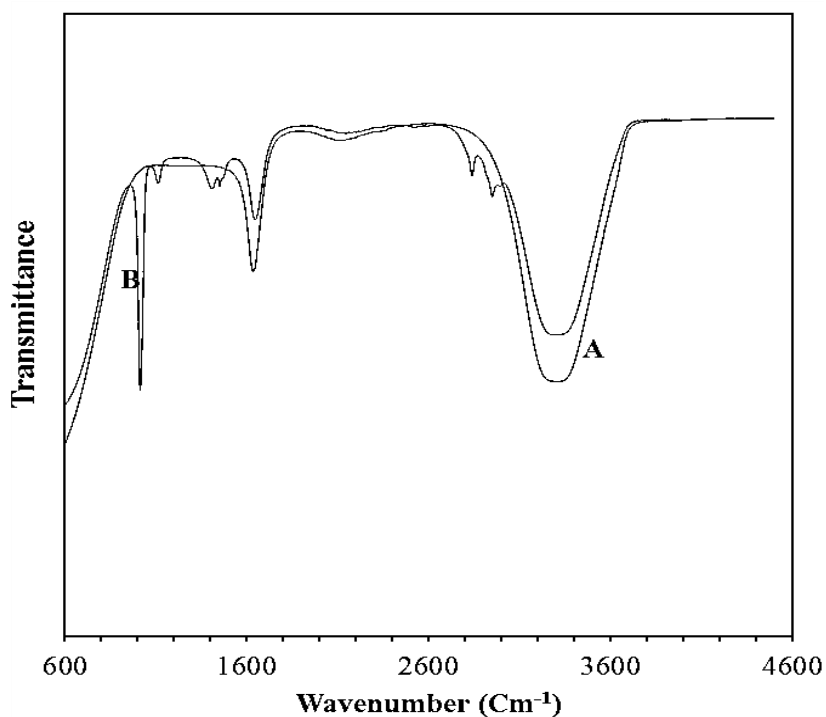


Figure 4.50. FTIR spectra of (A) raw atrazine; (B) extracted atrazine

This phenomenon is in agreement with the observation in section 4.5.7 where it was indicated that the As(III) reduction decreased in the presence of atrazine and humic acid since hydroxyl radicals and valence band holes rather than superoxide radicals were the dominating oxidizing species. The peaks at 1633 cm^{-1} and 1646 cm^{-1} were assigned to the $-\text{C}=\text{C}-$ stretch mode in the atrazine before the treatment and N-H deformation (Purcell *et al.*, 2001), respectively. The new

band after the treatment at 1408 cm^{-1} was assigned to C–C stretch (in-ring) aromatics. From this result, it can be proposed that the interaction between atrazine and the surface silanol OH group at the $\text{TiO}_2/\text{silica}$ takes place through hydrogen bonding mechanism.

The evolution of NO_3^- , SO_4^{2-} and PO_4^{3-} ions concentration during the degradative process is presented in Fig. 4.51. The concentration of SO_4^{2-} ions formed from atrazine mineralization decreased significantly in the first hour of degradation. This specifies that most of the $-\text{SO}_3^-$ group present in atrazine structure was oxidized at the early stage of the treatment. Mineralization of nitrogen atoms revealed an unexpected trend. The results showed that the nitrogen initially present in atrazine was not converted predominantly to NH_4^+ ions. The complete mineralization of SO_4^{2-} was very fast, whereas mineralization of nitrogen into nitrate was slow. Taking into account the overall atrazine degradation efficiency, it is clear that atrazine was not completely degraded. Konstantinou and Albanis (2003) reported cyanouric acid as one of the intermediate products and that this product is not easily mineralized and eventually accumulate in the reaction.

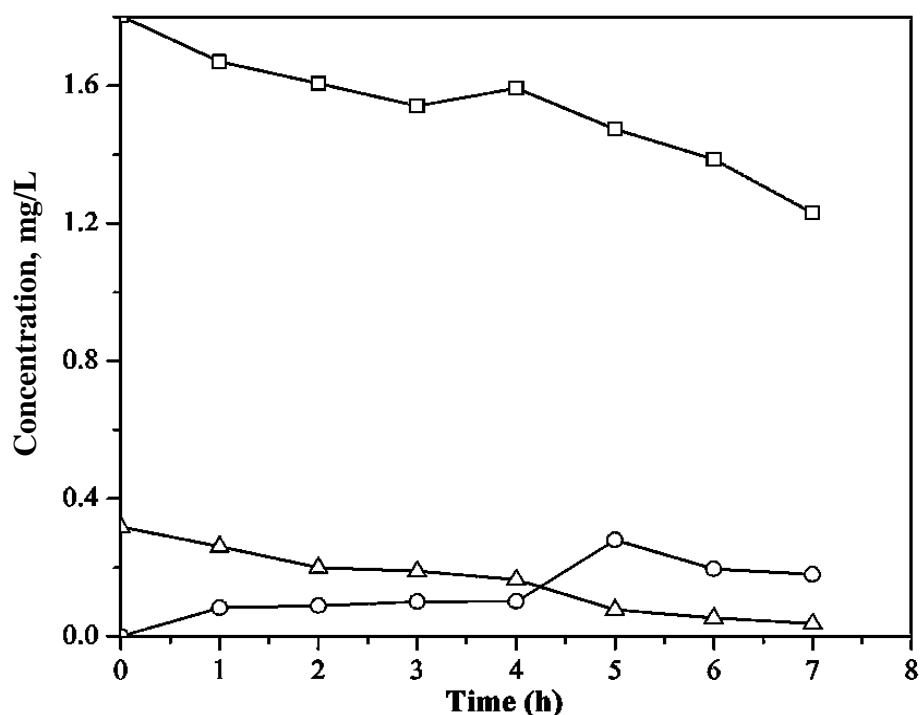


Figure 4.51. Time-course of inorganic ions concentration during heterogeneous photocatalysis treatment of atrazine: SO_4^{2-} (\square); PO_4^{3-} (\circ); NO_3^- (Δ)

CHAPTER 5

5. CONCLUSIONS AND RECOMMENDATIONS

The aim of this study was to investigate the heterogeneous photocatalytic degradation of dyes and pesticides in the presence of ions. In order to achieve this, different specific objectives were set up direct to the course of research. These conclusions and recommendation present the answers to the specific objective set. Organic and inorganic compounds such as methyl orange, Cr(VI), atrazine and As(III) are major pollutants being discharged into water bodies from various industries during mechanical operations. Human beings and animals are facing various health problems by being exposed to the polluted water. TiO₂ has been suggested to be an efficient and viable photocatalyst for the degradation and mineralization of various organic pollutants such as dye, pesticides and metal ions contaminants in wastewater in the presence of UV. Therefore, the consideration of the effect of ions was given due to the fact that most industrial wastewater streams contain both organic and inorganic pollutants.

5.1 Conclusions

In the first part of the work, TiO₂ was supported on zeolite and silica material with different particle sizes, for the photodegradation of methyl orange dye and atrazine herbicide in the absence and presence of ions. SEM with EDX microanalyses showed the homogeneity of the TiO₂ distribution inside the zeolite and silica supporting materials. The most favorable conditions for methyl orange degradation in the range studied were 10 wt% and 15 wt% loading of TiO₂ on zeolite and silica support, respectively, resulting in better degradation rate. It was observed that variation of the TiO₂/silica composite photocatalyst size plays an important role in degrading pollutants. The present study indicated that the photocatalytic degradation efficiency initially increases with composite photocatalyst concentration and then decreased at high values due to light scattering and screening effects. The optimum TiO₂/zeolite and TiO₂/silica concentration for methyl orange degradation were 6.25 g/L and 1.25 g/L, respectively. The composite photocatalysts showed higher efficiency at lower pH than at higher pH due to the strong adsorption of methyl orange on the composite photocatalyst surface. The optimum TiO₂/silica concentration for atrazine degradation was found to be 6.25 g/L. The TiO₂/silica composite photocatalyst showed high degradation efficiency at pH 5. The presence of inorganic salts such as SO₄²⁻ and Cl⁻, which are usually present in real wastewater produced

by textile industry have an inhibitory effect on methyl orange degradation on both composite photocatalyst in the sequence of $\text{SO}_4^{2-} > \text{Cl}^-$. The degradation of single dye/composite photocatalyst system continued faster than that of the respective binary dye/Cr (VI)/composite photocatalyst system at pH 6.5 and 3 for both composite photocatalysts.

The photodegradation efficiency of atrazine was decrease significantly in the water polluted by arsenic. This was ascribed to the competition between atrazine and As(III) for active site on $\text{TiO}_2/\text{silica}$ surface. The co-occurrence of humic acid and As(III) enhanced the degradation of atrazine. However, As(III) reduction declined due to the addition of humic acid. The hindrance by humic acid was ascribed to the combination effects of light attenuation and the competition between the As (III) and humic acid for the active sites on the $\text{TiO}_2/\text{silica}$ composite photocatalyst, resulting in a decrease in the metal reduction.

Comparing the two models applied using linear and non-linear regression techniques, the Langmuir model was found to be best fitting for both pollutants, methyl orange and atrazine photodegradation on $\text{TiO}_2/\text{zeolite}$ and $\text{TiO}_2/\text{silica}$ composite photocatalyst. Significant deviations between experimental and predicted data were observed with Freundlich model, implying that all the binding sites were similar on the composite photocatalyst in accordance with Langmuir's theory. The output for linear and nonlinear regression of pseudo-first-order and pseudo second-order regression models showed that the experimental data for methyl orange on composite photocatalysts were best fitted with pseudo second order model. The pseudo first order model was found to the best fit for atrazine experimental data, which indicates that the sorbent free sites are the rate-limiting step in the process.

Mineralization of methyl orange was achieved using heterogeneous photocatalytic degradation method, however, the mineralization rate was low especially at high pH values. The identified intermediates showed that the heterogeneous degradation of methyl orange took place through C–N cleavages. The atrazine was not completely removed at all experimental condition studied, this could be due to the release of cyanouric acid compound during the treatment. The results show that heterogeneous photocatalytic degradation could be more applicable as a pre-treatment method to enhance biodegradation of recalcitrant organic pollutants.

5.2 Recommendations

There is still a noticeable interest in the application of TiO₂ in the wastewater treatment processes based on its superior capabilities for photocatalytic processes. Thus, it is important to move forward with further modifications whether with more enhanced anion doping techniques or dye sensitizing approach. As mentioned in Section 2.6.4, structural impact can be significant in the case of employing interconnected structures synthesis. In this research, zeolites and silica have been utilized to meet this criterion with providing the nano-sized tetrahedral formation of the TiO₂ on the structured support. Further fundamental studies on the diffusion length of the photons inside structured materials such as zeolite and silica are necessary to estimate the effective impregnation depth of the semiconductor on the supporting material. This can be done via much more sophisticated analysis such as femtosecond studies in order to find the dynamics of charge carriers on the ultra-thin layers of the photocatalyst.

It is recommended that the lower pH conditions in the atrazine solution have to be investigated to clearly understand the impact of atrazine protonation onto the TiO₂/silica surface and to evaluate the strength of this interaction. The binding mechanism of the degradation products of atrazine need to be evaluated to provide further insight. Since this research was conducted using synthetic wastewater, it is recommended that photocatalytic efficiency of TiO₂ supported on zeolite and silica- materials should be further studied in various solution wastewater such as real wastewater samples. This would be significant prior to scaling up the process. In the industrial scale, the applications of novel composite photocatalyst can, for example, be in agriculture, textile and painting industry.

REFERENCES

- Agrios, A.G., Gray, K.A. & Weitz, E. 2003. Photocatalytic transformation of 2,4, trichlorophenol on TiO₂ under sub-band gap illumination. *Langmuir*, 19:1402.
- Aksu, Z. 2005. Application of biosorption for the removal of organic pollutants: review. *Process Biochemistry*, 40:997-1026.
- Allen, S.J., Gan, Q., Matthews, R. & Johnson, P.A. 2003. Comparison of optimized isotherm models for basic dye adsorption by kudzu. *Bioresources Technology*, 88:143-152
- Almquist, C.B. & Biswas, P. 2002. Role of synthesis method and particle size of Nanostructured TiO₂ and its Photoactivity. *Journal of Catalysis*, 212:145-156
- Alvey, S. & Crowley, D. E. 1996. Survival and activity of an atrazine-mineralizing bacterial consortium rhizosphere soil. *Environmental Science and Technology*, 30(5):1596-1603.
- Anderson, C. & Bard, A. 1997. Improved photocatalytic activity and characterization of mixed TiO₂/SiO₂ and TiO₂/Al₂O₃ materials. *Journal of Physical Chemistry, B*, 101:2611-2616.
- Armstrong, D.E., Chester, C. & Harris, J.H. 1967. Atrazine hydrolysis in soil. *Soil Science Society of American Proceedings*. 31:61-66.
- Artale, M.A., Augugliaro, V., Drioli, E., Golemme, G., Grande, C., Loddo, V., Molinari, R., Palmisano, L., Schiavello, M. 2001. Preparation and characterisation of membranes with entrapped TiO₂ and preliminary photocatalytic tests. *Annali di Chimica*, 91 (3-4):127-136.
- Asahi, R., Morikawa, T., Ohwaki, T., Aoki, K. & Taga, Y. 2001. Visible-light photocatalysis in nitrogen-doped titanium dioxides. *Science*, 293:269-271.
- Asuha, S., Zhou, X.G. & Zhao, S. 2010. Adsorption of methyl orange and Cr(VI) on mesoporous TiO₂ prepared by hydrothermal method. *Journal of Hazardous Material*, 181:204-210
- Augugliaro, V., Baocicchi, C., Prevot, A.B., Garcia-Lopez E., Loddo, V., Malato, S., Marci, G., Palmisano, L., Pazzi, M. & Pramauro, E. 2002. Azo-dyes photocatalytic degradation in aqueous suspension of TiO₂ under solar irradiation. *Chemosphere*, 49:1223-1230
- Azizian, S. & Bashiri, H. (2008). Adsorption kinetics at the solid/solution interface: statistical rate theory at initial times of adsorption and close to equilibrium. *Langmuir*, 24(20):11669-11676.
- Azizian, S. (2004). Kinetic models of sorption: a theoretical analysis. *Journal of Colloid and Interface Science*, 276:47-52.

- Bai, Y., Sun, Q., Xing, R., Wen, D. & Tang, X. 2010. Removal of pyridine and quinolone by bio-zeolite composed of mixed degrading bacteria and modified zeolite. *Journal of Hazardous Material*, 181:916-922.
- Bamba, D., Atheba, P., Robert, D., Trokourey, A. & Dongui, B. 2008. Photocatalytic degradation of the diuron pesticide. *Environmental Chemical Letter*, 6:163-167.
- Banat, I.M., Nigam, P., Singh, D. & Marchant, R. 1996. Microbiology decolourization of textile-dye containing effluents: review. *Bioresources Technology*, 58: 217-27.
- Beattie I.R, Gilson TR. 1968. Single crystal laser Raman spectroscopy. *Proceedings of the Royal Society of London Series a-Mathematical and Physical Sciences*, 307:407
- Beitz, H., Schmidt, H. & Herzel, F. 1994. Occurrence, toxicological and ecotoxicological significance of pesticides in groundwater and surface water. *Chemical Plant*, 8:3-53.
- Belsley, D.A., Kuh, E & Welsch, R.E. 1980. Regression diagnostics: Identifying Influential Data and Sources of Collinearity. New York: Wiley
- Bhatnagar, A & Sillanpää, M. 2009. Application of chitin and Chitosan-derivatives for the detoxification of water and wastewater. *Advances in Colloid and Interface Science*, 152:26-38.
- Boyd, G.E., Adamson J, A.W. & Myers, L.S. 1947. The exchange adsorption of ions from aqueous solutions by organic zeolites. *Journal of the American Chemical Society*, 69:2836-2848.
- Brown, A.M. 2001. A step-by-step guide to non-linear regression analysis of experimental data using a Microsoft Excel spreadsheet. *Computer Methods and Programs in Biomedicine*, 65(3):191-200.
- Calza, P., Sakkas, V.A., Medana, C., Baiocchi, C., Dimou, A., Giokas, D., Pelizzetti, E., Albanis, T. (2006). Photocatalytic degradation of diclofenac over aqueous TiO₂ suspensions. *Applied Catalysis B: Environmental*. 67, 197-205.
- Chakrabarti, S. & Dutta, B. K. 2004. Photocatalytic degradation of model textile dyes in wastewater using ZnO as semiconductor catalyst. *Journal of Hazardous Materials*. 112(3):269-78,
- Chen, C.C., Lu, C.S., Chung, Y.C. & Jan, J.L. 2007. UV light induced photodegradation of malachite green on TiO₂ nanoparticles. *Journal of Hazardous Materials*, 141:520-528
- Chen, D.W. & Ray, A.K. 2001. Removal of toxic metal ions from wastewater by semiconductor photocatalysis. *Chemical Engineering Science*, 56:1561-1570

- Chen, S. & Cao, G. 2005. Study on the photocatalytic reduction of dichromate and photocatalytic oxidation of dichlorvos, *Chemosphere*, 60:1308-1315.
- Chen, Y.P., Liu, S.Y., Yu, H.Q., Yin, H. & Liu, Q.R. 2008. Radiation-induced degradation of methyl orange in aqueous solutions. *Chemosphere*, 72:532-536
- Choi, H., Stathatos, E. & Dionysiou, D.D. 2007. Photocatalytic TiO₂ films and membranes for the development of efficient wastewater treatment and reuse systems. *Desalination*, 202:199- 206.
- Chong, M.N, Jin, B., Chow, C.W.K. & Saint, C. 2010. Recent developments in photocatalytic water treatment technology: review. *Water Research*. 44(10):2997–3027.
- Cohen, J.W. (1988). *Statistical power analysis for the behavioral science* (2nd edn). New York: Academic Press
- Colombini, M.P., Fuoco R., Giannarelli S. & Pospíšil L trsková. 1998. Protonation and degradation reactions of s-Triazine herbicides. *Microchemical Journal*, 59:239-245
- Colon, G., Hidalgo, M.C. & Navio, J.A. 2001. Photocatalytic deactivation of commercial TiO₂ samples during simultaneous photoreduction of Cr (VI) and photooxidation of salicylic acid. *Journal of Photochemistry and Photobiology A*, 138(1):79-85.
- Covelo, E.F., Vega, F.A. & Andrade, M.L. (2007). Simultaneous sorption and desorption of Cd, Cr, Cu, Ni, Pb and Zn in acid soils. I. Selectivity sequences, *Journal of Hazardous Material*, 147:852-861.
- Cox, G. 1993. The influence of silica structure on reversed-phase retention. *Journal of Chromatography*, 656:353-367
- Crini, G. 2005. Recent developments in polysaccharide-based materials used as adsorbents in wastewater treatment. *Progress in Polymer Science*. 30:38-70.
- De Laat, J., Le, G.T. & Legube, B. 2004. A comparative study of the effects of chloride, sulphate and nitrate ions on the rates of decomposition of H₂O₂ and organic compounds by Fe (II)/H₂O₂ and Fe (III)/H₂O₂. *Chemosphere*. 55:715-723.
- Dubey, N., Rayalu, S.S., Labhsetwar, N.K., Naidu, R.R., Chatti, R.V. & Devotta, S. 2006. Photocatalytic properties of zeolite-based materials for the photoreduction of methyl orange. *Applied Catalysis*. 303, 152–157.
- EPA Method 218.6. 1991. *Determination of Dissolved Hexavalent Chromium in Drinking Water, Groundwater and Industrial Wastewater Effluents by Ion Chromatography*, US Environmental Protection Agency, Cincinnati, OH.

- Eriksson, E., Baun, A., Mikkelsen, P.S. & Ledin A. 2007. Risk assessment of xenobiotic in storm water. *Desalination*. 215:187-197.
- Fallmann, H., Krutzler, T., Bauer, R., Malato, S. & Blanco, J. 1999. Applicability of the photo-Fenton method for treating water containing pesticides. *Catalysis Today*. 54: 309-319.
- Fogler, H.S. 1999. *Elements of Chemical Reaction Engineering: Catalysis and Catalytic Reactors*. Prentice-Hall, 581-685.
- Freundlich, H. M. F. 1906. Over the Adsorption in Solution. *The Journal of Physical Chemistry*, 57:385-471.
- Fujishima, A. & Honda, K. 1972. Electrochemical photolysis of water at a semiconductor electrode. *Nature*, 238:37-38.
- Fujishima, A., Rao, T.N. & Tryk, D.A. 2000. Titanium dioxide photocatalysis: review. *Journal of Photochemical. Photobiology C: Photochemical*, 1-21.
- Fujishima, A., Zhang, X. & Tryk, D.A. 2008. TiO₂ photocatalysis and related surface phenomena. *Surface Science Reports*. 63:515-582.
- Galindo, C., Jacques, P. & Kalt, A. 2001. Photochemical and photocatalytic degradation of an indigolid dye: a case study of acid blue 74 (AB74). *Journal of Photochemistry and Photobiology A: Chemistry*, 141:47-56.
- Gaya, U.I. & Abdullah, A.H. 2008. Heterogeneous photocatalytic degradation of organic contaminants over titanium dioxide: a review of fundamentals, progress and problems. *Journal of Photochemical. Photobiology, C: Photochemical: review*, 9:1-12.
- Gernjak, W., Krutzler, T. & Malato, S. 2007. Photo-Fenton treatment of olive mill wastewater applying a combined Fenton/flocculation pretreatment. *Journal of Solar Energy Engineering*, 129:53-59.
- Giles, C.H., Smith, D. & Huitson, A. 1974. A general treatment and classification of the solute adsorption isotherm. I. Theoretical. *Journal of Colloid Interface Science*, 47:755-765.
- Gomez, S., Marchena, C.L., Pizzio, L. & Pierella, L. 2013. Preparation and characterization of TiO₂/HZSM-11 zeolite for photodegradation of dichlorvos in aqueous solution. *Journal of Hazardous Materials*, 258-259:19-26
- Guivarch, E., Trevin, S., Lahitte, C. & Oturan, M.A. 2003. Degradation of azo dyes in water by electro-Fenton process. *Environmental Chemical Letter*. 1(1):38-44.

- Gupta, V.K., Mittal, A., Gajbe, V. & Mittal, J. 2006. Removal and recovery of the hazardous azo dye acid orange 7 through adsorption over waste materials: Bottom Ash and De-Oiled. Soya. *Industrial & Engineering Chemistry Research*, 45(4):1446-1453.
- Gupta, V.K., Pathania, D., Sharma, S., Agarwal, S. & Singh, P. 2013. Remediation and recovery of methyl orange from aqueous solution onto acrylic acid grafted Ficus carica fiber: Isotherms, kinetics and thermodynamics. *Journal of Molecular Liquids*, 177:325-334
- Han, R., Wang, Y., Zou, W., Wang, Y. & Shi, J. 2007. Comparison of linear and nonlinear analysis in estimating the Thomas model parameters for methylene blue adsorption onto natural zeolite in fixed-bed column. *Journal of Hazardous Materials*, 145(1-2):331-335.
- Hao, O.J., Kim, H. & Chiang, P.C. 2000. Decolorization of wastewater: critical review, *Environmental Science*, 30:449-505.
- Herrmann, J.M. 1999. Heterogeneous photocatalysis: fundamentals and applications to the removal of various types of aqueous pollutants. *Catalysis Today*, 53:115-129.
- Hoffmann, M.R, Martin ST. 1995. Environmental applications of semiconductor photocatalysis. *Chemical Review*, 95:69-95.
- Hu, C., J.C. Yu, Hao, Z. & Wong, P.K. 2003. Effects of acidity and inorganic ions on the photocatalytic degradation of different azo dyes. *Applied Catalysis B: Environmental*, 46: 35-47.
- Hua, R.M, Yue, Y.D., Qi, C.Y., Tang, F., Li, X.Q, & Fan, D.F. 2000. Photoquenching effect of nine pesticides on the photolysis of butachlor in water. *Acta Scientiae Circumstantiae*, 20(3):360-364.
- Ichiura, H., Kitaoka, T. & Tanaka, H. 2003. Preparation of Composite TiO₂- Zeolite Sheets Using a Papermaking Technique and Their Application to Environmental Improvement. *Journal of Material Science*, 38:1611-1615.
- Jal, P.K., Patel, S. & Mishra, B.K. 2004. Chemical modification of silica surface by immobilization of functional groups for extractive concentration of metal ions. *Talanta*, 62: 1005-1028.
- Joana, M.D., Maria, C.M., Manuel, F., Jose, R.U. & Manuel, S.P. 2007. Waste materials for activated carbon preparation and its use in aqueous-phase treatment. *Journal of Environmental Management*, 85:833-846.

- Kabra, K., Chaudhary, R. & Sawhney, R.L. 2004. Treatment of hazardous organic and inorganic compounds through aqueous-phase photocatalysis: review. *Indian Engineering Chemical Research*, 43:7683-7696.
- Kamat, P. 2012. TiO₂ nanostructures: Recent physical chemistry advances. *Journal of Physical Chemistry Letter*, 116:11849-11851.
- Kansal, S.K., Singh, M. & Sud, D. 2007. Studies on photodegradation of two commercial dyes in aqueous phase using different photocatalyst. *Journal of Hazardous Material*, 12:141.
- Kawahara, T., Konishi, Y., Tada, H., Tohge, N., Nishii, J. & Ito, S. 2002. A patterned TiO₂ (anatase)/TiO₂ (rutile) bilayer-type photocatalysis: effect of the anatase/rutile junction on the photocatalytic activity. *Angewandte Chemie International Edition*. 41:2811-2813.
- Khan, A.Y. 2003. TiO₂ coated activated carbon: a regenerative technology for water recovery, Masters's Thesis. University of Florida
- Kiwi, J. Lopez, A. & Nadtochenko, V. 2000. Mechanism and kinetics of the OH-radical intervention during Fenton oxidation in the presence of a significant amount of radical scavenger (Cl⁻). *Environmental Science and Technology*. 34:2162-2168.
- Konstantinou, I.K. & Albanis, T.A. 2004. TiO₂-assisted photocatalytic degradation of azo dyes in aqueous solution: kinetic and mechanistic investigations: review, *Applied Catalysis*. 49:1-14.
- Konstantinou, K.I. & Albanis, T.A. 2003. Photocatalytic transformation of pesticides in aqueous titanium dioxide suspensions using artificial and solar light: intermediates and degradation pathways. *Applied Catalysis B: Environmental*, 49:1-14.
- Kuriakose, S. Singh, T.S. & Pant, K.K. 2004. Adsorption of As(III) from aqueous solution onto iron oxide impregnated activated alumina. Water Quality Research. *Journal of Canada*, 39(3):258-266.
- Kwak, S.Y. & Kim, S.H., 2001. Hybrid organic/inorganic reverse osmosis (RO) membrane for bactericidal anti-fouling. Preparation and characterization of TiO₂ nanoparticle self-assembled aromatic polyamide thin-film-composite (TFC) membrane. *Environmental Science and Technology*, 35:2388-2394.
- Langmuir, I. 1918. The Constitution and Fundamental Properties of Solids and Liquids. *Journal of the American Chemical Society*, 40(9):1361-1403.
- Lee, H. & Choi, W. (2002). Photocatalytic oxidation of arsenite in TiO₂ suspension: Kinetics and mechanisms. *Environmental Science and Technology*, 6:3872-3878.

- Li, J., Zhang, S.W., Chen, C.L, Zhao, G.X., Yang, X. & Li, J.X. 2012. Removal of Cu (II) and fulvic acid by grapheme oxide nanosheets decorated with Fe₃O₄ nanoparticles. *Applied Material Interfaces*, 4(9):4991-5000.
- Liu, S., Lim, M., Amal, R. 2014. TiO₂-coated natural zeolite: Rapid humic acid adsorption and effective photocatalytic regeneration. *Chemical Engineering Science*, 105:46-52
- Liu, Y., Liu, Y-J, 2008. Biosorption isotherms, kinetics and thermodynamics. *Separation and Purification Technology*, 61:229-242.
- Londeree, D.J. 2002. Silica-titania composites for water treatment, Masters's dissertation. University of Florida
- MacKay, A.A. & Pignatello, J.J. 2001. Application of Fenton-based reactions for treating dye wastewaters: Stability of azo dyes in the presence of Fe(III), *Helvetica Chimica Acta*, 84: 2589-2600.
- Maji, S.K. and Pal, A. & Pal, T. 2007. Arsenic removal from aqueous solutions by adsorption on laterite soil. *Journal of Environmental Science and Health, Part A*. 42(4):453-462,
- Malato, S., Ferná'ndez-Iba'nez, P., Maldonado, M.I., Blanco, J. & Gernjak, W. 2009. Decontamination and disinfection of water by solar photocatalysis: recent overview and trends. *Catalysis Today*, 147:1-59.
- Manju, G.N, Raji, C. & Anirudhan, T.S. 1998. Evaluation of coconut husk carbon for the removal of arsenic from water. *Water Research*, 32:3062-3070.
- Matatov-Meytal, Y.I. & Sheintuch, M. 1998. Catalytic abatement of water pollutants. *Industrial and Engineering Chemistry Research*, 37(2):309-326.
- Material Safety Data Sheet. 2012. Titanium dioxide MSDS, ScienceLab.com, <http://www.sciencelab.com/msds.php?msdsId=992-5268>
- Meng, X.G., Bang, S. & Korfiatis, G.P. 2000. Effects of silicate, sulfate, and carbonate on arsenic removal by ferric chloride. *Water Research*, 34:1255-1261.
- Mills, A. & Morris, S. 1993. Photo-mineralization of 4-chlorophenol sensitized by titanium dioxide: a study of the initial kinetics of carbon dioxide photo-generation. *Journal of Photochemistry and Photobiology A: Chemistry*, 71:75-83.
- Ming, D.W. & Dixon, J.B. 1987. Quantitative determination of clinoptilolite in soils by a cation exchange capacity method. *Clays Clay Mineral*, 35:463-468.

- Morales, J., Manso J.A., Cid A. & Mejuto J.C. 2012. Degradation of carbofuran and carbofuran-derivatives in presence of humic substances under basic conditions. *Chemosphere*, 89(11):267-271.
- Moura, M.N, Martín, M.J. & Burguillo, F.J. 2007. A comparative study of the adsorption of humic acid, fulvic acid and phenol onto *Bacillus subtilis* and activated sludge. *Journal of Hazardous Material*, 149(1):42-8.
- Muthukumar, M. & Selvakumar, N. 2004. Studies on the effect of inorganic salts on decolouration of acid dye effluents by ozonation. *Dyes Pigmentation*, 62:221-228
- Neppolian, B., H.C. Choi, S. Sakthivel, B. Arabindoo and V. Murugesan. 2002. Solar light induced and TiO₂ assisted degradation of textile dye reactive blue 4. *Chemosphere*, 46:1173-1181.
- Ni, M., Leung, M.K.H., Leung, D.Y.C. & Sumathy, K. 2007. A review and recent developments in photocatalytic water-splitting using TiO₂ for hydrogen production. *Renewable and Sustainable Energy Reviews*. 11:401-425.
- Nikazar, M., GholVIand, K. & Mahanpoor, K. 2007. Enhancement of photocatalytic efficiency of TiO₂ by supporting on clinoptilolite in the decolorization of azo dye direct yellow 12 aqueous solutions. *Journal of Chinese Chemical society*, 54:1261-1268.
- Nowacka, M., Ambrohewicz, D. & Jesionowski. T. 2013. TiO₂-SiO₂/Ph-POSS Functional Hybrids: Preparation and Characterisation. *Journal of Nanomaterials*, 1-10.
- Ou, X.X., Chen S, Zhao, H.M. & Quan, X. 2009. Photochemical activity and characterization of the complex of humic acids with iron(III). *Journal of Geochemical Exploration*, 102, 49-55.
- Pallant, J. 2007. *SPSS Survival manual* (3rd Ed.). London: Open University Press.
- Papadam, T., Xekoukoulotakis N.P., Ioannis, P., Dionissios, M. 2007. Photocatalytic transformation of acid orange 20 and Cr(VI) in aqueous TiO₂ suspensions, *Journal Photochemistry. Photobiology. A: Chemistry*, 186:308-315.
- Papirer, E. 2000. *Adsorption on Silica Surfaces*, New York: Wiley
- Park, D., Yun, Y.S. & Park, J.M. 2005. Use of dead fungal biomass for the detoxification of hexavalent chromium: screening and kinetics. *Process Biochemistry*, 40:2559-2565.
- Parra, S., Stanca, S.E., Guasaquillo, I., Thampi, K.R., 2004. Photocatalytic degradation of atrazine using suspended and supported TiO₂. *Applied Catalysis B: Environmental*, 51:107- 116.

- Pera-Titus, M., Garcí'a-Molina, V., Ban˜ os, M.A., Gime´nez, J. & Esplugas, S. 2004. Degradation of chlorophenols by means of advanced oxidation processes: review. *Applied Catalysis B: Environmental*, 47:219-256.
- Pignatello, J.J., 1992. Dark and photoassisted iron (III)-catalyzed degradation of chlorophenoxy herbicides by hydrogen peroxide. *Environmental Science and Technology*, 26:944-951.
- Pirkanniemi, K. & Sillanpää. M. 2002. Heterogeneous water phase catalysis as an environmental application: review. *Chemosphere*, 48:1047-1060.
- Pitoniak, E.R. 2004. Evaluation of nanostructured silica-titania composites in an adsorption/photocatalytic oxidation system for elemental mercury vapor control, Masters of Engineering thesis, University of Florida.
- Plazinski, W., Rudzinski, W. & Plazinska, A. 2009. Theoretical models of sorption kinetics including a surface reaction mechanism: review. *Advances in Colloid and Interface Science*, 15(1-2):2-13.
- Purcell, M., Neault, J. F.; Malonga, H. Arakawa, H., Carpentier, R. & Tajmir-Riahi, H.A. 2001. Interactions of atrazine and 2,4-D with human serum albumin studied by gel and capillary electrophoresis, and FTIR spectroscopy. *Biochimica et Biophysica Acta*, 1548:129-138
- Raghavacharya, C. 1997. Colour removal from industrial effluents—a comparative review of available technologies. *Chemical Engineering World*, 32:53-54.
- Ren, J. & Jiang, K. 2002. Impact of atrazine on the water resources of the Yang River in Zhangjiakou area in China. *Bulletin of Environmental Contamination and Toxicology*, 68(6):893-900.
- Repo, E. 2011. EDTA- and DTPA-functionalized silica gel and chitosan adsorbents for the removal of heavy Metals from aqueous solutions. PhD. Thesis. Finland: Lappeenranta University of Technology.
- Robinson, T, McMullan, G, Marchant, R. & Nigam P. 2001. Remediation of dyes in textile effluent: a critical review on current treatment technologies with a proposed alternative. *Bioresources Technology*, 77:247-55.
- Saien, J. & Khezrianjoo, S. 2008. Degradation of the fungicide carbendazim in aqueous solutions with UV/TiO₂ process: optimization, kinetics and toxicity studies. *Journal of Hazardous Materials*. 157:269-276.

- Sakthivel, S., Shankar, M.V., Palanichamy, M., Banumathi A., Bahnemanna, D.W. & Murugesan, V. 2004. Enhancement of photocatalytic activity by metal deposition: Characterization and photonic efficiency of Pt, Au and Pd deposited on TiO₂ catalyst. *Water Research*, 38:3001-3008
- Sakthivel, S., Neppolian, B., Shankar, M. V., Arabindoo, B., Palanichamy, M. & Murugesan, V. 2003. *Solar Energy Materials and Solar Cells*, 77(1):65-82.
- Schrank, S.G., José, H.J. & Moreira, R.F.P.M. 2002. Simultaneous photocatalytic Cr(VI) reduction and dye oxidation in a TiO₂ slurry reactor. *Journal of Photochemistry and Photobiology. A: Chemistry*. 147:71-76.
- Shan, A.Y., Ghazi, T.I.M. Rashid, S.A. 2010. Immobilisation of titanium dioxide onto supporting materials in heterogeneous photocatalysis: review. *Applied Catalysis A: General*, 389:1-8
- Sharma, V.K. & Sohn, M. 2009. Aquatic arsenic: toxicity, speciation, transformations, and remediation. *Environmental International*, 35:743-759.
- Silverstein, M., Basseler, G.C. & Morill, C. 1981. *Spectrometric Identification of Organic Compounds*, New York:Wiley
- Sing, K.S.W., Everett, D.H., Haul, R.A.W., Moscou, L., Pierotti, R.A., Rouquerol, J. & Siemieniewska, T. 1985. Reporting physisorption data for gas/solid systems: with Special reference to the determination of surface area and porosity, *Pure and Applied Chemistry*, 57(4):603-619, IUPAC.
- Slokar, Y.M. & Le Marechal, A.M. 1997. Methods of decoloration of textile wastewaters. *Dyes Pigments*, 37:335-356.
- Solozhenko, E.G., Soboleva, N.M. & Goncharuk, V.V. 1995. Decolorization of azo dye solutions by Fenton's oxidation. *Water Research*, 29 (9):2206-2210.
- Sun, X., Liu, H., Zhang, Y., Zhao, Y., Quan. X. (2011). Effects of Cu (II) and humic acid on atrazine photodegradation. *Journal of Environmental Science*, 23(5):773-777.
- Tang, W.W, Zeng, G.M., Gong J.L., Liu Y., Wang X.Y., Liu Y.Y., Liu, Z.F., Chen, L., Zhang, X.Y. & Tu, D.Z. 2012. Simultaneous adsorption of atrazine and Cu(II) from wastewater by magnetic multi-walled carbon nanotube. *Chemical Engineering Journal*, 211-212:470-478.
- Tao, Q.H. & Tang, H.X. 2004. Effect of dye compounds on the adsorption of atrazine by natural sediment. *Chemosphere*, 56:31-38.

- Torimoto, T., Ito, S., Kuwabata, S. & Yoneyama, H. 1996. Effects of adsorbents used as supports for titanium dioxide loading photocatalytic degradation of propyzamide. *Environmental Science and Technology*, 30:1275-1281.
- Turchi, C. & Ollis, D. 1990. Photocatalytic degradation of organic water contaminant: mechanisms involving hydroxyl radical attack. *Journal of Catalysis*, 122:178-192.
- Turner, M., Golovko, V.B., Vaughan, O.P.H. Abdulkin, P., Berenguer-Murcia, A., Tikhov, M.S., Johnson B.F., Lambert, R.M. (2008). Selective oxidation with dioxygen by gold nanoparticle catalysts derived from 55-atom clusters. *Nature*, 454: 981-983.
- Uchida, H., Itoh, S. & Yoneyama, H., 1993. Photocatalytic decomposition of propyzamide using TiO₂ supported on activated carbon. *Chemistry Letters*, 1995-1998.
- Venceslau, M.C., Tom, S. & Simon, J.J. 1994. Characterization of textile wastewaters: review. *Environmental Technology*, 15(9):17-29.
- Vilhunen, S.H. & Sillanpää M. E.T. 2009. Ultraviolet light emitting diodes and hydrogen peroxide in the photodegradation of aqueous phenol. *Journal of Hazardous Materials*, 161:1530-1534.
- Vinodgopal, K. & Kamat, P.V. 1992. Photochemistry on surfaces: photodegradation of 1, 3-diphenylisobenzofuran over metal oxide particles. *Journal of Physical Chemistry*, 96:5053-5059.
- WHO. 2006. Guidelines for Drinking-Water Quality First Addendum to third edition Recommendations, WHO Library Cataloguingin- Publication Data.
- Xu, Y. & Lebrun, R.E. 1999. Treatment of textile dye plant effluent by nano filtration membrane. *Separation Science and Technology*, 34:2501-2519.
- Yamazaki, S., Matsunaga, S. & Hori, K. 2001. Photocatalytic degradation of trichloroethylene in water using TiO₂ pellets. *Water Resources*, 35:1022-1028.
- Yu, H., Yu, J. Cheng, B. & Lin, J. 2007. Synthesis, characterization and photocatalytic activity of mesoporous Titania nanorod/titanate nanotube composites. *Journal of Hazardous Materials*, 147:581-587.
- Zhuravlev L. T. 2000. The surface chemistry of amorphous silica. Zhuravlev model. *Colloidal surfaces*. 173, 1-45.

APPENDIX: Characterization of composite photocatalystsTable A1 Physical characteristics of zeolite and composite (TiO₂/zeolite)

Catalyst TiO ₂ on composite, wt%	BET surface area (m ² g ⁻¹)
0	22.095
3	21.468
10	22.2005
15	21.88
20	20.904

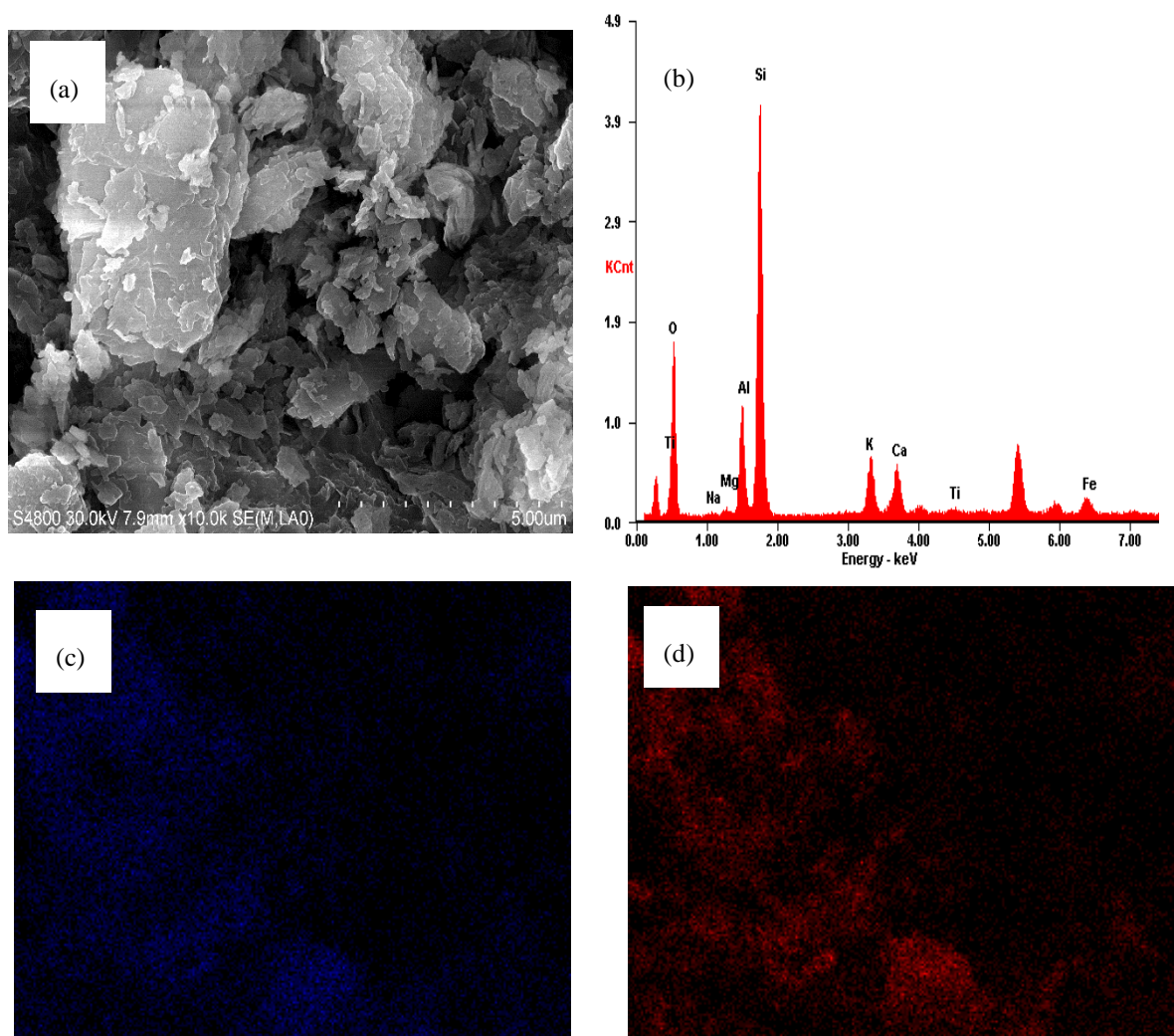


Figure A1. Zeolite analysis, (a) SEM image; (b) EDX spectra; EDX mapping of (c) Al and (d) O

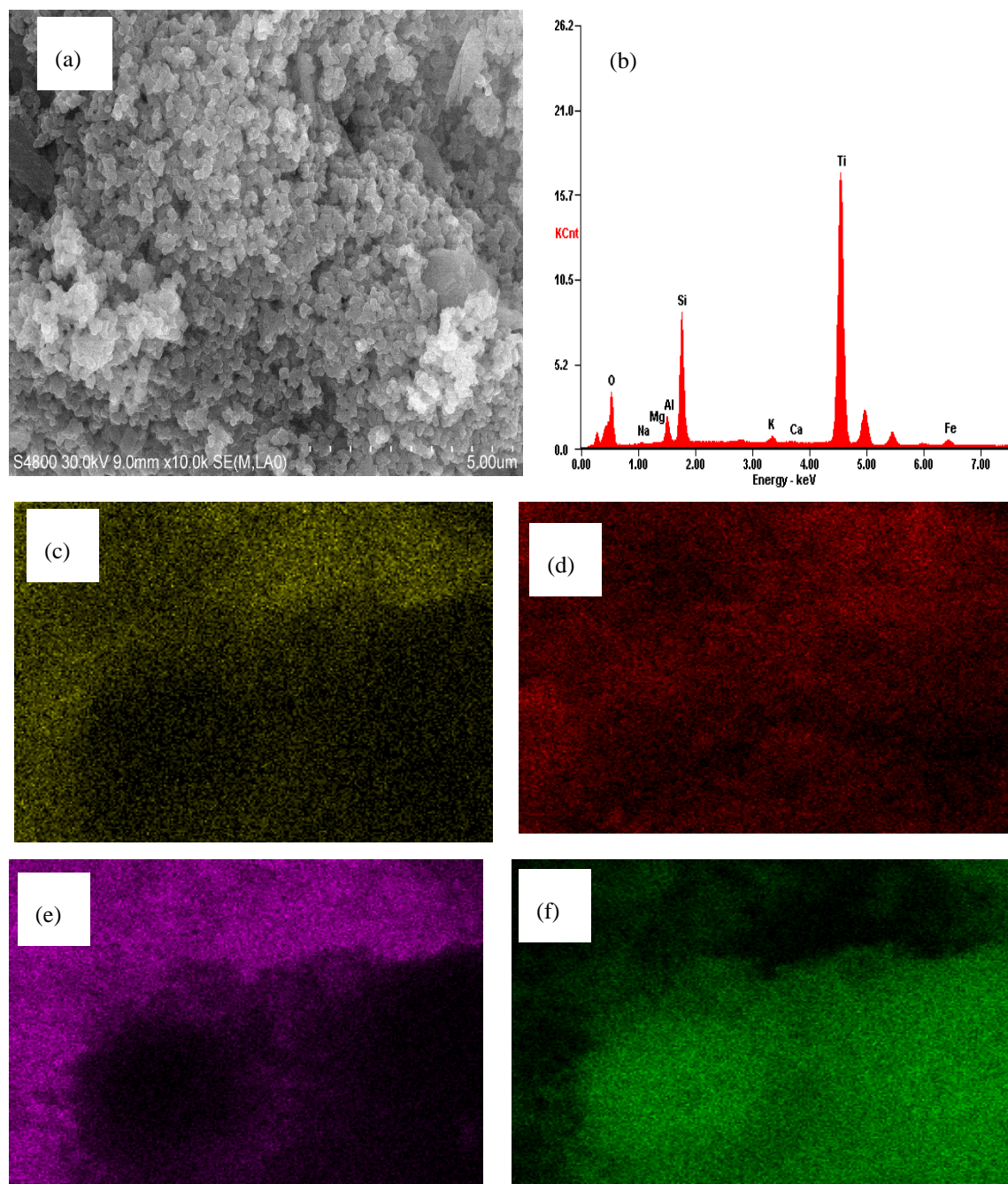


Figure A2. Analysis of TiO₂ supported on 0.2-0.5 mm zeolite, (a) SEM images (b) EDX spectra; EDX mapping of (c) Al, (d) O, (e) Si (f) Ti

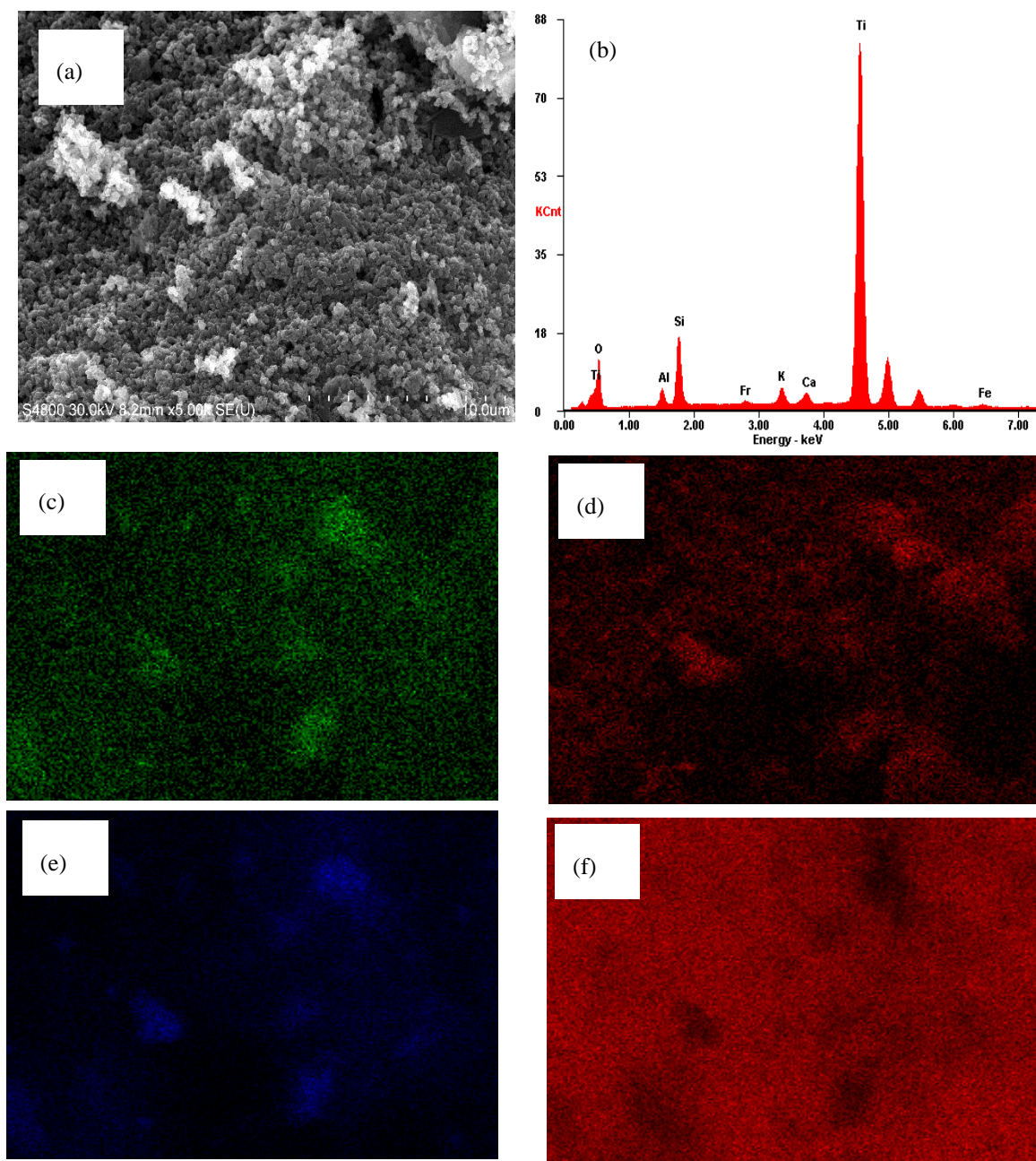


Figure A3. Analysis of TiO₂ supported on 0.5-1 mm zeolite, (a) SEM images (b) EDX spectra; EDX mapping of (c) Al, (d) O, (e) Si (f) Ti

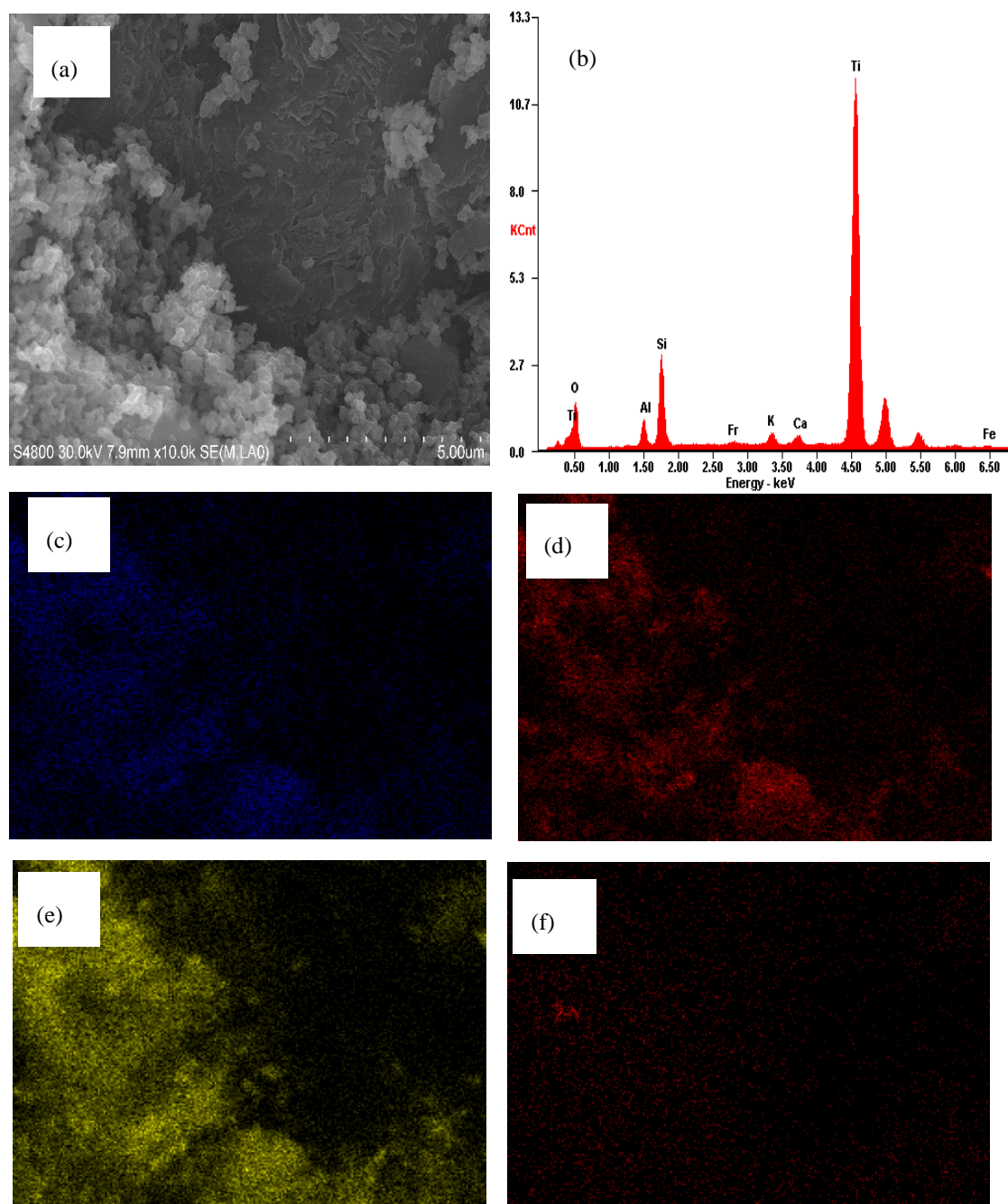


Figure A4. Analysis of TiO_2 supported on 1-1.2 mm zeolite, (a) SEM images (b) EDX spectra; EDX mapping of (c) Al, (d) O, (e) Si (f) Ti

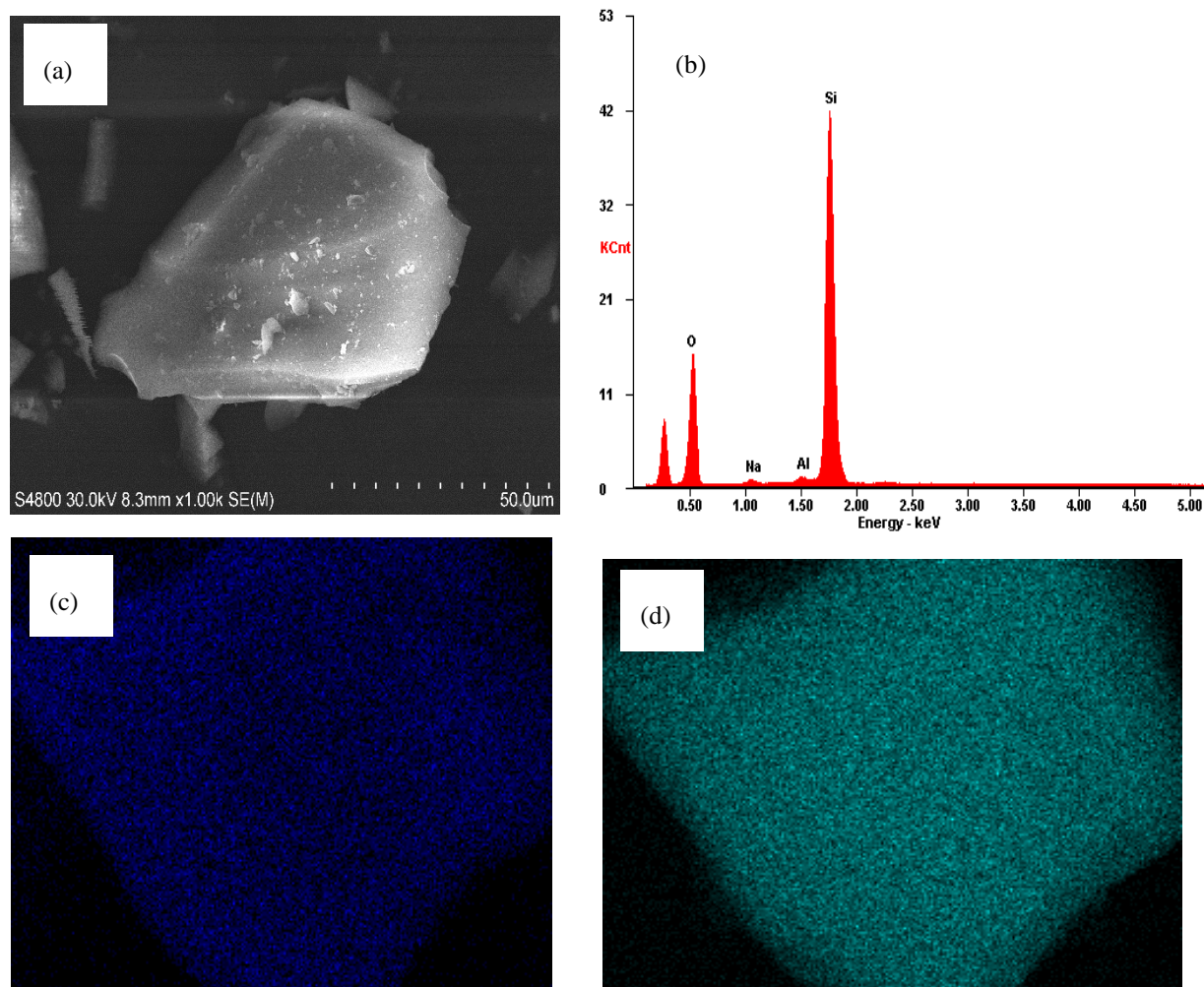


Figure A5. Silica analysis, (a) SEM image; (b) EDX spectra; EDX mapping of O (c) and Si (d)

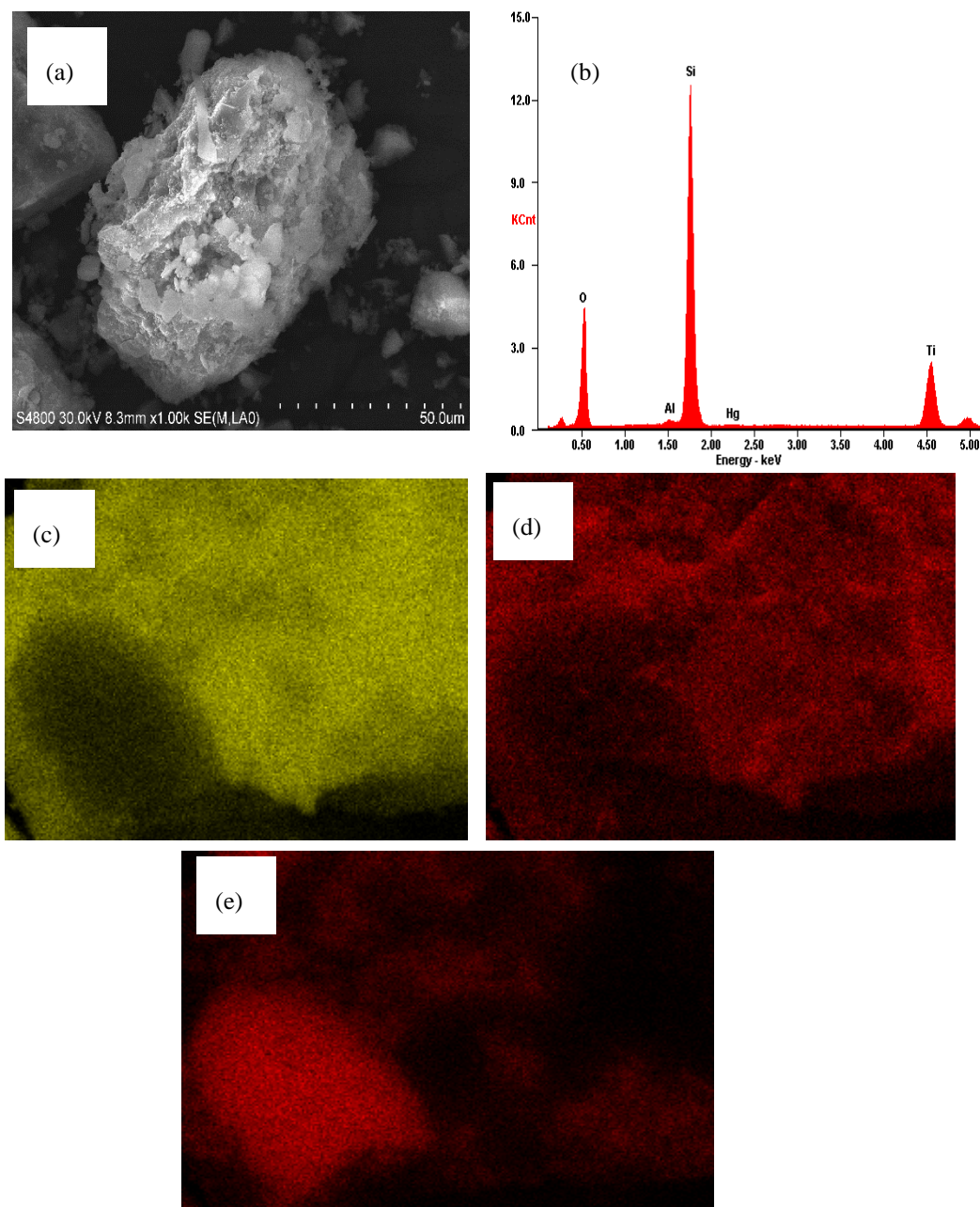


Figure A6. Analysis of 38-75 μm TiO_2 /silica composite photocatalyst (a) SEM images (b) EDX spectra; EDX mapping of (c) O, (d) Si (e) Ti

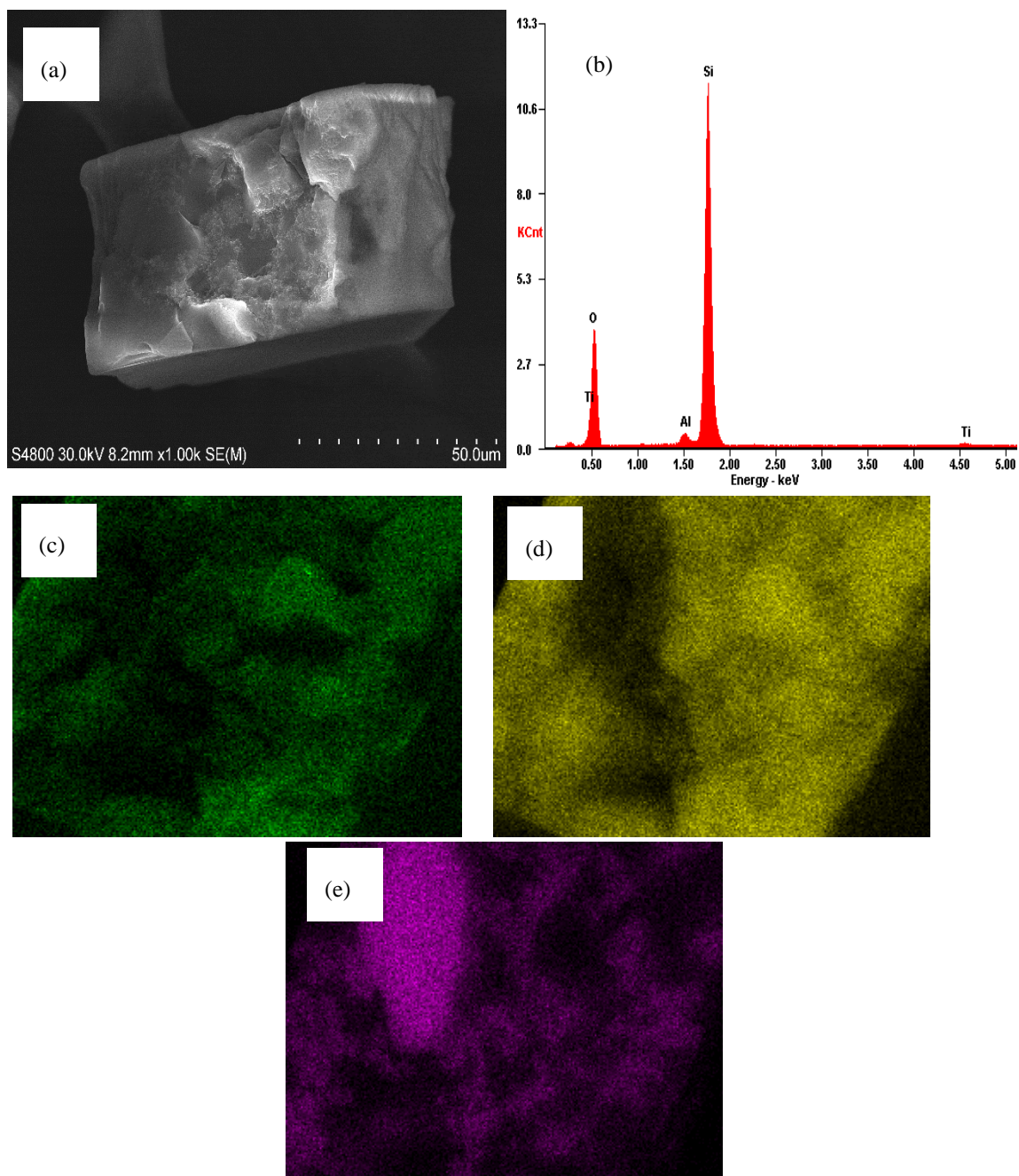


Figure A7. Analysis of 75-150 μm TiO_2 /silica composite photocatalyst (a) SEM images (b) EDX spectra; EDX mapping of (c) O, (d) Si (e) Ti

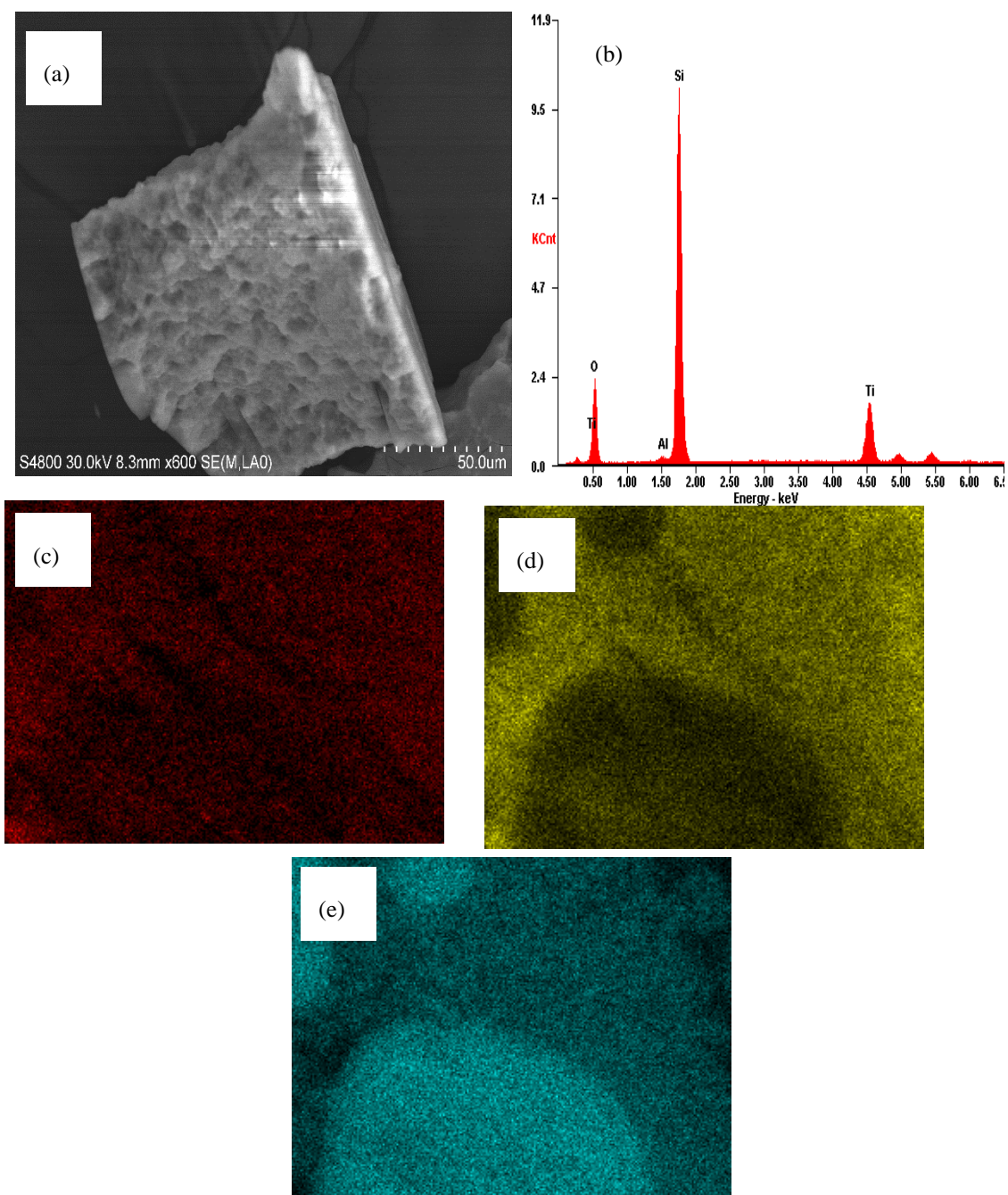


Figure A8. Analysis of 150-250 μm TiO_2 /silica composite photocatalyst (a) SEM images (b) EDX spectra; EDX mapping of (c) O, (d) Si (e) Ti